

**INTEGRATION OF WELL TEST ANALYSIS INTO A NATURALLY
FRACTURED RESERVOIR SIMULATION**

A Thesis

by

LAURA ELENA PEREZ GARCIA

Submitted to the Office of Graduate Studies of
Texas A&M University
in partial fulfillment of the requirements for the degree of

MASTER OF SCIENCE

December 2005

Major Subject: Petroleum Engineering

**INTEGRATION OF WELL TEST ANALYSIS INTO A NATURALLY
FRACTURED RESERVOIR SIMULATION**

A Thesis

by

LAURA ELENA PEREZ GARCIA

Submitted to the Office of Graduate Studies of
Texas A&M University
in partial fulfillment of the requirements for the degree of

MASTER OF SCIENCE

Approved by:

Chair of Committee,	David S. Schechter
Committee Members,	W. John Lee
	Wayne M. Ahr
Head of Department,	Stephen A. Holditch

December 2005

Major Subject: Petroleum Engineering

ABSTRACT

Integration of Well Test Analysis into a Naturally Fractured Reservoir Simulation.

(December 2005)

Laura Elena Perez Garcia, B.S., Universidad Surcolombiana

Chair of Advisory Committee: Dr. David S. Schechter

Naturally fractured reservoirs (NFR) represent an important percentage of the worldwide hydrocarbon reserves and production. Reservoir simulation is a fundamental technique in characterizing this type of reservoir. Fracture properties are often not available due to difficulty to characterize the fracture system.

On the other hand, well test analysis is a well known and widely applied reservoir characterization technique. Well testing in NFR provides two characteristic parameters, storativity ratio and interporosity flow coefficient. The storativity ratio is related to fracture porosity. The interporosity flow coefficient can be linked to shape factor, which is a function of fracture spacing.

The purpose of this work is to investigate the feasibility of estimating fracture porosity and fracture spacing from single well test analysis and to evaluate the use of these two parameters in dual porosity simulation models.

The following assumptions were considered for this research: 1) fracture compressibility is equal to matrix compressibility; 2) no wellbore storage and skin effects are present; 3) pressure response is in pseudo-steady state; and 4) there is single phase flow.

Various simulation models were run and build up pressure data from a producer well was extracted. Well test analysis was performed and the result was compared to the simulation input data.

The results indicate that the storativity ratio provides a good estimation of the magnitude of fracture porosity. The interporosity flow coefficient also provides a reasonable estimate of the magnitude of the shape factor, assuming that matrix permeability is a known parameter. In addition, pressure tests must exhibit all three flow regimes that characterizes pressure response in NFR in order to obtain reliable estimations of fracture porosity and shape factor.

DEDICATION

I dedicate my thesis:

First to God, for so many blessings;

To my wonderful kids, Maria Fernanda, Maria Paula and Juan Felipe,
for you I did all this journey.

and

To Ricardo, my love, my husband, and my best friend,
without you this dream would never have come true.

ACKNOWLEDGEMENTS

I wish to express my sincere gratitude and appreciation to Dr. David S. Schechter, chair of my advisory committee, for encouraging me through these two years. I thank Dr. W. John Lee, and Dr. Wayne Ahr, for their support and guidance, and also for the wonderful courses I had the opportunity to take with them. I appreciate the continuous support and advice of Dr. Erwin Putra, and Dr. Dewi Hidayati, especially in the hardest moments. Finally, I want to thank Empresa Colombiana de Petroleos ECOPETROL for sponsoring my studies at Texas A&M University.

TABLE OF CONTENTS

	Page
ABSTRACT	iii
DEDICATION	iv
ACKNOWLEDGEMENTS	v
TABLE OF CONTENTS	vii
LIST OF FIGURES	ix
LIST OF TABLES	xiii
 CHAPTER	
I INTRODUCTION.....	1
1.1 Objectives.....	2
1.2 Problem Description.....	2
1.3 Scope of the Work.....	3
1.4 Motivation	3
II NATURALLY FRACTURED RESERVOIRS	4
2.1 Fracture Properties	4
2.2 Classification of Fractured Reservoirs	6
III WELL TEST ANALYSIS IN NATURALLY FRACTURED RESERVOIRS	9
IV NUMERICAL SIMULATION IN NFR	15
V TECHNICAL FRAMEWORK	18
5.1 Shape Factor	18
5.2 Storativity Ratio	22

CHAPTER	Page
5.3 Interporosity Flow Coefficient	24
VI SIMULATION CASES AND WELL TEST RESULTS	29
6.1 Radial Model – Gas System	30
6.2 Radial Model – Oil System	38
6.3 Cartesian Model	44
6.4 Anisotropic Matrix Permeability Model	48
6.5 Anisotropic Fracture Permeability Model	53
6.6 Heterogeneous Field Model	54
6.7 Anisotropic Field Model	69
VII CONCLUSIONS	78
NOMENCLATURE	80
REFERENCES	81
APPENDIX A	84
APPENDIX B	89
VITA	96

LIST OF FIGURES

FIGURE		Page
2.1	Schematic plot of fracture porosity and permeability percentage for the four fractured reservoir types.	7
3.1	Ideal model for a natural fractured reservoir.....	9
3.2	Semilog plot for pressure response in NFR	10
3.3	Idealization of a naturally fractured reservoir	11
3.4	Ideal model for a nonintersecting natural fracture	12
3.5	Derivative type curve for double-porosity reservoir, pseudo-steady state flow	14
3.6	Idealized pressure response in quadruple porosity reservoirs	14
4.1	Schematic representation of fractured reservoir simulation model.....	15
4.2	Different approaches to simulate NFR.....	16
4.3	Discrete Fracture Network	17
5.1	Shape factor as function of fracture spacing	19
5.2	Gas rates obtained for different values of fracture spacing.....	21
5.3	Cumulative gas production obtained for different values of fracture spacing	21
5.4	Matrix porosity distribution in NFR.....	23
5.5	Fracture porosity distribution in NFR	23
5.6	Storativity ratio distribution from field data	24
5.7	Shape factor vs. λ/r_w^2	26
5.8	L_{ma} vs. λ/r_w^2	26

FIGURE		Page
5.9	Matrix permeability distribution in NFR	27
5.10	Fracture permeability distribution in NFR	28
5.11	Interporosity flow coefficient distribution from field data.....	28
6.1	Schematic representation of the 216 simulation cases run for gas cases	32
6.2	Example of semilog analysis.....	33
6.3	Example of type curve analysis.....	34
6.4	Well test response with no system radial flow	35
6.5	Fracture porosity estimated from storativity ratio for 179 simulation runs; radial model, gas system	36
6.6	Shape factor estimated from λ ; radial model, gas system.....	37
6.7	Fracture spacing estimated from λ ; radial model, gas system	38
6.8	Simulation cases run for radial model-oil system case	40
6.9	Well test response with no system radial flow	41
6.10	Fracture porosity estimated from storativity ratio for 164 simulation runs; radial model, oil system.....	42
6.11	Shape factor estimated from storativity ratio from 164 simulation runs; radial model, oil system.....	43
6.12	Fracture spacing estimated from storativity ratio from 164 simulation runs; radial model, oil system	43
6.13	Comparison of bottom-hole pressure from radial and cartesian models	45
6.14	Bottom hole pressure in cartesian and radial models	46

FIGURE		Page
6.15	Comparison bottom hole pressure using cartesian local refinement.....	47
6.16	Bottom hole pressure comparison using cartesian and hybrid refinements	47
6.17	Comparison pressure response in radial and cartesian models	49
6.18	Type curve analysis showing the effect of anisotropic matrix permeability on well test response	51
6.19	Type curve analysis showing the effect of anisotropic fracture permeability on well test response	55
6.20	Log normal distribution used to generate fracture permeability values.....	56
6.21	Triangular distribution used to generate fracture spacing values.....	57
6.22	Well locations in heterogeneous field model	58
6.23	Example of pressure response in a low fracture permeability heterogeneity zone. Well 22.....	60
6.24	Example of pressure response in a moderate fracture permeability heterogeneity zone. Well 4.....	61
6.25	Example of pressure response in a high fracture permeability heterogeneity zone.....	62
6.26	Fracture porosity estimated from well test storativity ratio for heterogeneous field model	63
6.27	Well block fracture permeability vs. well test estimated permeability.....	64
6.28	Well block vs. well test estimated fracture spacing correlation.....	65
6.29	Example of fracture permeability averages.....	66
6.30	Simulation average vs. well test estimated fracture permeability.....	68

FIGURE		Page
6.31	Simulation average vs. well test estimated fracture spacing	68
6.32	Fracture porosity estimated from well test storativity ratio	72
6.33	Well block vs. well test estimated effective fracture permeability correlation.....	73
6.34	Well block vs. well test estimated Shape factor correlation.....	74
6.35	Effect of matrix permeability value on Shape factor estimation.....	75
6.36	Well block vs. well test estimated fracture spacing in x direction	76
6.37	Well block vs. well test estimated fracture spacing in y direction	77

LIST OF TABLES

TABLE		Page
2.1	Characteristics and examples of type I to III fractured reservoirs	8
5.1	Shape factor constants proposed by several authors	18
6.1	Main reservoir characteristics for radial model, gas reservoir	31
6.2	Main reservoir characteristics; cartesian model	44
6.3	Matrix permeability values in x and y directions. Anisotropic matrix permeability case	50
6.4	Well test analysis results for anisotropic matrix permeability cases	51
6.5	Shape factor and fracture spacing estimation using effective and maximum matrix permeability	52
6.6	Fracture permeability values in x and y directions. Anisotropic fracture permeability case	53
6.7	Well test analysis results. Anisotropic fracture permeability cases .	54
6.8	Main Reservoir Characteristics; heterogeneous field model.....	56
6.9	Well test results for heterogeneous field model	59
6.10	Average input values that closely matched well test results	67
6.11	Well test results. Anisotropic field model	71

CHAPTER I

INTRODUCTION

Naturally fractured reservoirs (NFR) are those reservoirs that contain fractures created by nature that have or could have an effect, either positive or negative, on fluid flow. NFR has two different porous media, the matrix, which has high storage but low flow capacity, and the fractures, which provide high flow path but low storage capacity.

A number of authors have developed different models for interpreting the pressure response in fractured reservoirs considering, among others, the characteristics of flow from matrix to fractures, fracture orientation, and block-size distribution. In general, pressure-transient tests in NFR show a behavior consistent with the Warren and Root¹ model. The characteristic behavior of pressure response can be described with two dimensionless parameters, namely storativity ratio (ω) and interporosity flow coefficient (λ).

Standard simulation models for NFR are based on the same principle of two porous media, where the simulation model is divided into two superimposed grids, one grid for matrix and other for fractures. Fluid flow from matrix to fractures is represented by transfer function. In specific cases where matrix cannot be represented with idealized models, discrete fracture network approach is preferred.

This thesis follows the style of the *SPE Reservoir Evaluation and Engineering Journal*.

Success of a simulation model in depicting observed behavior and predicting the future performance depends highly on the accuracy of reservoir description. In NFR, knowing how fractures are distributed and interconnected is one of the most important tasks. Information from different sources is incorporated during the process of understanding the fractures system, but there is no documented evidence that ω and λ , the two parameters obtained from well test in NFR, had been used as input data in building simulation models.

1.1 Objectives

The main objective of this project is to determine the feasibility to integrate the parameters obtained from well test analysis into simulation models. The specific objectives are 1) to validate the use of storativity ratio from well test analysis to estimate fracture porosity and 2) to validate the use of interporosity flow coefficient to estimate shape factor or fracture spacing.

1.2 Problem Description

Well test analysis is a well known and widely used reservoir management tool. Besides for short-term actions such as damage identification, well optimization and stimulation evaluation, well test results are often incorporated into other reservoir management processes such as numerical simulation.

Effective permeability and average reservoir pressure are two parameters commonly estimated from well test and later incorporated into simulation models as input data. Well test has also been used as a calibration tool in building simulation models by comparing pressure response from the model with actual data.

In NFR, there are two characteristic parameters, ω and λ , which are related to fracture porosity and shape factor, respectively. Fracture porosity and shape factor (expressed in

terms of fracture spacing) are required as input data to build dual-porosity simulation models.

1.3 Scope of the Work

This research is focused on single well, dual-porosity, pseudosteady state well tests without wellbore storage and skin. Simulation study is limited to radial and cartesian grid geometries and only considers single phase flow (either gas or oil).

1.4 Motivation

NFR represent an important percentage of worldwide hydrocarbon reserves and production. One fundamental technique to characterize this type of reservoirs is using reservoir simulation. In some cases, the actual complexities that occur in NFR can not be accurately represented by the classic simplification of dual-porosity models. However, the current state of the art model using DFN is not yet applicable for field scale. Thus, for the immediate future, the dual-porosity model is still widely used.

Simulation of NFR using dual porosity models requires shape factor and fracture porosity as input data. Shape factor is most of the time expressed in terms of fracture spacing. In theory, Shape factor could be obtained from well test data, but for practical purposes, it is considered as a matching parameter.

The main goal of this research is to find practical applications of single-well pressure test performed in NFR beyond permeability and average reservoir pressure estimation. The results of the study will show whether storativity ratio and interporosity flow coefficient could be a valid basis to obtain reliable estimates of fracture porosity and fracture spacing to be used as input parameters in building simulation models.

CHAPTER II

NATURALLY FRACTURED RESERVOIRS

Naturally fractured reservoirs (NFR) have increasingly gained attention in the past two decades. Many reservoirs, initially classified as classical matrix reservoirs, have been reclassified as fractured reservoirs during advanced stages of development, carrying significant losses on recoverable reserves. Identifying the fractured nature of a reservoir during early time is critical for an adequate reservoir management to maximize the economical benefit.

Fractures have been defined in different terms depending on the specific purpose or context of the definition. From reservoir point of view, Nelson² has defined fracture as a naturally macroscopic planar discontinuity in rock due to deformation or physical diagenesis. Fractures can be produced by brittle or ductile failure. The characteristic of fractures will also be different depending on generation process. Fractures can have positive or negative effects on fluid flow. NFR are those reservoirs where fractures have, or could have, any influence on reservoir performance. Nelson² has stressed the importance to collect information that allows identifying a reservoir as fractured in early stages of development.

2.1 Fracture Properties

The two major factors that govern permeability and porosity of fractures are fracture width and spacing. Fracture width (e) is the distance between two parallel surfaces that represent the fracture. Fracture spacing (D) is the average distance between parallel regularly spaced fractures.

According to Nelson², the four most relevant properties of fractured reservoirs, in order of increasing difficulty to determine, are:

- Fracture porosity
- Fracture permeability
- Fluid saturations within fractures
- Expected recovery factor.

Fracture Porosity

Fracture porosity is a percentage of void space in fractures compared to the total volume of the system. Fracture porosity is estimated using the following expression:

$$\phi_f = \left(\frac{e}{D + e} \right) \times 100 \dots\dots\dots(2.1)$$

As can be noticed from the expression, fracture porosity is very scale-dependent. The value of ϕ_f can be 100% in a particular location of reservoir, but the value for the whole reservoir is generally less than 1%. According to Nelson², fracture porosity is always less than 2%; in most reservoirs is less than 1% with a general value of less than 0.5%. An exception to this rules-of-thumb is vuggy fractures where porosity can vary from 0 to a very large value.

The importance of fracture porosity in reservoir performance depends on the type of fractured reservoir. If the fracture system provides an essential porosity and permeability to the reservoir, then fracture porosity is a critical parameter to be determined in early stages of development. As contribution of matrix porosity to the whole system increases, the relevance of fracture porosity decreases. The estimation of fracture porosity in early stages is not so crucial in reservoirs where matrix porosity is several orders of magnitude greater than fracture porosity.

Fracture porosity is one of the fracture properties that is difficult to determine. The common sources of fracture porosity estimation are: 1) core analysis; 2) porosity-permeability relationships; 3) field/lab determinations; 4) Logs; and 5) multiple-well tests.

Fracture Permeability

Permeability defines the ability of porous medium to transmit fluids. The presence of open fractures has a great impact in reservoir flow capacity. Therefore, fracture permeability is an important factor that determines reservoir quality and productivity.

Darcy's equation that is used to model fluid flow through porous media can not be used to represent flow through fractures. Thus, parallel plate theory was developed to model fluid flow in fractures. The parallel plate model is based on fracture width and spacing concepts.

Nelson² cited the work of Parsons (1966), who combined the model for fracture and matrix fluid flow and obtained the following equation for fracture permeability:

$$k_f = \frac{e^2}{12} x \frac{\rho g}{\mu} \dots\dots\dots(2.2)$$

This equation assumes laminar flow between smooth, non-moving, parallel plates and homogeneous fractures with respect to orientation, width and spacing. Parson's relationship is simple but is applicable to fluid flow through fractured reservoirs.

Fractures do not always improve fluid flow in a reservoir. In some cases, partially or total filled fractures can act as flow barriers. The effect of fractures on permeability depends on several factors such as morphology, orientation, and others.

Fracture width and permeability are difficult to determine from direct sources such as core data or laboratory test. Well test analysis is the most common source of fracture permeability information.

2.2 Classification of Fractured Reservoirs

Based on Hubbert and Willis work (1955), Nelson² proposed the following classification of fractured reservoirs:

- Type 1: Fractures provide the essential reservoir porosity and permeability.
- Type 2: Fractures provide the essential reservoir permeability.

Type 3: Fractures assist permeability in an already producible reservoir.

Type 4: Fractures provide no additional porosity or permeability but create significant reservoir anisotropy, such as barriers to flow.

As shown in Figure 2.1, the effect of fractures is of paramount importance for type 1 reservoirs, decreases for type 2 and so on. In the same way, the importance of proper characterization of porosity and permeability changes with reservoir type.

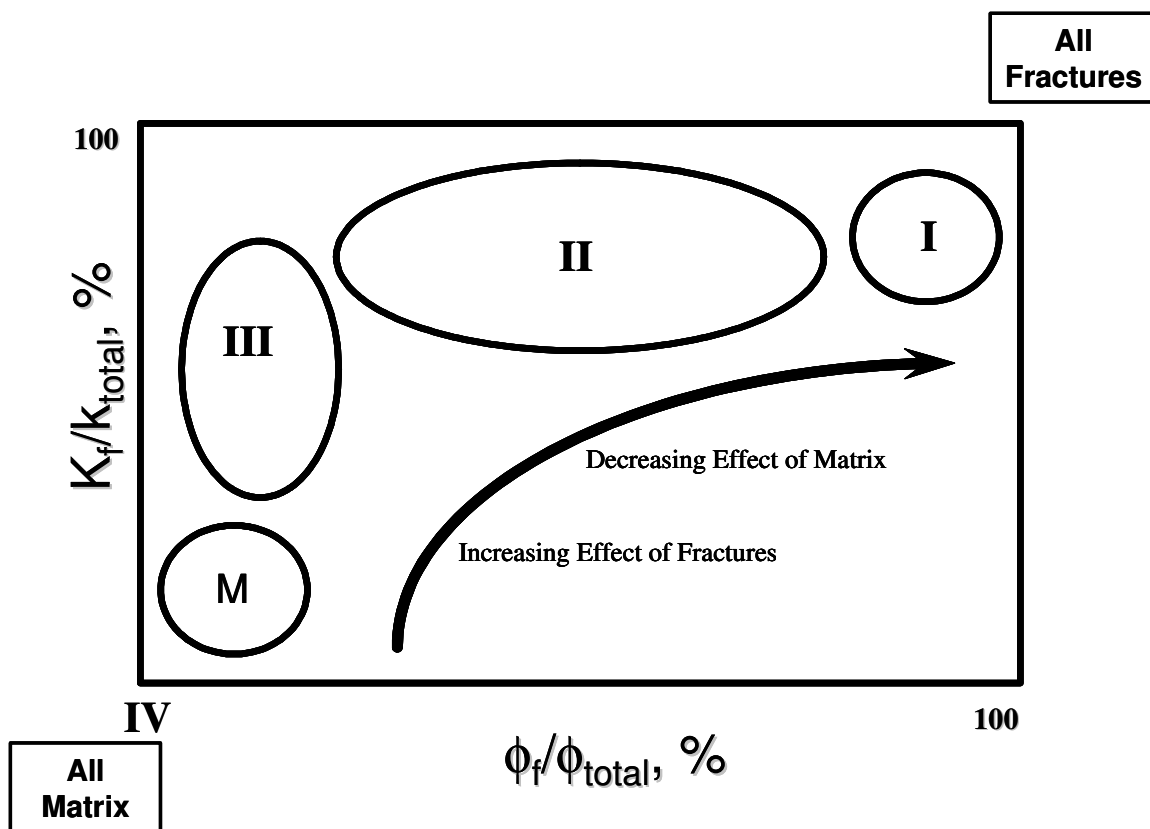


Figure 2.1- Schematic plot of fracture porosity and permeability percentage for the four fractured reservoir types. (After Nelson²).

Table 2.1 shows the characteristic, potential problems and some examples of the I, II and III fractured reservoirs types. Type IV reservoirs show the same characteristics as the conventional matrix reservoirs with fractures acting as heterogeneities.

Table 2.1- Characteristics and examples of type I to III fractured reservoirs.

Reservoir Type	Characteristics	Problems	Field Examples
Type 1	<p>Large drainage areas per well</p> <p>Few wells needed for development</p> <p>Good reservoir quality-well information correlation</p> <p>Easy good well location identification</p> <p>High initial potential</p>	<p>Rapid decline rates</p> <p>Possible early water encroachment</p> <p>Size/shape drainage area difficult to determine</p> <p>Reserves estimation complex</p> <p>Additional wells accelerate but not add reserves</p>	<p>Amal, Libia</p> <p>Ellenburger, Texas</p> <p>Edison, California</p> <p>Wolf Springs, Montana</p> <p>Big Sandy, Kentucky</p>
Type 2	<p>Can develop low permeability rocks</p> <p>Well rates higher than anticipated</p> <p>Hydrocarbon charge often facilitated by fractures</p>	<p>Poor matrix recovery (poor fracture-matrix communication)</p> <p>Poor performance on secondary recovery</p> <p>Possible early water encroachment</p> <p>Recovery factor variable and difficult to determine</p> <p>Fracture closure may occur in overpressured reservoir</p>	<p>Agha Jari, Iran</p> <p>Hart Kel, Iran</p> <p>Rangely, Colorado</p> <p>Spraberry, Texas</p> <p>La Paz/Mara, Venezuela</p>
Type 3	<p>Reserves dominated by matrix properties</p> <p>Reserve distribution fairly homogeneous</p> <p>High sustained well rates</p> <p>Great reservoir continuity</p>	<p>Highly anisotropic permeability</p> <p>Unusual response in secondary recovery</p> <p>Drainage areas often highly elliptical</p> <p>Interconnected reservoirs</p> <p>Poor log/core analysis correlation</p> <p>Poor well test performance</p>	<p>Kirkuk, Iraq</p> <p>Gachsaran, Iran</p> <p>Hassi Mesaoud, Algeria</p> <p>Dukhan, Qatar</p> <p>Cottonwood Creek, Wyoming</p> <p>Lacq, France</p>

CHAPTER III

WELL TEST ANALYSIS IN NATURALLY FRACTURED RESERVOIRS

One of the first documented approaches to model a NFR was presented by Pollard³ in 1953, which provides the method for selecting candidates for acid stimulation. Later Pirson and Pirson⁴ extended Pollard's method to calculate matrix pore volume. Despite the usefulness of Pollard's method in field applications, some authors^{1,6} have shown its inaccuracies.

Warren and Root¹ developed an idealized model for studying fluid flow in heterogeneous reservoirs, as shown in Figure 3.1. The model is composed of rectangular parallelepipeds where the blocks represent the matrix and the space in between represents the fractures. The general assumptions of the model are homogeneity and isotropy of the two porous media, uniform block-size distribution, and occurrence of fluid flow from matrix to fracture and from fracture to well, but not between matrix elements. The flow from matrix to fractures is pseudosteady state.

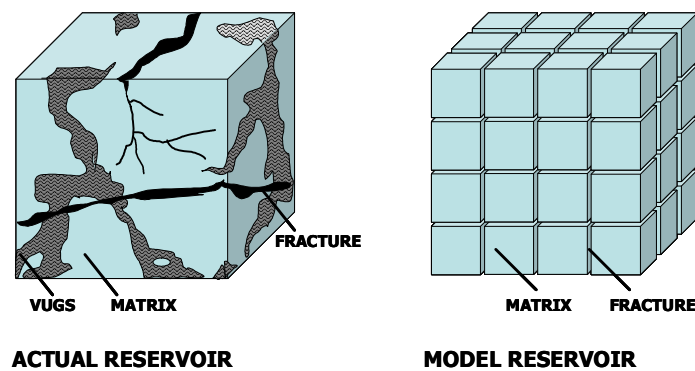


Figure 3.1– Ideal model for a natural fractured reservoir (after Warren and Root¹).

Warren and Root¹ found that buildup pressure response exhibits two semilog straight lines, Figure 3.2. The first straight line corresponds to the transient flow in the fracture media, and the second to the transient flow in the total system. The slopes of those lines are related to the flow capacity of the formation. The vertical separation of the two lines is related to the relative storage capacity of the fracture. They also defined two parameters describing the pressure behavior in a fractured system. The first parameter is storativity ratio (ω) which is the ratio of fracture storage capacity to the total storage capacity of the system. The second parameter is interporosity flow coefficient (λ) which governs the flow from matrix to fracture and is related to heterogeneity of the system. Mavor and Cinco⁵ later extended the Warren and Root¹ model to account for wellbore storage and skin.

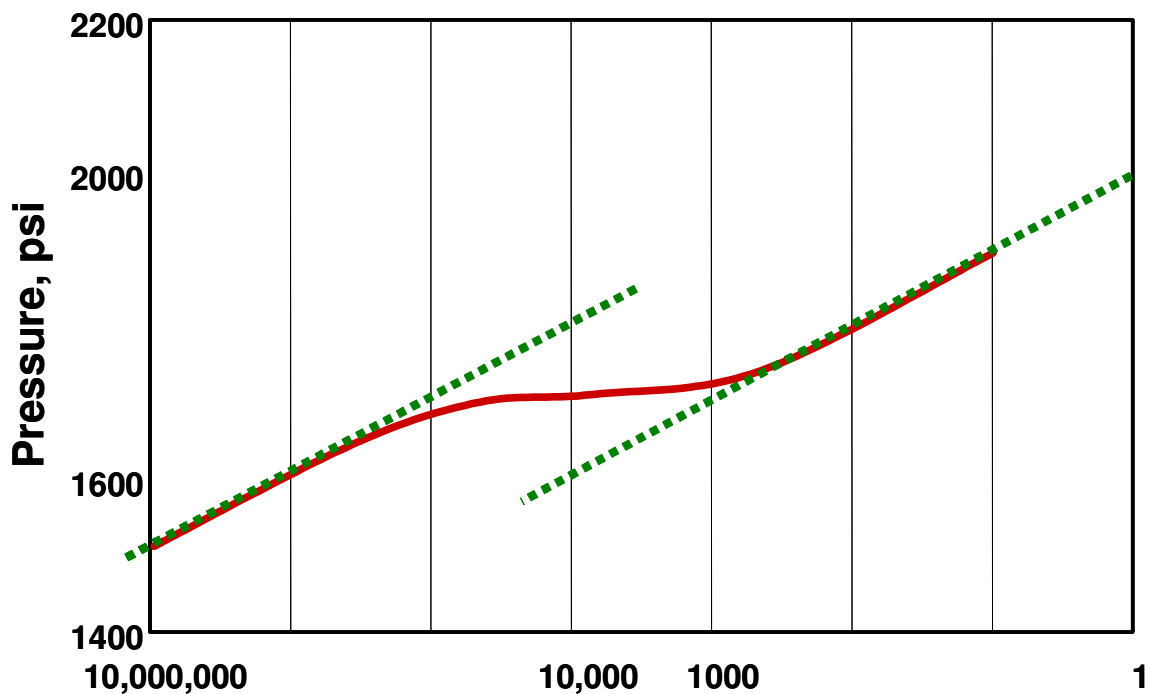


Figure 3.2- Semilog plot for pressure response in NFR.

Kazemi⁶ adopted a special case of the Warren and Root¹ model, a circular, finite reservoir with a centrally located well, where all fractures are horizontal. Figure 3.3 shows the Kazemi⁶ idealized model. The general assumptions of the model are: 1) single-phase flow; 2) flow in radial and vertical direction in unsteady-state; 3) fluid flows from matrix (high storage and extremely low flow capacity) to fracture (high flow capacity and low storage); and fracture produces fluid into the wellbore.

Kazemi⁶ simulated three hypothetical cases, analyzed the drawdown and buildup responses, and obtained three semilog straight lines. The first and third straight lines are equivalent to those observed in Warren and Root¹ model. The second line corresponds to transition regime from a fracture-dominated flow to a total system dominated flow. Kazemi⁶ concluded that Warren and Root¹ model for fractured reservoirs is valid for unsteady-state flow, and the value of interporosity flow coefficient depends on matrix-to-fracture flow regime.

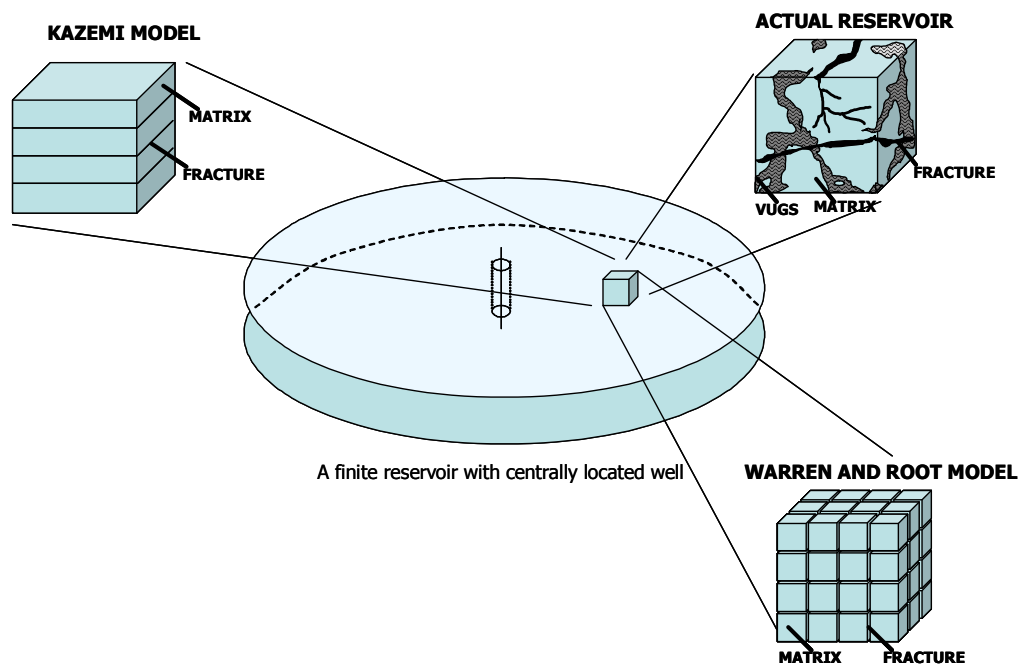


Figure 3.3- Idealization of a naturally fractured reservoir (after Kazemi⁶).

De Swaan⁷ presented analytical solutions for interporosity transient flow for different geometries than those used by Kazemi⁶. The results were similar and showed familiar semilog straight lines. Later, Najurieta⁸ extended the theory to include the transition period and Moench⁹ included the effect of pseudosteady-state skin between matrix and fracture system.

Cinco *et al.*¹⁰ considered a theoretical circular model with a centrally located well and a vertical fracture nearby the well, shown in Figure 3.4. Other assumptions of the model were: 1) isotropy of the two porous media; 2) fluid has low compressibility and constant viscosity; 3) constant system compressibility; and 4) fully penetrating well with constant production rate.

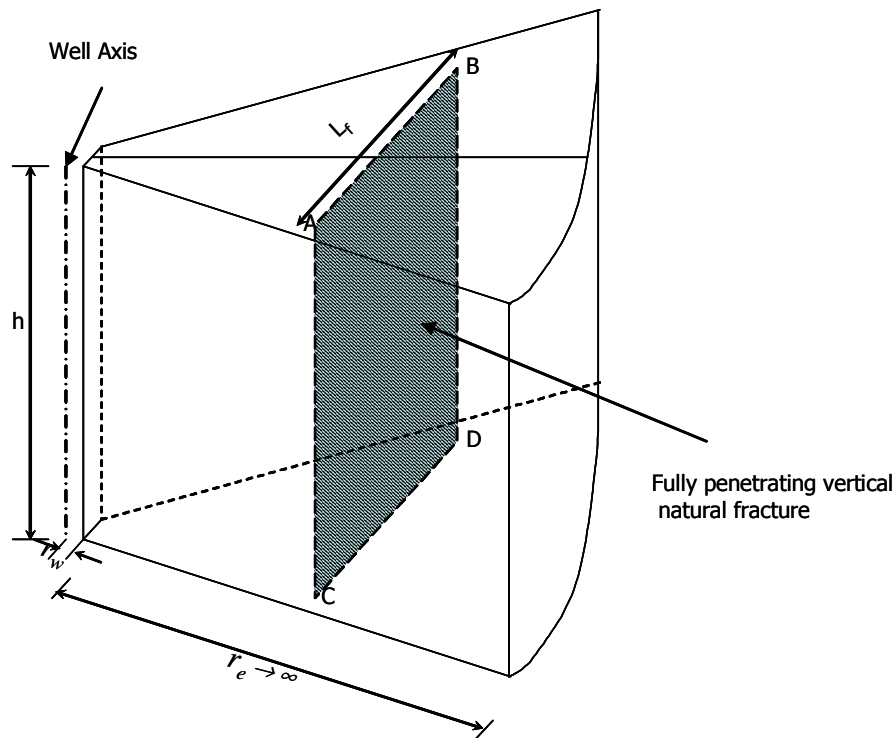


Figure 3.4 - Ideal model for a nonintersecting natural fracture (after Cinco *et al.*¹⁰).

The results showed that although the assumption of only one fracture, the pressure response was similar to the uniformly fractured reservoir with three semilog straight lines: fracture, transition, and total-system flow periods.

Cinco *et al.*¹⁰ also considered the effect of fracture orientation on pressure response. They concluded the semilog straight lines are present in all cases, with the transition period varying as a function of fracture orientation.

Bourdet *et al.*^{11, 12} introduced the use of pressure-derivative type curves in well-test interpretation. For NFR, they considered both pseudosteady-state and transient flow. They also included the effects of wellbore storage and skin. The pressure responses show different behaviors. For pseudosteady-state flow, the derivative curve shows a V-shape during the transition time. If the flow is transient, the derivative shows a constant value of 0.25 during the transition regime. Figure 3.5 presents an example of Bourdet type curves for fractured reservoirs considering pseudosteady flow.

A number of authors have discussed the inability of the dual-porosity approach in accounting for more complex reservoirs. Abdassah and Ershaghi¹³ introduced the triple porosity model in 1986. More recently, in 2004, Dreier *et al.*¹⁴ presented two quadruple porosity models. Figure 3.6 shows an example of the pressure response in a quadruple porosity system presented by Dreier *et al.*¹⁴. Nevertheless the basis of the mostly-used well-test analysis techniques for naturally fractured reservoir is the Warren and Root¹ theory with some modifications taking into account different types of matrix-to-fracture flow regimes, wellbore storage, and skin; such that the parameters ω and λ are valid for describing those reservoirs.

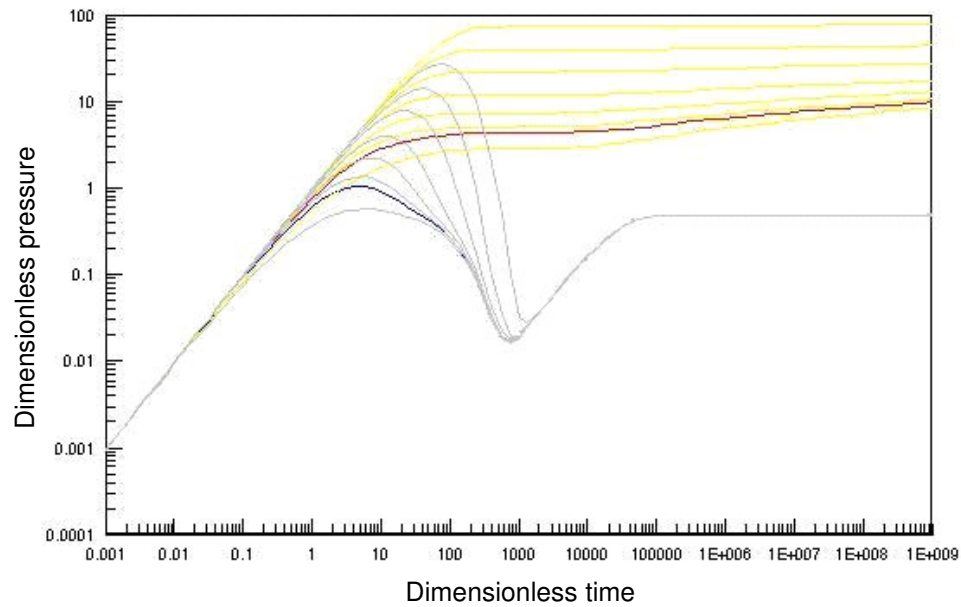


Figure 3.5- Derivative type curve for double-porosity reservoir, pseudo-steady state flow. (after Bourdet *et al.*¹¹).

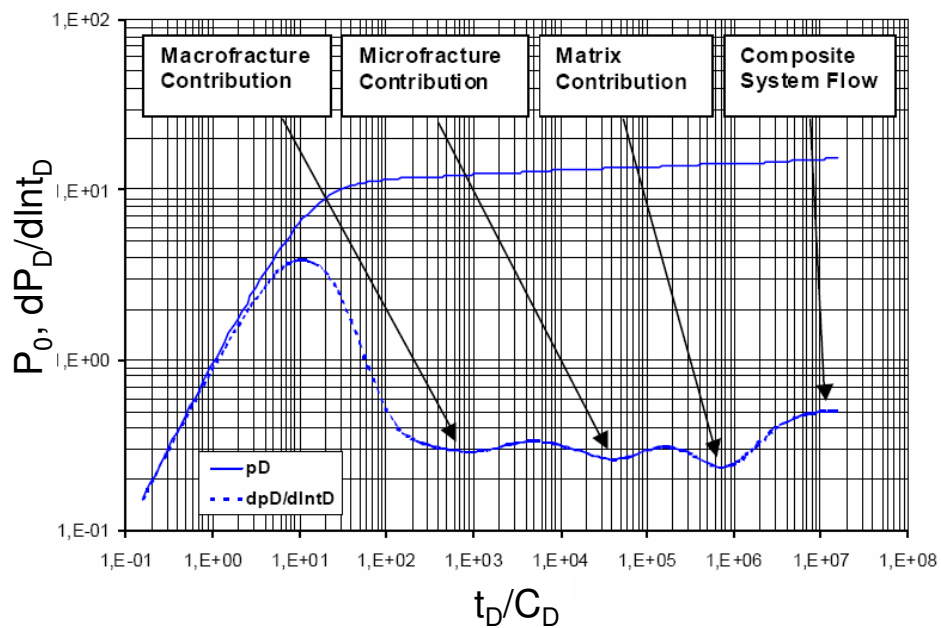


Figure 3.6-. Idealized pressure response in quadruple porosity reservoirs (from Dreier *et al.*¹⁴).

CHAPTER IV

NUMERICAL SIMULATION IN NFR

Simulation of NFR is a challenging task. Intensive research^{15,23} has been conducted in efforts to obtain the best way to represent the complexities involved. The most efficient approach is the idealization of two equivalent continuous media. Figure 4.1 shows a representation of a fractured-reservoir simulation model. The matrix and fracture system are represented as two separate grids, and the continuity equations for each system are connected by a transfer function that characterizes the flow from matrix to fractures.

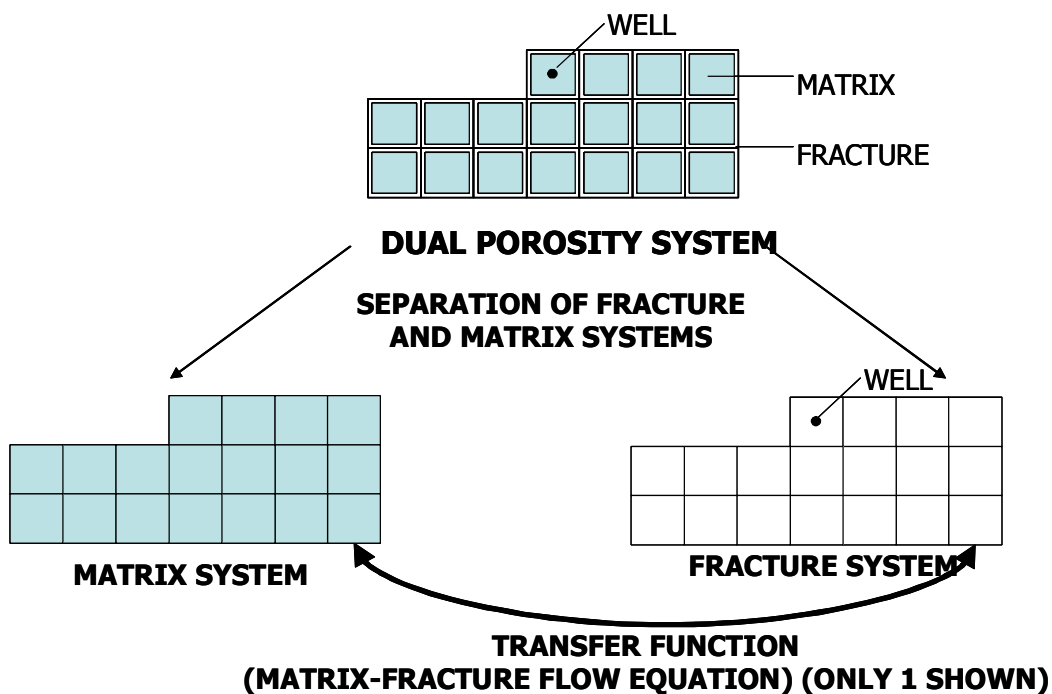


Figure 4.1- Schematic representation of fractured reservoir simulation model.

The transfer function's ability to represent the complex fluid-flow phenomena in NFR distinguishes four main types of simulation models. Figure 4.2 shows the basic concepts used in each model. In the dual-porosity model approach¹⁵, fluid flows from matrix blocks into fractures, but there is no flow between or into the matrix blocks. The subdomain model approach refines each matrix block in the vertical direction to account for the transient flow. The Multiple Interacting Continua (MINC)¹⁶ uses discretization of each matrix block in a nested configuration. The dual-permeability model allows flow between matrix elements; fluid flow occurs in both fracture and surrounding matrix blocks.

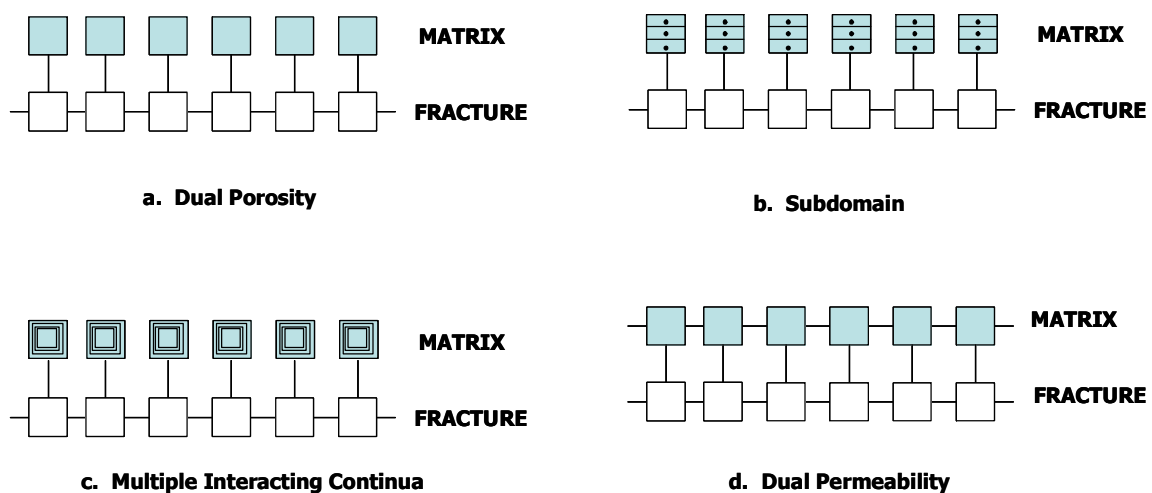


Figure 4.2- Different approaches to simulate NFR.

For modeling a more complex fractured porous medium, where two-continuum simplification is not valid, fractures are represented explicitly in the model. This methodology is called Discrete Fracture Network (DFN). Figure 4.3 shows an example of a reservoir simulation model using this approach.

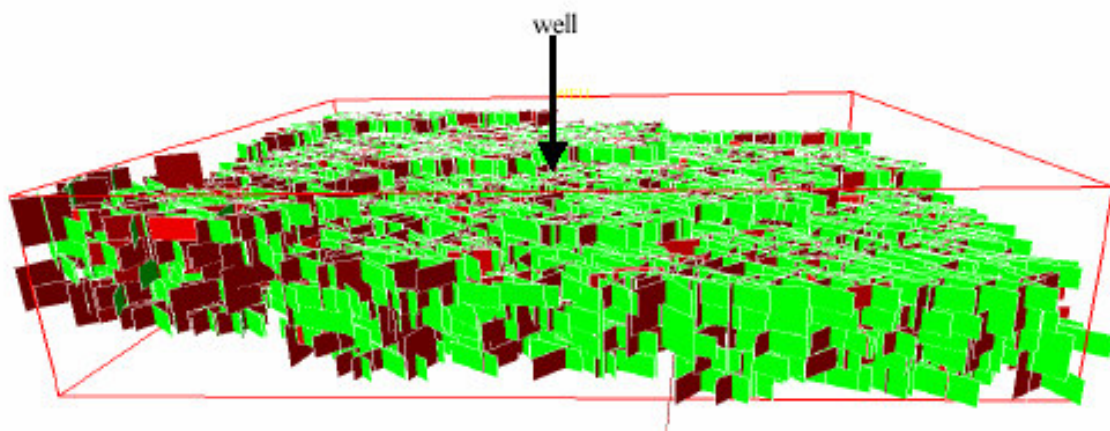


Figure 4.3- Discrete Fracture Network (from Bourbiaux *et al.*²⁰).

Several authors^{21,23} have shown some advantages of the DFN approach, as well as its limitations. Currently, DFN models are considered impractical for field-size simulations due to the limitations in adequate descriptions of flow networks and matrix-fracture interactions, as well as the excessive number of elements required for modeling flow in each individual fracture.

CHAPTER V

TECHNICAL FRAMEWORK

5.1 Shape Factor

NFR simulation requires an additional parameter, namely shape factor, besides those parameters needed in conventional reservoirs simulation. Shape factor is a function of fracture spacing. Several authors have proposed different expressions for shape factor including analytical derivations, numerical derivation and time-dependent functions.

Gilman²⁴ described the shape factor as a second-order, distance-related, geometric parameter used to estimate the mass transfer from matrix to fracture. The general form of shape factor is expressed as C/L^2 , where C is a constant that depends on the number of fracture sets occurring in a reservoir, and L is fracture spacing. Table 5.1 shows some of the most commonly used shape factor constants.

Table 5.1 Shape factor constants proposed by several authors.

Set of fractures	Warren and Root	Kazemi and Gilman	Coats <i>et al.</i>	Lim and Aziz
1	12	4	8	π^2
2	32	8	16	$2\pi^2$
3	60	12	24	$3\pi^2$

For practical applications, such as well testing and simulation, Gilman and Kazemi equation is the most widely used shape factor expression. The expression for a 3 set of fractures is given by

$$\sigma = 4 \left[\frac{1}{L_x^2} + \frac{1}{L_y^2} + \frac{1}{L_z^2} \right] \dots\dots\dots (5.1)$$

L_x , L_y and L_z refer to fracture spacings in x, y and z directions, respectively.

In cases where $L_x = L_y = L_z$, fracture spacing is frequently called L_{ma} and shape factor expression reduces to

$$\sigma = \frac{12}{L_{ma}^2} \dots\dots\dots (5.2)$$

From Equations 5.1 and 5.2, it is evident that shape factor is inversely proportional to fracture spacing. Figure 5.1 illustrates the shape factor as a function of fracture spacing, assuming $L_x = L_y = L_z$.

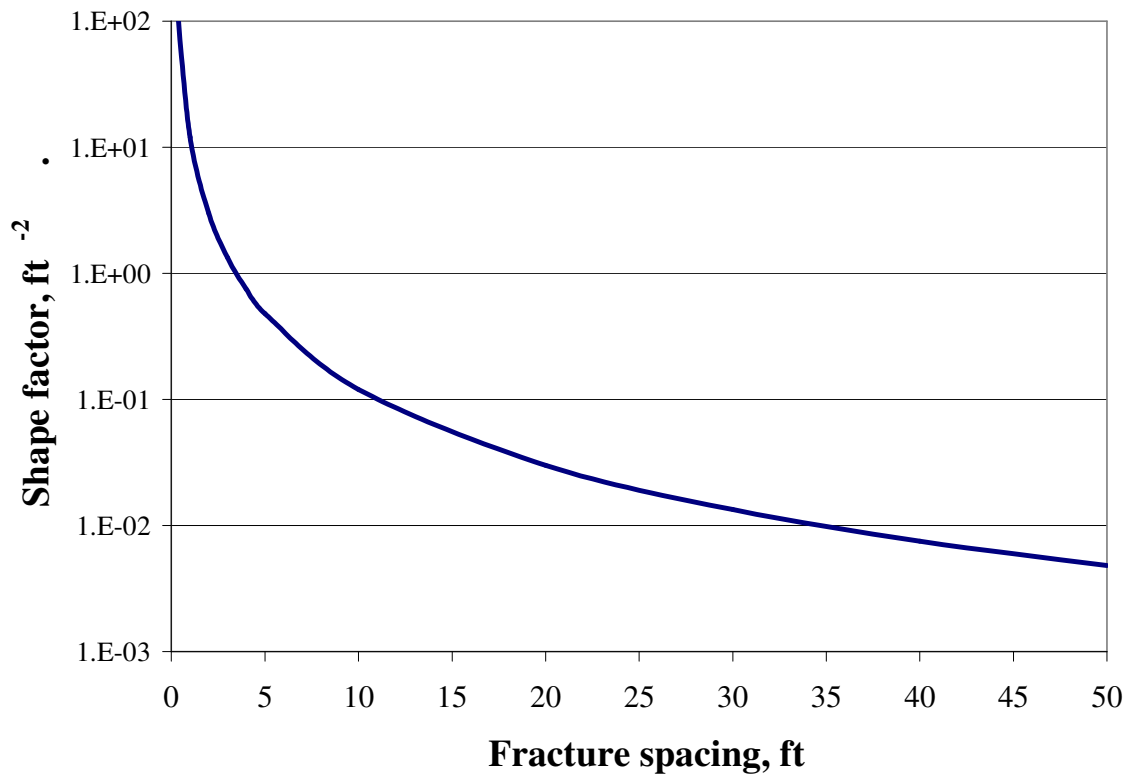


Figure 5.1- Shape factor as function of fracture spacing.

Figure 5.1 suggests the following two conclusions. First, as fracture spacing approaches zero the shape factor becomes infinite. This means the fractures are too close together that the system acts as a continuous media. Second, fracture spacing increases as shape factor decreases. For fracture spacing of 50ft, shape factor is in the order of 10^{-3} . Based on those observations and the comparison with the values reported in the literature, fracture spacing could be limited in the range of 1 to 50 ft for practical purposes.

In dual-porosity simulator, the NFR can be seen as two overlying porous media linked by a transfer function. This transfer function is directly proportional to shape factor. Therefore shape factor is one of the most important parameters in NFR simulation.

To illustrate the importance of shape factor, a 10 acres, dual-porosity, gas reservoir with a producing well in the center was simulated. The initial reservoir pressure is 3,600 psi and the producing well is constrained by a bottom hole pressure of 1,000 psi. Simulation was run up to 5 years or until the production rate reaches 1 MSCF/day. Fracture spacing was assumed equal in all three directions, x, y and z (L_{ma}). Sensitivity to different values of L_{ma} was performed with variable L_{ma} values of 1, 2, 5, 10, 20, 30 and 50 ft.

Figure 5.2 shows gas rate for variable L_{ma} values. Higher rates are obtained when the fracture spacing is smaller. Gas rate changes from 13,500 SCF/D to 7,500 SCF/D. Cumulative gas production is presented in Figure 5.3. All cases show the same amount of final recovery, but the time required to reach the same amount of recovery increases as the fracture spacing decreases.

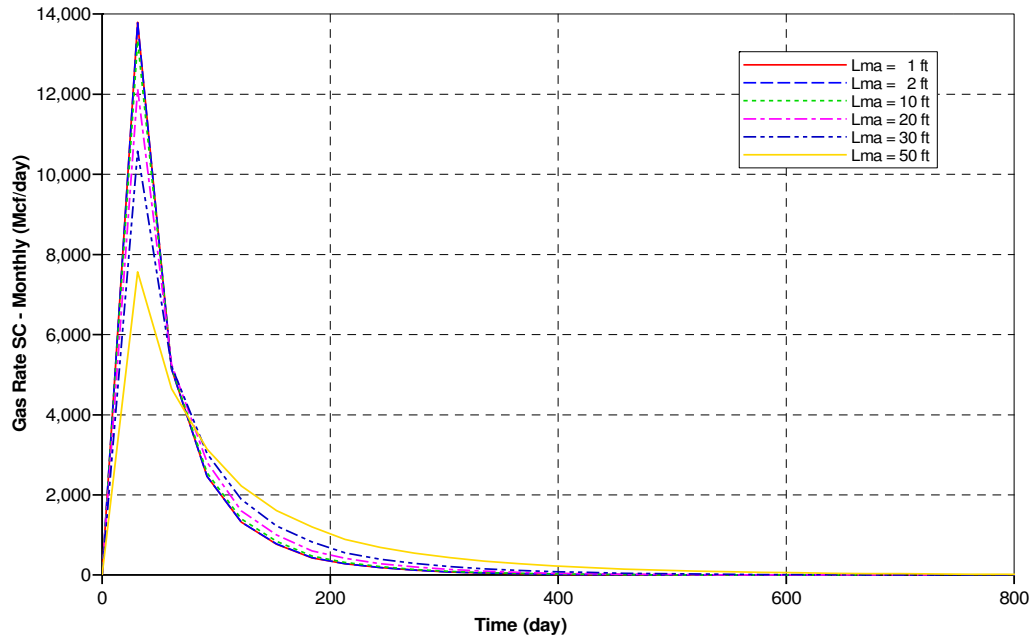


Figure 5.2- Gas rates obtained for different values of fracture spacing.

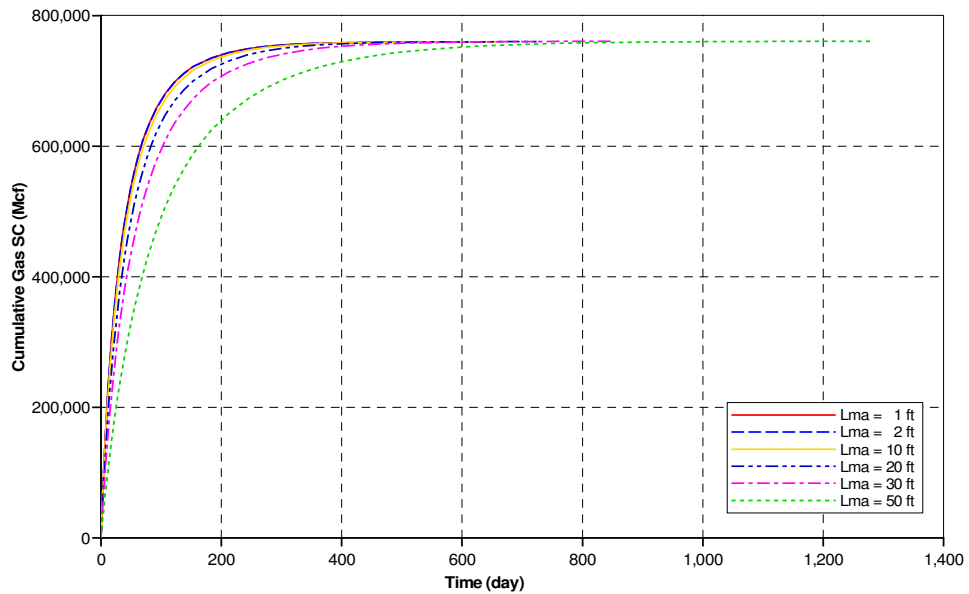


Figure 5.3- Cumulative gas production obtained for different values of fracture spacing.

5.2 Storativity Ratio

The storativity ratio, ω , is expressed as

$$\omega = \frac{\phi_f C_f}{\phi_f C_f + \phi_m C_m} \dots\dots\dots (5.3)$$

where ϕ is porosity and C is total compressibility. Subscripts f and m represent fracture and matrix, respectively.

The fracture compressibility is difficult to determine. For many reservoirs a value for this parameter is not available. Therefore, it is common to assume the fracture compressibility is equal to matrix compressibility. This assumption simplifies the equation to

$$\omega = \frac{\phi_f}{\phi_f + \phi_m} \dots\dots\dots (5.4)$$

Accordingly, the fracture porosity can easily be obtained from storativity ratio using the following equation:

$$\phi_f = \left(\frac{\omega}{1 - \omega} \right) \phi_m \dots\dots\dots (5.5)$$

Therefore, well test analysis could provide a useful indication of fracture porosity.

To define a practical range of values for storativity ratio, information reported by Nelson for 25 NFRs around the world was used. Figs. 5.4 and 5.5 show matrix porosity and fracture porosity distributions, respectively, based on that information. Both porosities shows log normal distributions. Matrix porosity ranges from 1% to 55%; the mean is 9% and the mode is 4%. Fracture porosity ranges from 0.005% to 5%; the mean is 1% and the mode is 0.4%.

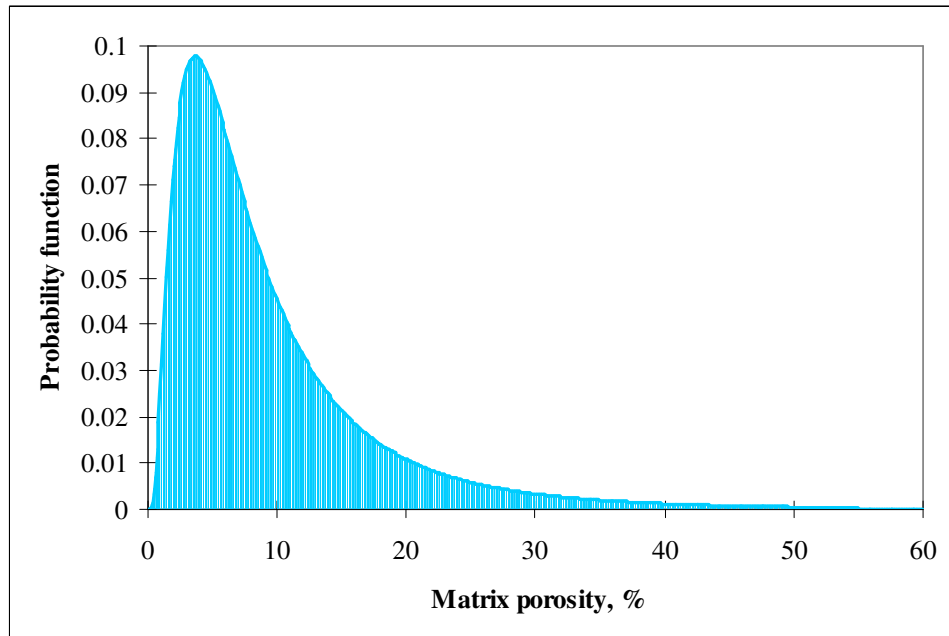


Figure 5.4 – Matrix porosity distribution in NFR.

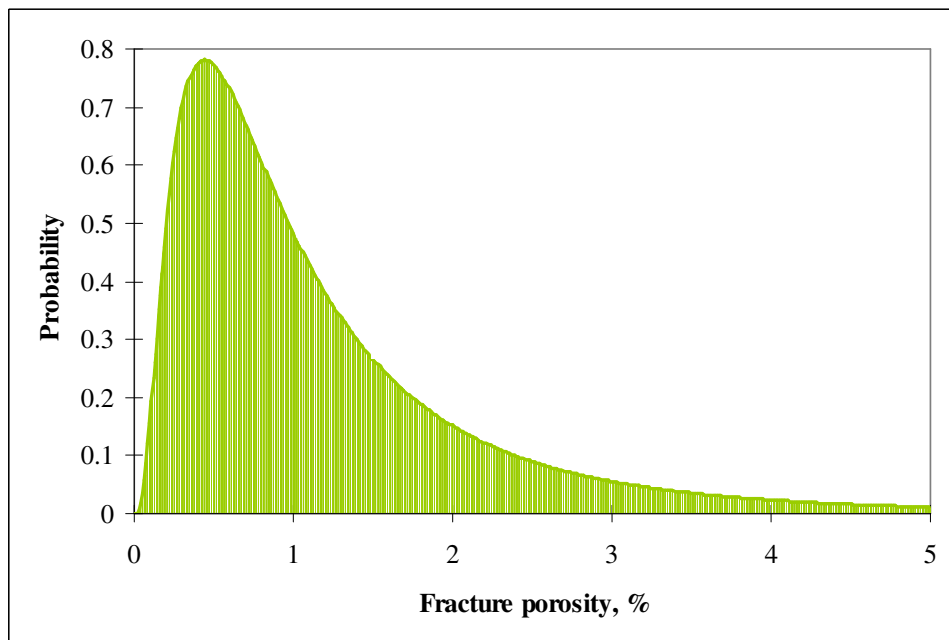


Figure 5.5- Fracture porosity distribution in NFR.

Assuming fracture compressibility is the same as matrix compressibility, the values of storativity ratio were calculated using Equation 5.4. The results are presented in Figure 5.6. The values of storativity ratio ranges from 0.003 to 0.75; the mean is 1.5 and the mode is 0.04.

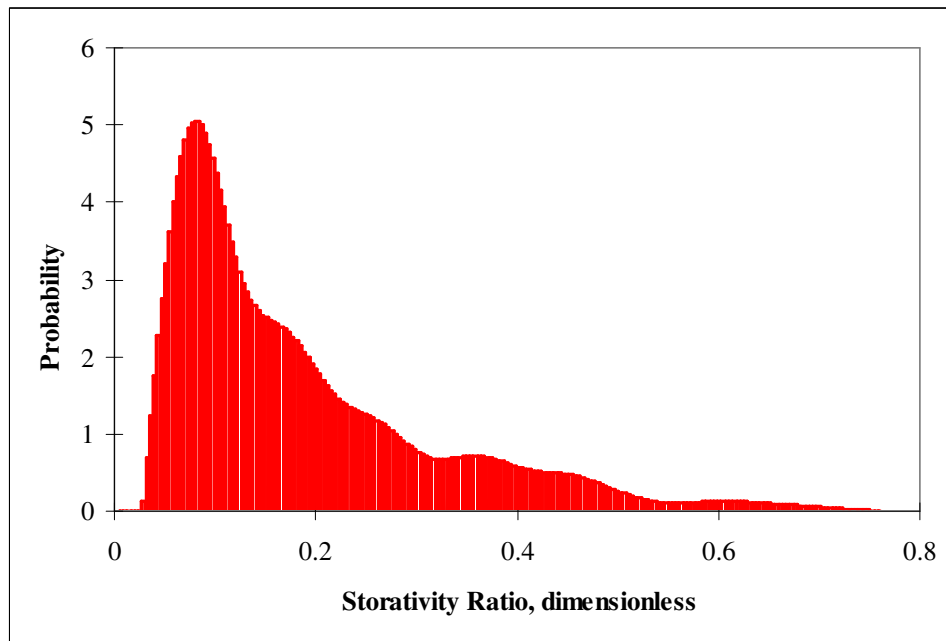


Figure 5.6 – Storativity ratio distribution from field data.

5.3 Interporosity Flow Coefficient

The interporosity flow coefficient, λ , for a system with matrix-to-fracture pseudo steady-flow is given as:

$$\lambda = \frac{\sigma k_m r_w^2}{k_f}, \dots \dots \dots (5.6)$$

Fracture permeability, k_f , is generally obtained from well test analysis. Wellbore radius, r_w , is normally a known parameter. Then, provided that the matrix permeability value, k_m , is available, shape factor can be estimated from λ using the following equation:

$$\sigma = \frac{\lambda k_f}{k_m r_w^2} \dots\dots\dots (5.7)$$

This value can be used directly in simulation models or expressed as fracture spacing.

Based on the above equation, shape factor can be expressed as a linear function of λ by rearranging equation 5.6 and taking logarithm of both left and right sides of the equation,

$$\text{Log } \sigma = \log\left(\frac{\lambda}{r_w^2}\right) + \log\left(\frac{k_f}{k_m}\right) \dots\dots\dots (5.8)$$

Then, a log-log plot of σ vs. $\frac{\lambda}{r_w^2}$ exhibits a series of parallel unit-slope straight lines as is

shown in Figure 5.7. Each line corresponds to a specific $\frac{k_f}{k_m}$ ratio.

In cases where fracture spacing can be assumed equal in all directions, a similar log-log plot can be obtained. Figure 5.8 presents fracture spacing as a function of $\frac{\lambda}{r_w^2}$ for cases

where $L_x = L_y = L_z = L_{ma}$.

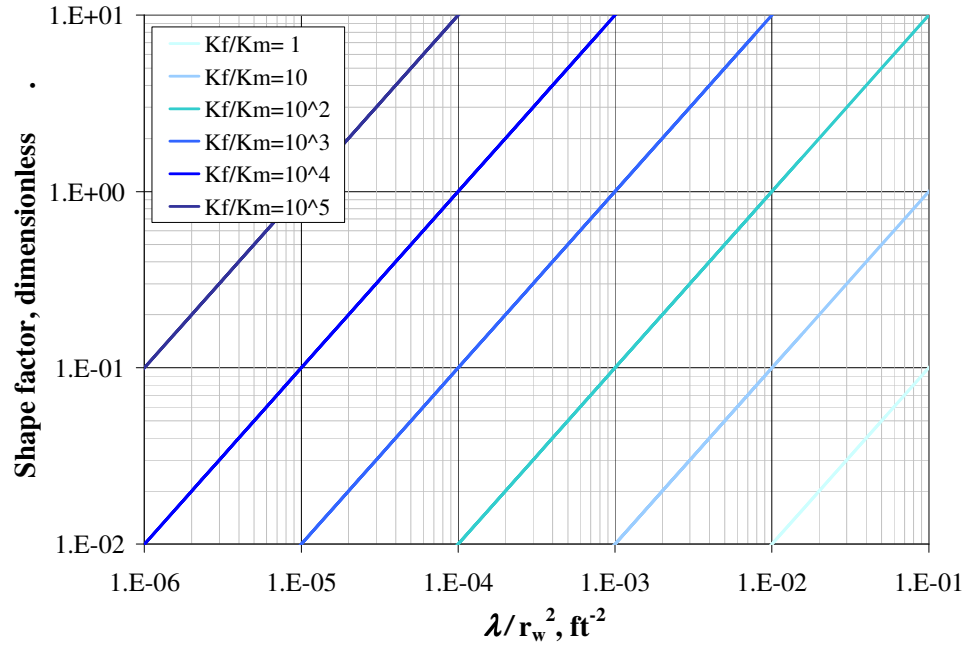


Figure 5.7- Shape factor vs. λ/r_w^2 .

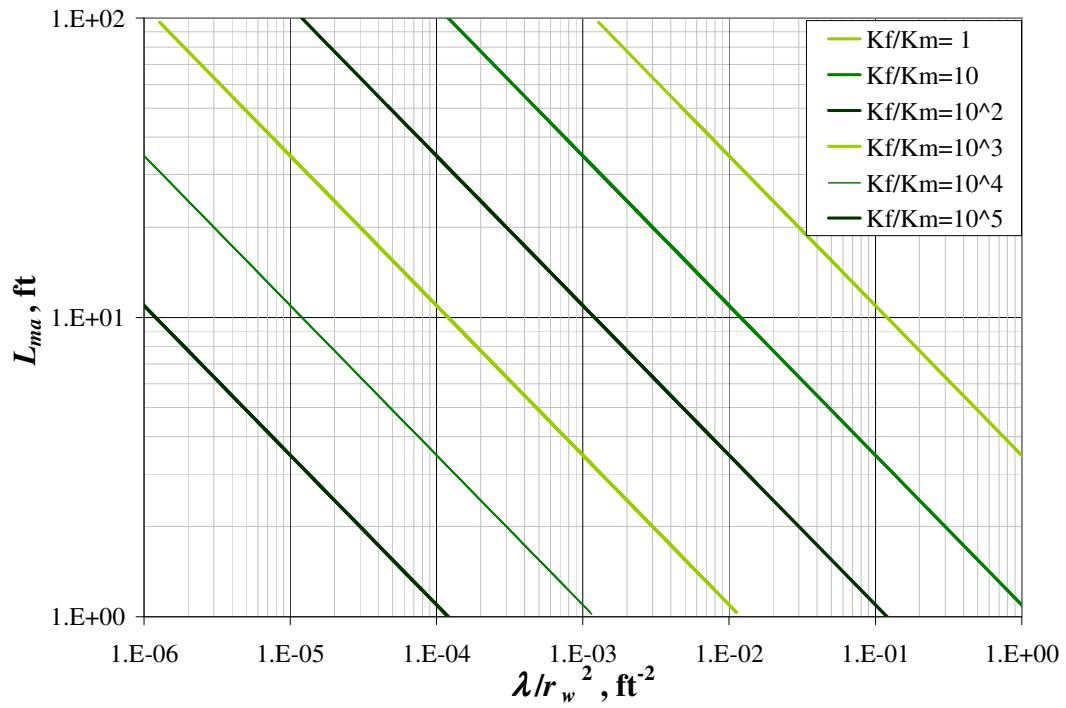


Figure 5.8- L_{ma} vs. λ/r_w^2 .

To establish a practical range of interporosity flow coefficient, information reported by Nelson was used. Figs. 5.9 and 5.10 show the distributions of reported matrix and fracture permeabilities, respectively. Permeability is commonly assumed to be log normally distributed, but the provided data shows exponential distributions for both matrix and fracture permeabilities.

Using the range of shape factor values defined previously, wellbore radius from 0.17 (4 3/4" hole size) to 0.502 (12 1/4" hole size) and permeability distributions presented above, a distribution of interporosity flow coefficient was obtained. The values range from 7×10^{-7} to 0.22. The mean is 2×10^{-3} and the mode is 1×10^{-5} . Despite its wide range, most values are clustered around 2×10^{-5} to 5×10^{-4} . This range matches with values reported in the literature. Figure 5.11 presents the results in the 90% range of confidence (1×10^{-5} to 1×10^{-2}).

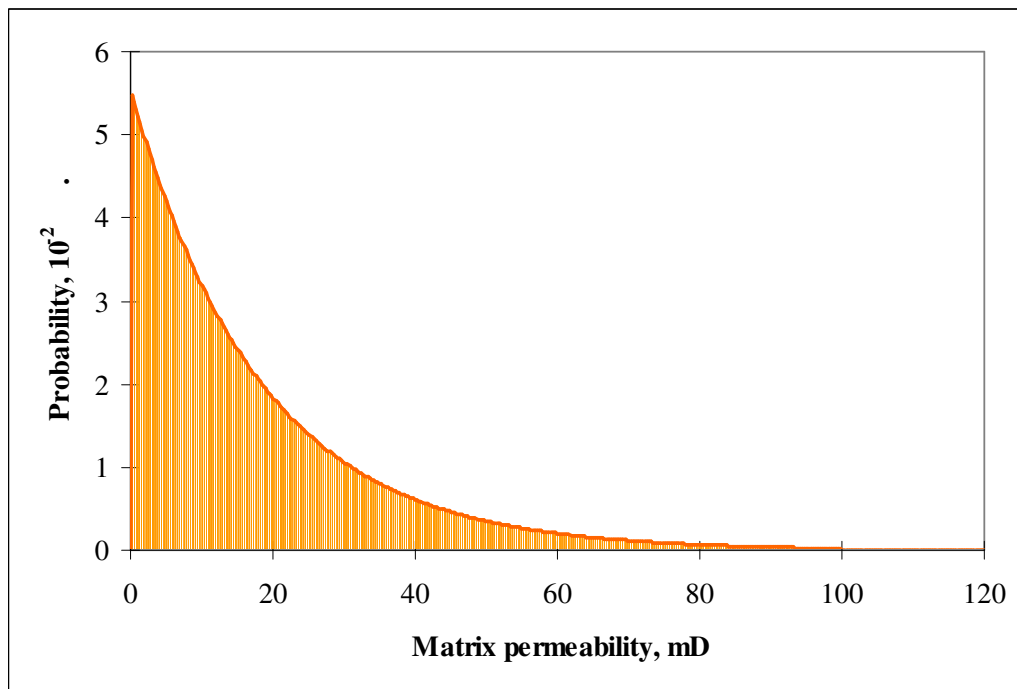


Figure 5.9 – Matrix permeability distribution in NFR.

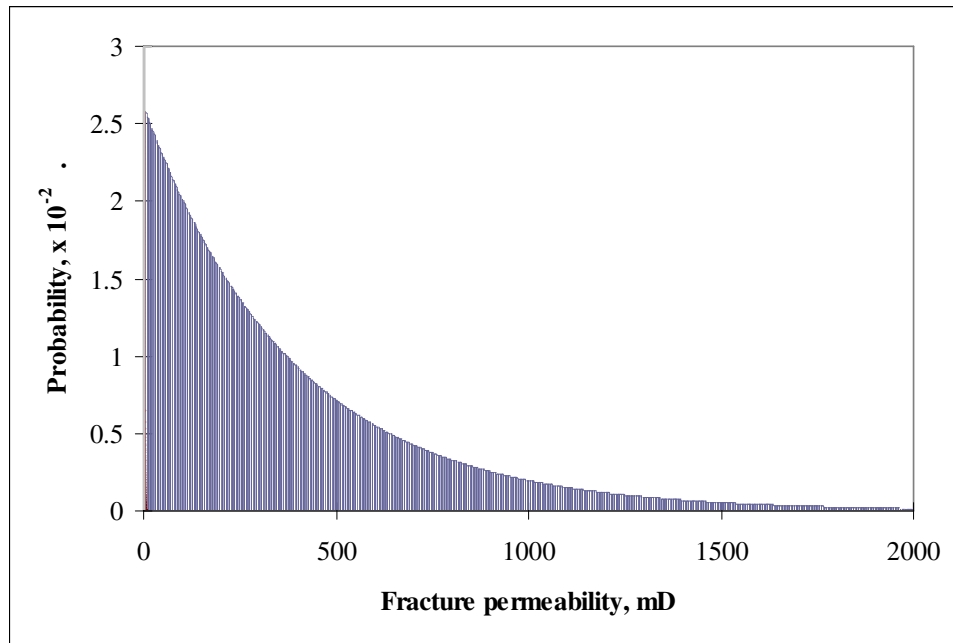


Figure 5.10 – Fracture permeability distribution in NFR.

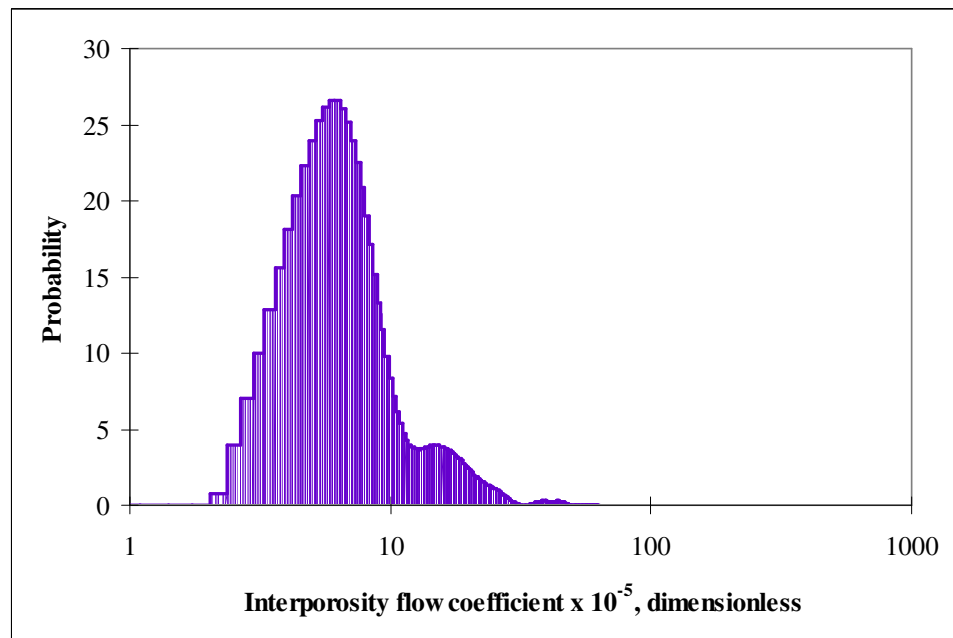


Figure 5.11 – Interporosity flow coefficient distribution from field data.

CHAPTER VI

SIMULATION CASES AND WELL TEST RESULTS

All simulation models were built and run in IMEX™, a three-dimensional, three-phase black-oil simulator software from CMG. To perform well test analysis, WELLTEST™ from Schlumberger was used. WELLTEST™ is a pressure transient test design and analysis tool that allows manual type curve matching, traditional straight line analysis methods and automatic type curve matching.

This study used dual porosity approach and considered the following models: 1) Radial, homogeneous, and isotropic; 2) cartesian, homogeneous, and isotropic; 3) cartesian, homogeneous, and anisotropic; 4) cartesian, heterogeneous, and isotropic; and 5) cartesian, heterogeneous, and anisotropic.

Radial, homogeneous, dual-porosity simulation models were built considering gas-water and oil-water fluid systems, with a wide range of values for the following parameters: matrix permeability, fracture permeability, wellbore radius, and fracture spacing. A producer well was centrally located in the model. The well was produced at a constant rate for 15 days for gas system and 30 days for oil system and shut-in for the same period of time. Pressure data was extracted from the simulation run and the buildup period was analyzed using WELLTEST™. The values of permeability, storativity ratio and interporosity flow coefficient obtained from well test analysis were used to estimate fracture spacing and fracture porosity. The results were then compared to the simulation input data.

Cartesian, homogeneous, dual-porosity simulation models were built with the same properties as the radial models. Sensitivity analysis to local refinement in cartesian grid was conducted to obtain a better approximation of pressure response to the radial model.

Once a better match was obtained, pressure data was collected and analysis was performed in the same manner as previously described.

Cartesian, homogeneous, anisotropic dual-porosity simulation models were used to investigate the effect of permeability anisotropy on pressure response. Both matrix and fracture permeability anisotropies were considered.

Cartesian, heterogeneous, isotropic dual-porosity simulation models were run to identify the effects of heterogeneity on pressure response. Fracture permeability and fracture spacing were randomly generated using statistical distributions. Pressure transient data was collected from 25 different locations in the model. Parameters estimated from well test analysis were compared to simulation input data.

Finally, to represent the actual conditions of a field case simulation, a cartesian, heterogeneous, anisotropic dual-porosity simulation model was built. The following properties were obtained from statistical distributions: 1) matrix permeability; 2) fracture permeability in the x direction; 3) fracture spacing in the x direction; and 4) fracture spacing in the y direction. A permeability anisotropy ratio of 6:1 was used to estimate fracture permeability in y direction. Then pressure transient data was collected from 25 different locations in the model and parameters estimated from well test analysis were compared to simulation input data.

6.1 Radial Model – Gas System

The first approach was to determine relationships between parameters estimated from well test analysis and input data in numerical simulation using dual-porosity radial models taking into account that well test theory is based mostly on radial flow. The radial model is $30 \times 1 \times 1$, with 10,000 ft as external radius to assure an infinite acting. Three set of fractures were considered to model fractured type rock. All properties were

homogeneous and isotropic, including fracture spacing in x , y and z directions. Table 6.1 summarizes other characteristics of the reservoir.

Fluid properties were generated using correlations based on specific gas gravity of 0.75. Matrix relative permeabilities were generated from correlations as well. Fracture permeabilities curves were set as straight lines and capillary pressures were ignored for both the matrix and the fracture.

A producer well was located in the center of the reservoir. The well was set to produce at a constant rate of 10 MMSCF/days for 15 days and then, was shut-in for another 15 days. The minimum time step was set at 1×10^{-5} days and the maximum was 0.1 days to obtain detailed bottom-hole pressure for well test analysis.

Simulation was run for different values of matrix permeability, fracture permeability, wellbore radius and fracture spacing. Figure 6.1 shows the values used for each of those properties.

Table 6.1- Main reservoir characteristics for radial model, gas reservoir.

Reservoir Parameter	Values
External radius	1,000 ft
Reservoir thickness	100 ft
Initial pressure	3626 psi
Reservoir temperature	120 °F
Matrix porosity	20%
Matrix compressibility	6.8×10^{-7} psi ⁻¹
Fracture porosity	1%
Fracture compressibility	6.8×10^{-7} psi ⁻¹
Connate water saturation	20%

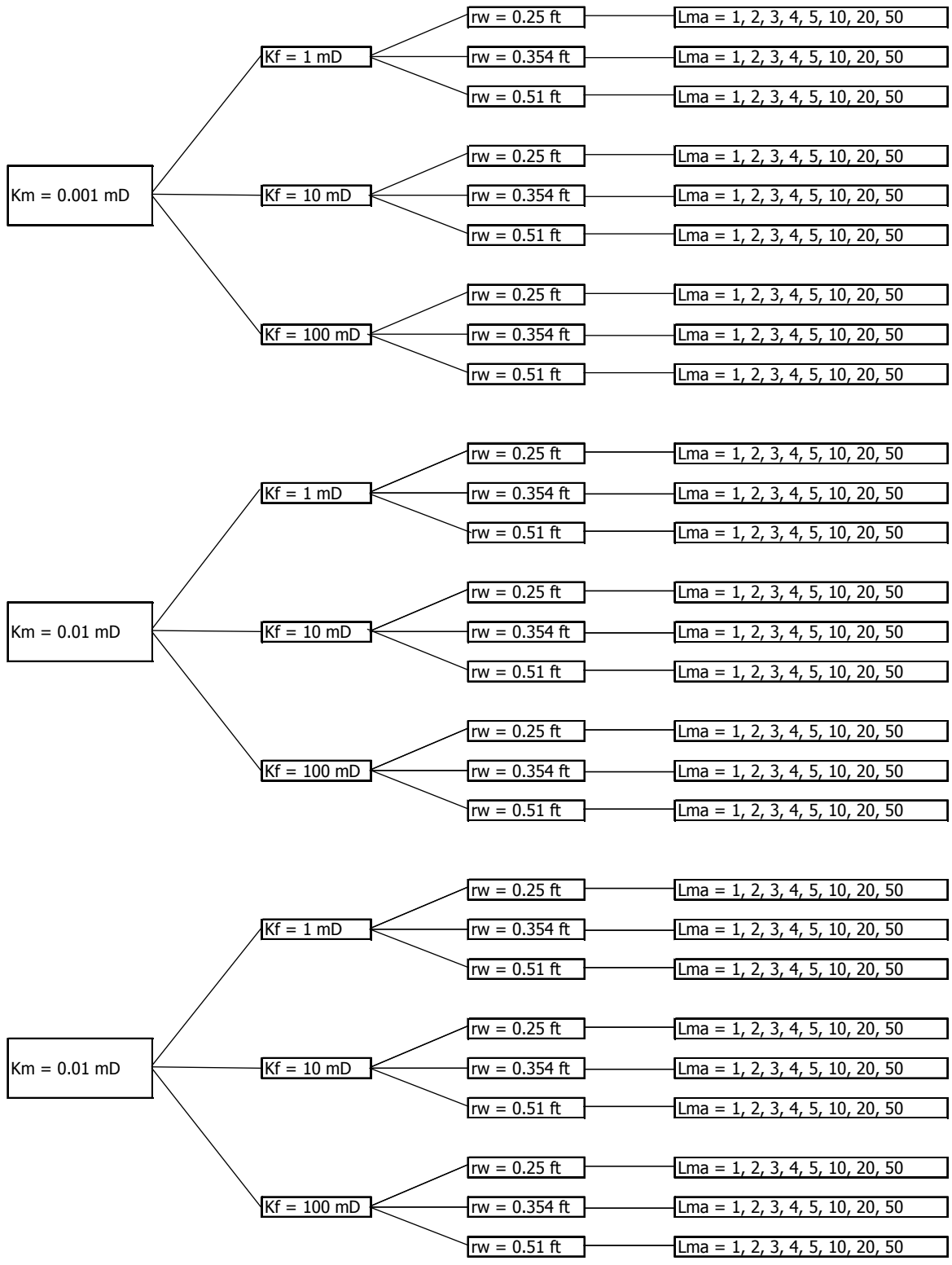


Figure 6.1- Schematic representation of the 216 simulation cases run for gas cases.

A total of 216 simulation cases were run, covering ranges of $\frac{k_f}{k_m}$ ratios from 10^2 to 10^6 .

Well radii corresponded to the most common well configurations in producing zones: 6", 8 1/2" and 12 1/4" hole size. Fracture spacing values covered the practical range defined in Chapter V.

Bottom-hole pressure data was extracted from each simulation case result file. The data corresponding to build-up period was imported into WELLTEST™. Reservoir and fluid properties in WELLTEST™ were set at the same values as in the simulation model. Semilog and type curve analysis were performed. Figure 6.2 shows an example of the semilog analysis that was performed. Figure 6.3 presents an example of the type curve analysis.

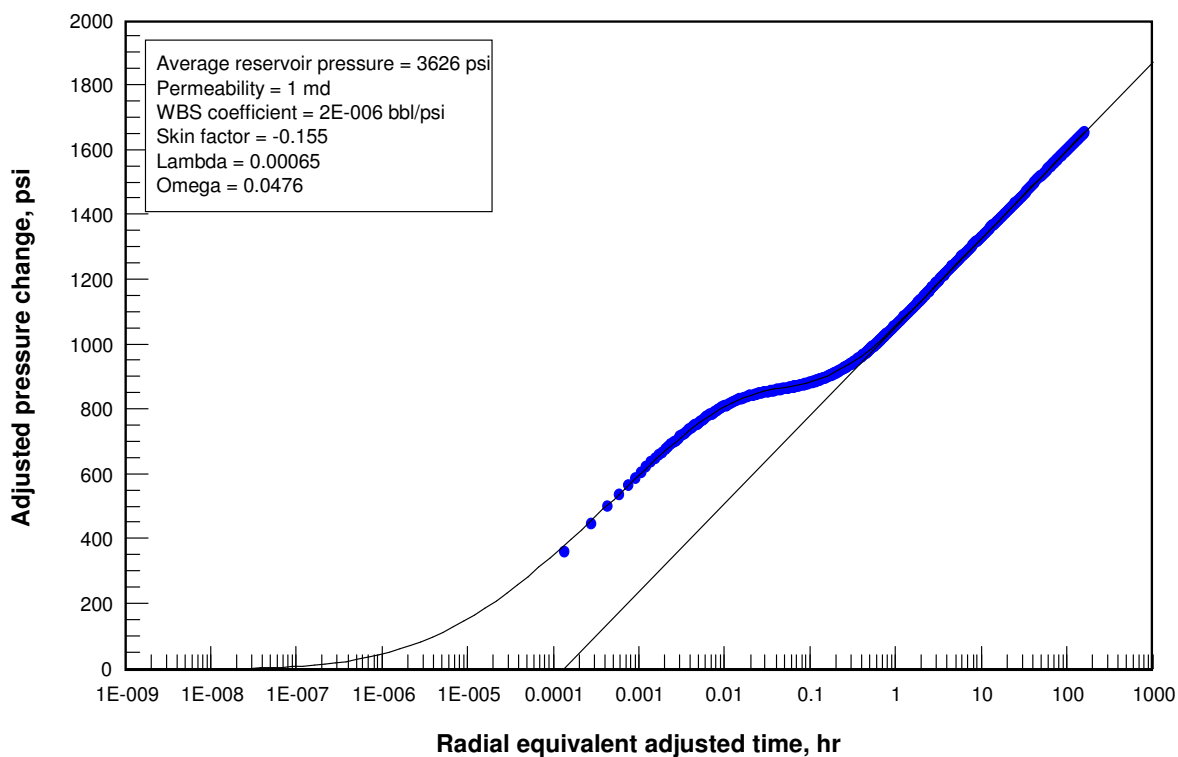


Figure 6.2- Example of semilog analysis.

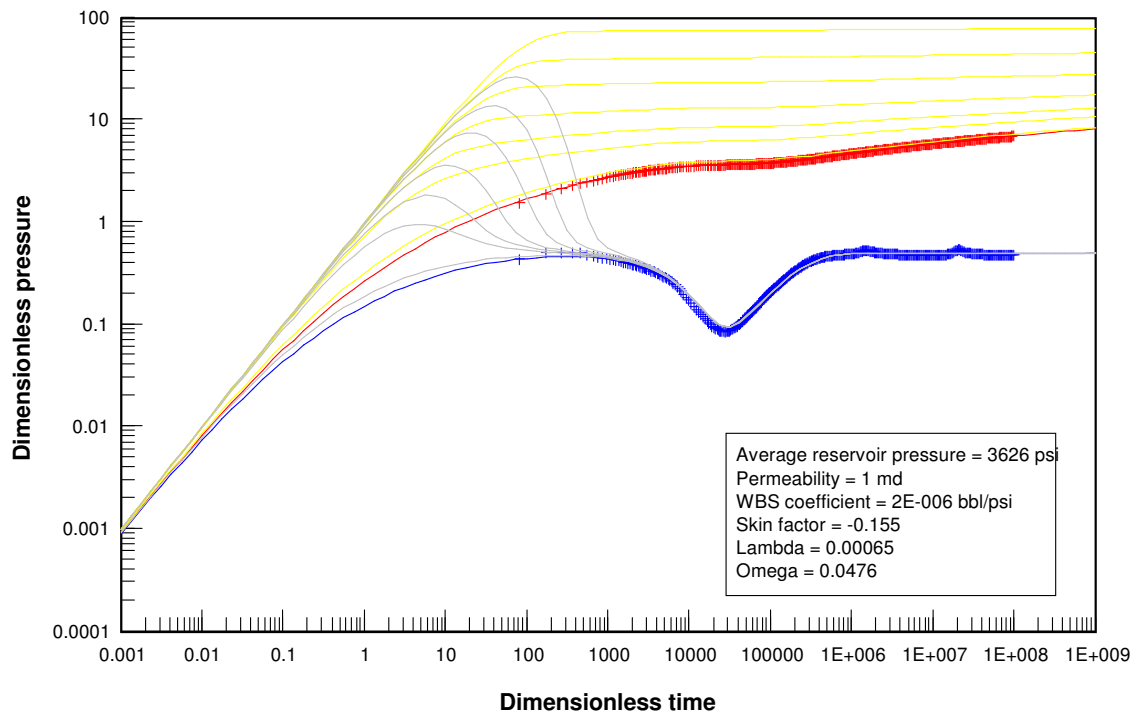


Figure 6.3- Example of type curve analysis.

From the 216 cases, 179 cases showed all the flow regions expected in a dual-porosity well test: fracture radial flow, transition flow and system radial flow. The duration of the fracture and system radial flow periods is a function of fracture spacing. As fracture spacing increases, fracture radial flow period increases and system radial flow period decreases.

The system radial flow was not reached in 28 cases; all of which were run with fracture spacing values from 20 to 50 ft. The absence of system radial flow was possibly the result of a short shut-in period. In an attempt to reach the system radial flow, the flowing and shut in times for those 28 cases were increased up to 45 days. However, the system radial flow was still not reached. Figure 6.4 shows an example of a well test where system radial flow is not reached.

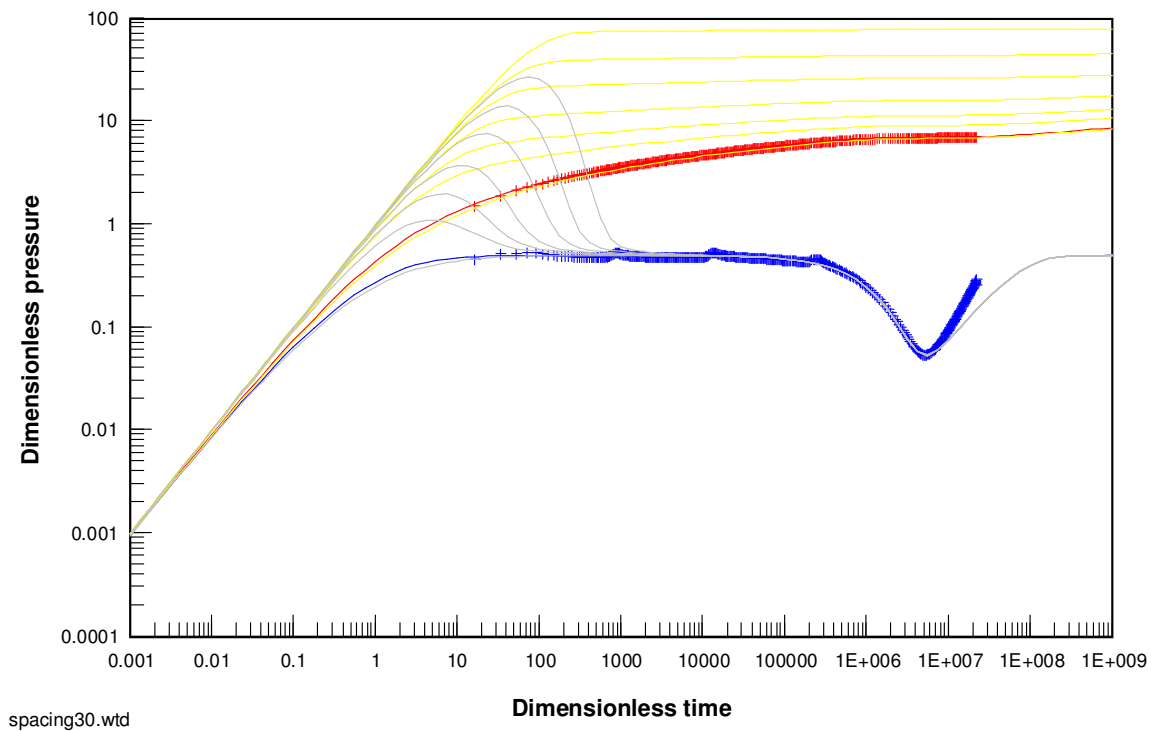


Figure 6.4- Well test response with no system radial flow.

In 9 cases with 1 ft fracture spacing the fracture radial flow was not present. In order to accurately estimate fracture spacing and porosity from well test analysis, only those cases showing a complete flow region were considered. Appendix A presents the summary of parameters estimated from well tests for the 179 cases.

Radial Model – Gas system results

Based on ω values obtained from well test analysis, fracture porosity was calculated using Equation 5.4. Estimated fracture porosity values varied in the range from 0.5% to 1.7% as presented in Figure 6.5.

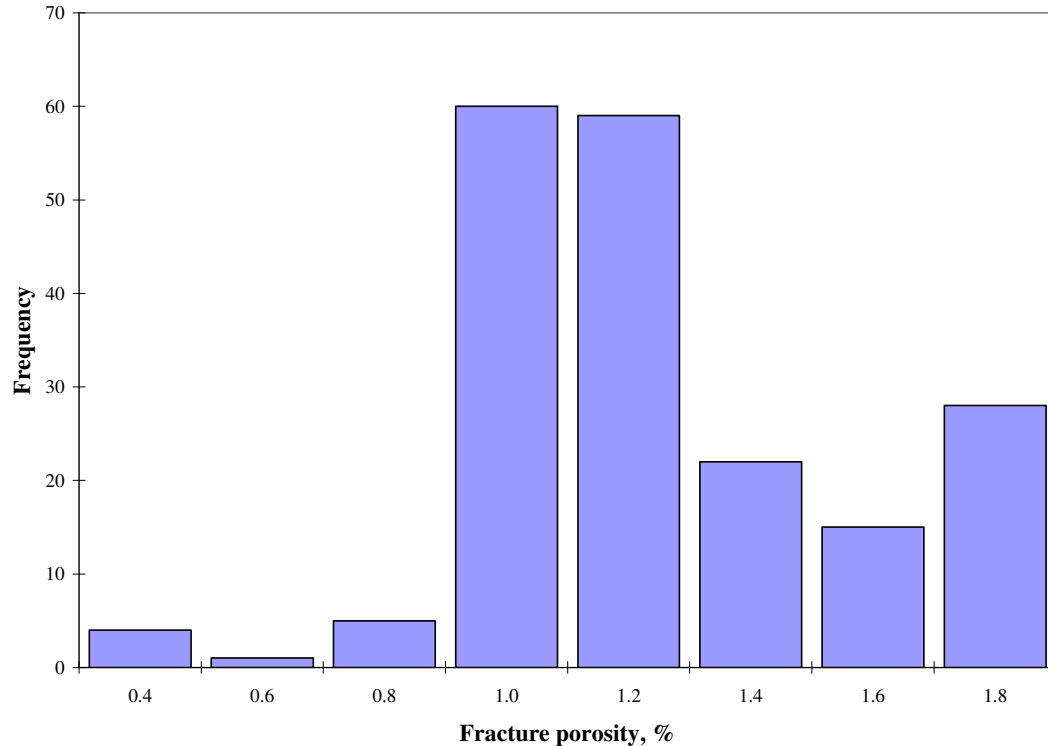


Figure 6.5- Fracture porosity estimated from storativity ratio for 179 simulation runs; radial model, gas system.

The mean value is 1.1%, and most values are from 1.0% to 1.2%, showing a good match with the input data (1%). However, a considerable amount of data lies in the edge of the histogram, from 1.6% to 1.8%. It is worth noting that ω increases as fracture permeability increases. Higher values of ω were obtained from cases with a fracture permeability of 100 mD. Based on these observations, fracture porosities estimated from ω are not very accurate, especially for high fracture permeabilities.

To compare the simulation input values with the well test results, shape factor was estimated using Equation 5.1. IMEX™ does not use shape factor as input data but calculate the value using the Gilman and Kazemi or Warren and Root formulation,

depending on user settings. For this study, the Gilman and Kazemi formulation was selected.

Shape factor was estimated using Equation (5.7) whereas λ and permeability values were obtained from well test analysis of 179 cases. Note that matrix permeability can not be estimated from single-well pressure analysis. Calculation of shape factor requires the matrix permeability input data and therefore it is necessary to have a matrix permeability value from other sources such as core data or multi-well pressure tests.

Shape factor estimated from well test were compared with simulation input values in a log-log plot of σ vs. $\frac{\lambda}{r_w^2}$. In all cases, perfect matches were obtained, as can be observed in Figure 6.6.

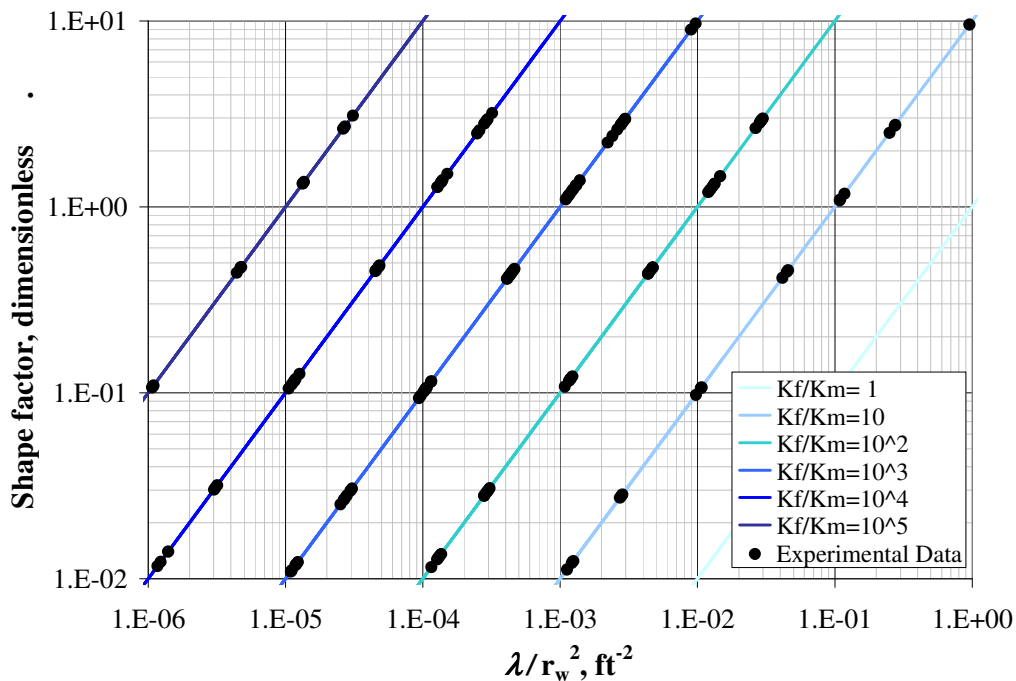


Figure 6.6- Shape factor estimated from λ ; radial model, gas system.

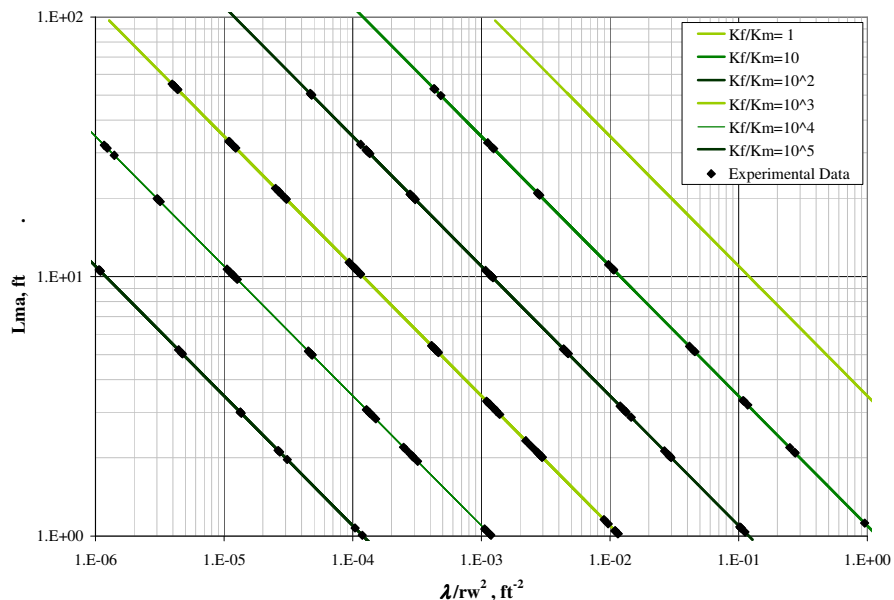


Figure 6.7- Fracture spacing estimated from λ ; radial model, gas system.

The fracture spacing (L_{ma}) estimated from shape factor using Equation 5.2 is shown in Figure 6.7.

6.2 Radial Model – Oil System

The radial model with oil as the fluid system was built to determine the existence of any effect of reservoir fluids on the match obtained between simulation input data and estimated well test parameters. The radial model is essentially similar to the one used in the radial-gas system case, but with a different fluid system. This particular system contains 35° API, black oil, with 500 SCF/B GOR. Other properties were determined from correlations. Oil compressibility was set constant for pressures above saturation pressure.

Production rate was set at 1,000 STB/Day. Flowing and shut-in periods were set for 30 days. Under that production scenario, all of the cases showed flowing bottom-hole

pressures above saturation pressure. Minimum and maximum time step remained the same as in the gas case.

Since oil viscosity is considerably higher than gas viscosity, the values of matrix and fracture permeabilities were increased to allow the fluid to flow. Figure 6.8 presents matrix permeability, fracture permeability, wellbore radius and fracture spacing values that were used to generate 288 simulation cases.

Bottom-hole pressure was extracted from the result file for all simulation cases and loaded into WELLTEST™. Although all tests showed a typical dual-porosity shape in type curve analysis, only 164 cases presented the complete dual-porosity behavior with the complete flow regimes. In 115 cases, fracture radial flow was not developed. The remaining 9 cases did not show the system radial flow because the external boundary at 10,000 ft was reached during the transition flow as shown in Figure 6.9.

For all cases with fracture spacing of 1 ft, fracture radial flow did not exist. As matrix and fracture permeabilities increased, fracture spacing values had shown an increase for those cases that did not exhibit fracture radial flow. For cases with matrix permeability of 5 mD and fracture permeability of 5,000 mD fracture radial flow could be observed only for cases with 20, 30 and 50 ft fracture spacing values. These observations stress the difficulty to observe fracture radial flow in actual well tests because this phenomenon occurs at very early times and has a short duration. See Appendix B for well test results and examples of interpreted tests.

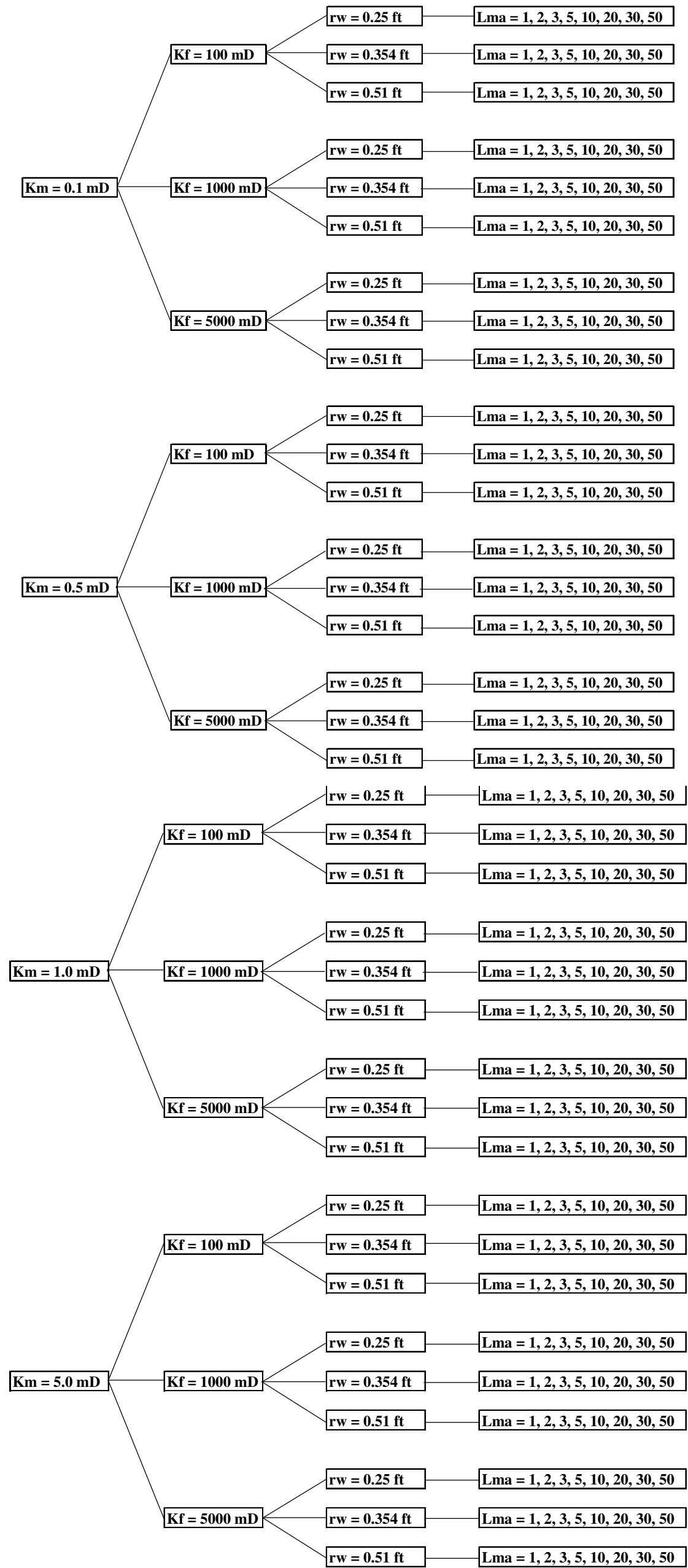


Figure 6.8- Simulation cases run for radial model-oil system case.

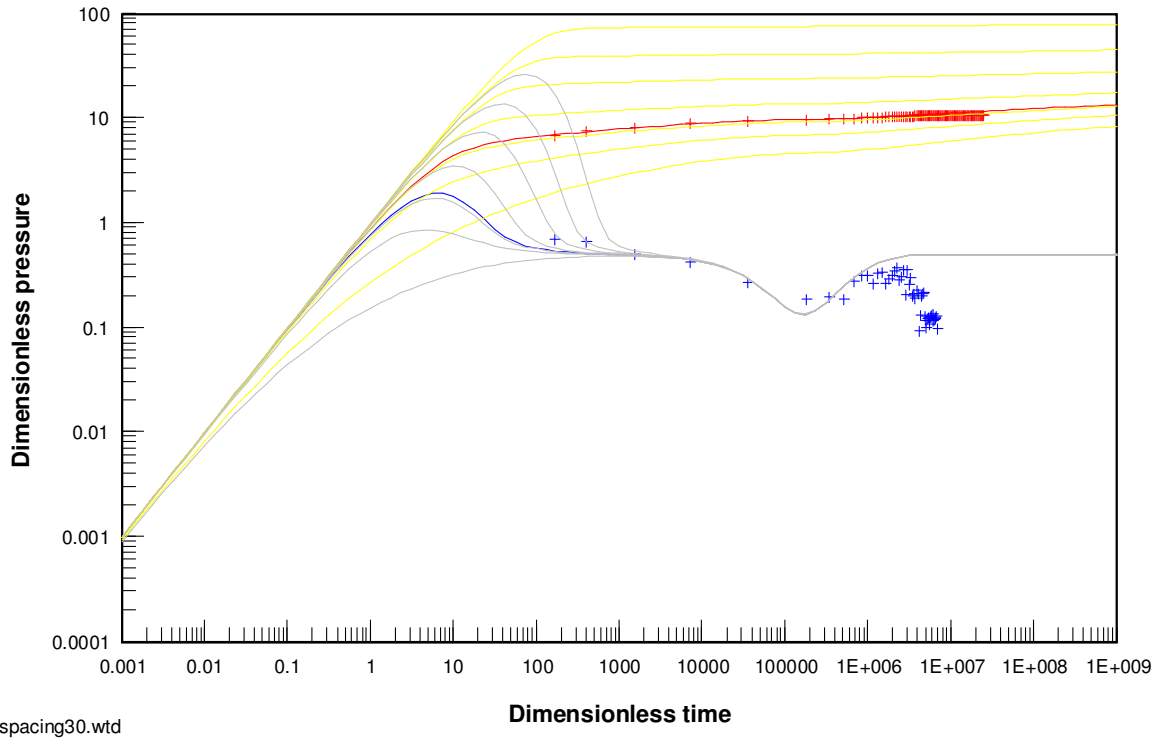


Figure 6.9- Well test response with no system radial flow. External boundary reached during transition flow.

Radial Model – Oil system results.

Fracture porosity for the 164 cases with complete dual-porosity behavior were calculated using ω estimated from well test analysis. Figure 6.10 shows the histogram of the fracture porosity values obtained. The mean value is 1.2%, and the mode and median are 1.1%. Most of the values (129 data points) are in the range of 0.9% to 1.3%, matching closely with the simulation input data of 1%. Nevertheless, there are 35 data points higher than 1.6%. As in the gas case, the accuracy of fracture porosity estimated from ω is lower for higher fracture permeabilities.

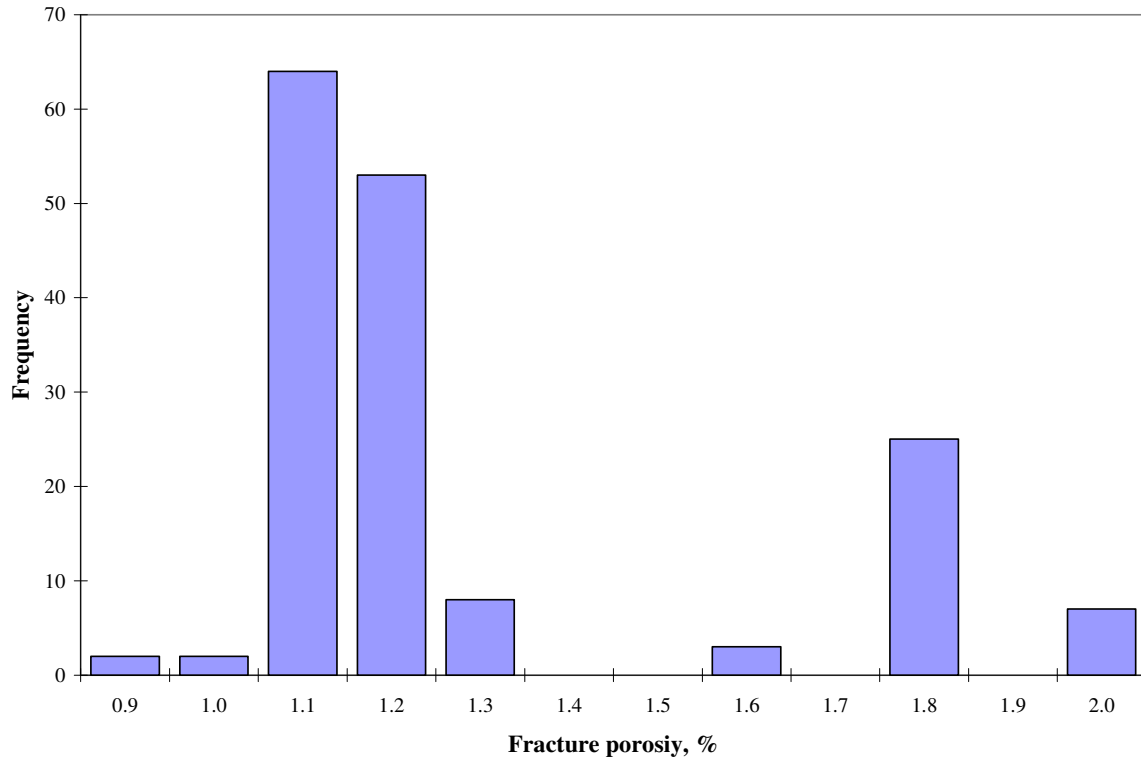


Figure 6.10- Fracture porosity estimated from storativity ratio for 164 simulation runs; radial model, oil system

Shape factor and fracture spacing were estimated from well test analysis results using λ and simulation input matrix permeability. A very good match with simulation input data was obtained as is shown in Figures 6.11 and 6.12.

Despite important differences in fluid properties, particularly in viscosity (that is one of the most important fluid parameters both in simulation and well testing), oil and gas models results were very similar. For that reason, all the next cases were run only for the oil system. PVT properties for all cases are the same as those used in the radial model- oil case presented in section 6.2.

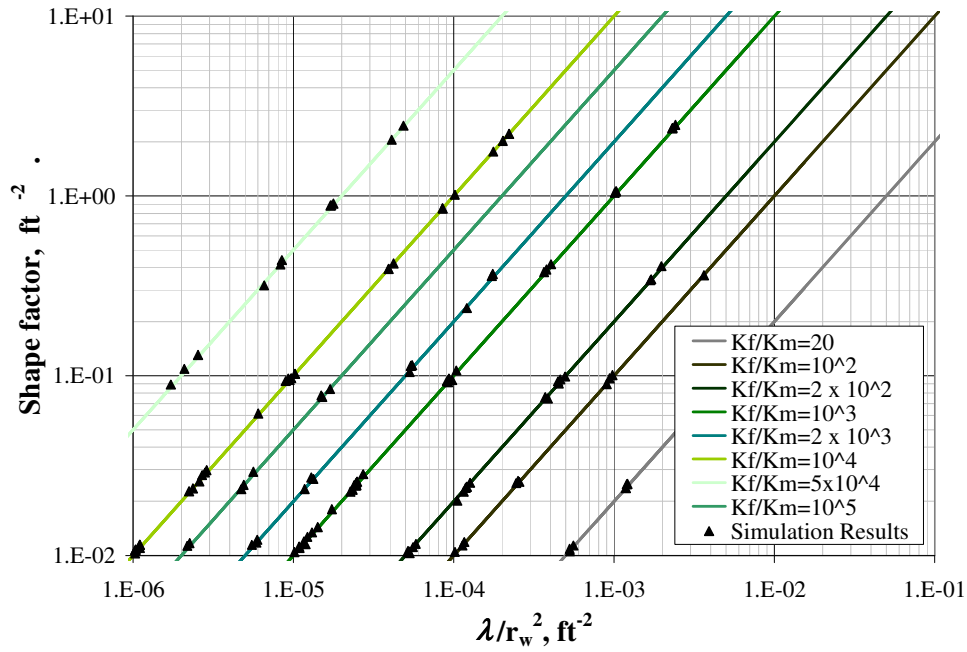


Figure 6.11- Shape factor estimated from storativity ratio from 164 simulation runs; radial model, oil system.

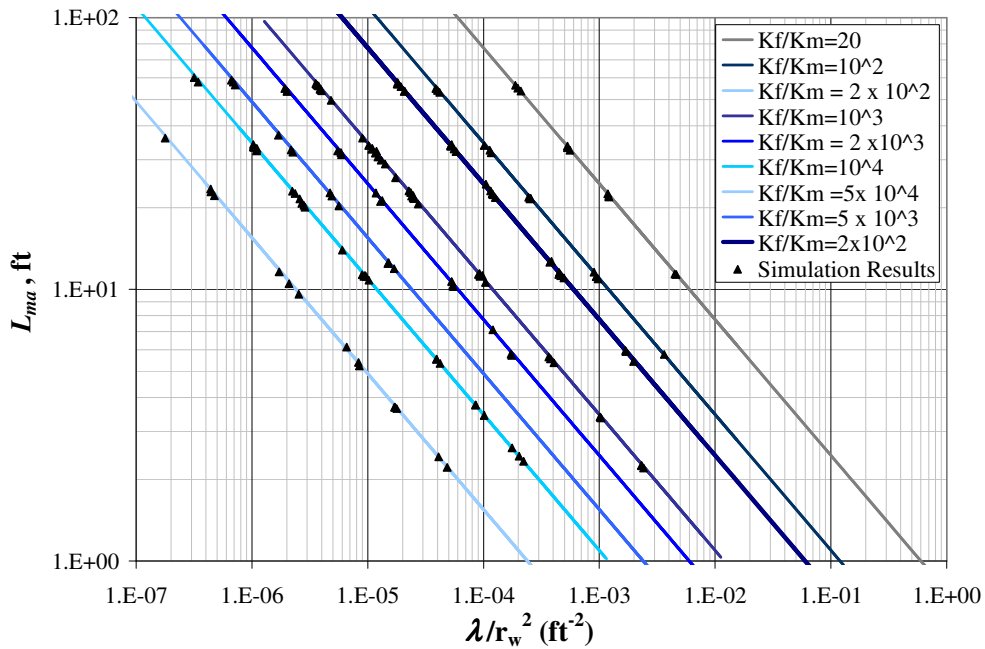


Figure 6.12- Fracture spacing estimated from storativity ratio from 164 simulation runs; radial model, oil system.

6.3 Cartesian Model

Actual field simulations do not use radial grids, but other geometries such as cartesian, corner point (orthogonal and non-orthogonal). To determine the applicability of λ and ω concepts in non-radial models, well test results from the radial model were compared with results from an equivalent cartesian model.

The cartesian model is dual porosity, homogeneous and isotropic. The grid dimension is 99 x 99 x 1 cells. Grid block dimensions were defined such that the reservoir area was similar to that defined in radial model. Rock and fluid properties are the same as those described for radial model-oil system. A producer well was centrally located in cell 50, 50. Distance from well to grid boundaries is 10,000 ft. Other reservoir characteristics are presented in Table 6.2.

Table 6.2- Main reservoir characteristics; cartesian model.

Reservoir Parameter	Values
Grid cell dimensions	202 ft x 202 ft
Reservoir thickness	100 ft
Initial pressure	3626 psi
Reservoir temperature	120 °F
Matrix porosity	20%
Matrix compressibility	6.8×10^{-7} psi ⁻¹
Fracture porosity	1%
Fracture compressibility	6.8×10^{-7} psi ⁻¹
Connate water saturation	20%

First, a simulation case using 0.1 mD matrix permeability, 10 mD fracture permeability and 1 ft fracture spacing was run. Bottom hole pressure response was compared with

the equivalent radial case. Results were different, as expected, because the differences in well block size (Figure 6.13).

In radial models, the block radius is similar in magnitude to the wellbore radius. In cartesian models, well radius is estimated using Peaceman approximation. For isotropic models wellbore radius is

$$r_w \cong 0.21\Delta x \dots\dots\dots (6.1)$$

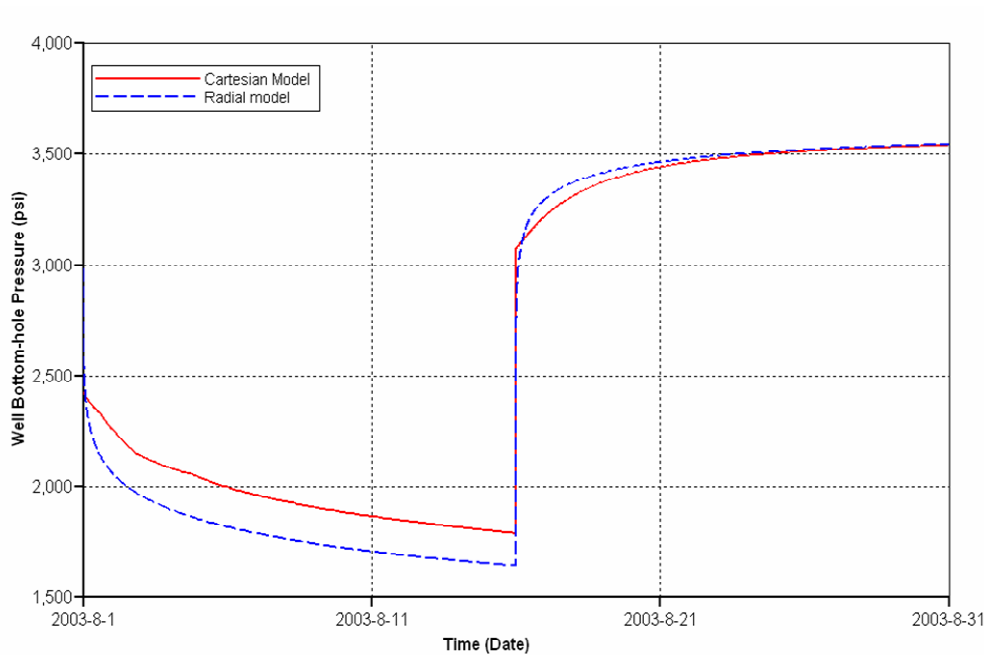


Figure 6.13- Comparison of bottom-hole pressure from radial and cartesian models.

Based on Equation 6.1, the wellbore radius estimated in the cartesian model is around 40.2 ft. Since pressure changes are more dramatic near the wellbore, using a higher wellbore radius for calculations results in lower pressure drops, as shown in Figure 6.14. For that reason, local refinement around the producer well was used to improve pressure response match between the two models.

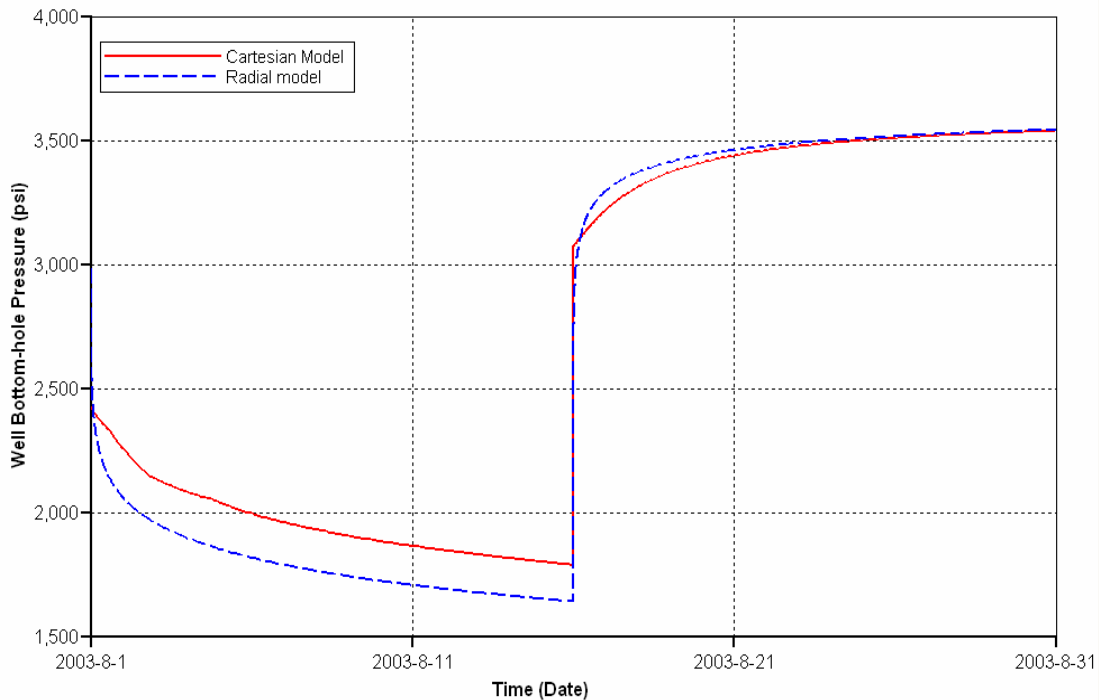


Figure 6.14- Bottom hole pressure in cartesian and radial models.

IMEX™ allows cartesian and hybrid refinements. Cartesian refinement divides a block into a user defined number of equal subdivisions. The hybrid grid refinement divides a block from a cartesian grid into a local cylindrical grid, either in radial alone or radial and angular directions.

Cartesian refinement was tested, dividing the well grid block into 3, 5, and 9 subdivisions in x and y direction. Pressure results are presented in Figure 6.15. The best match of cartesian and radial models was obtained using a 3x3 refinement, but the early build up period could not be matched very well.

Hybrid refinement was performed in the well grid cell and pressure results were compared with 3x3 cartesian refinement. As a result, pressure match between radial and cartesian model was slightly improved (Figure 6.16). Based on these results, hybrid refinement was selected to run cartesian model simulation cases.

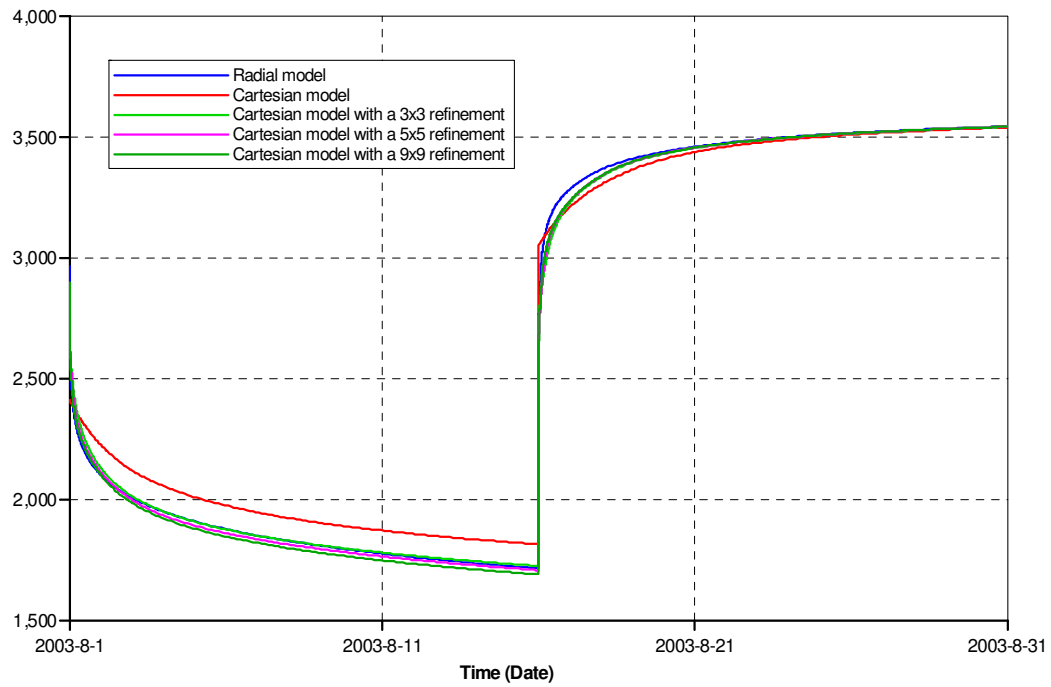


Figure 6.15- Comparison bottom hole pressure using cartesian local refinement.

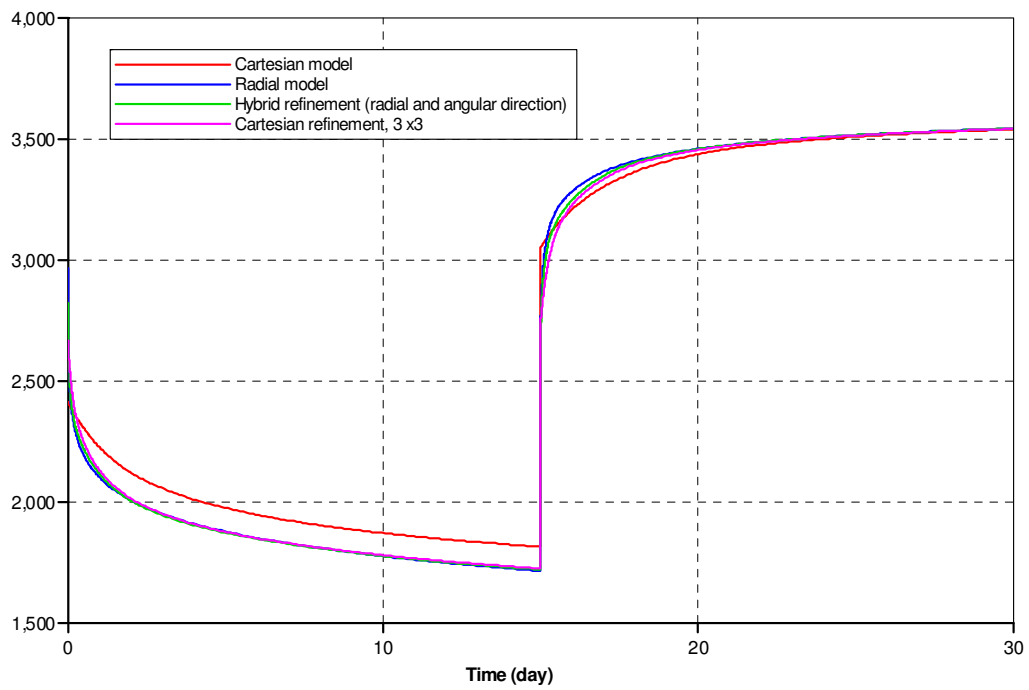


Figure 6.16- Bottom hole pressure comparison using cartesian and hybrid refinements.

Simulation was run using different values of matrix permeability, fracture permeability, and fracture spacing. Values are the same as those used in the radial model-oil case, shown in Figure 6.7. Only one value of wellbore radius was used, which was 0.25 ft.

A total of 96 simulation cases were run. Well test analysis of build up period was performed and the results were compared with those obtained from the radial case with the same properties. In all cases, parameters obtained from both models were similar. Only minor differences were found, mainly in early times. Figure 6.17 presents examples of radial and cartesian pressure response comparison in WELLTEST™. According to these results, parameters obtained from single well pressure tests can be incorporated into cartesian models with appropriate grid assignment.

6.4 Anisotropic Matrix Permeability Model

A cartesian, homogeneous, black oil model was built with the same characteristics presented in Table 6.1. Fracture spacing was defined as 10 ft in the three directions, and fracture permeability was set as 100 mD.

Matrix permeabilities in x and y directions (k_{mx} and k_{my}) were defined to maintain a constant effective permeability. Effective permeability is defined as

$$K_e = \sqrt{K_x K_y} \dots\dots\dots (6.2)$$

Effective matrix permeability was set at 0.1 mD and 10 simulation cases, including one isotropic case, were run. Fracture permeability combinations used in each case are shown in Table 6.3.

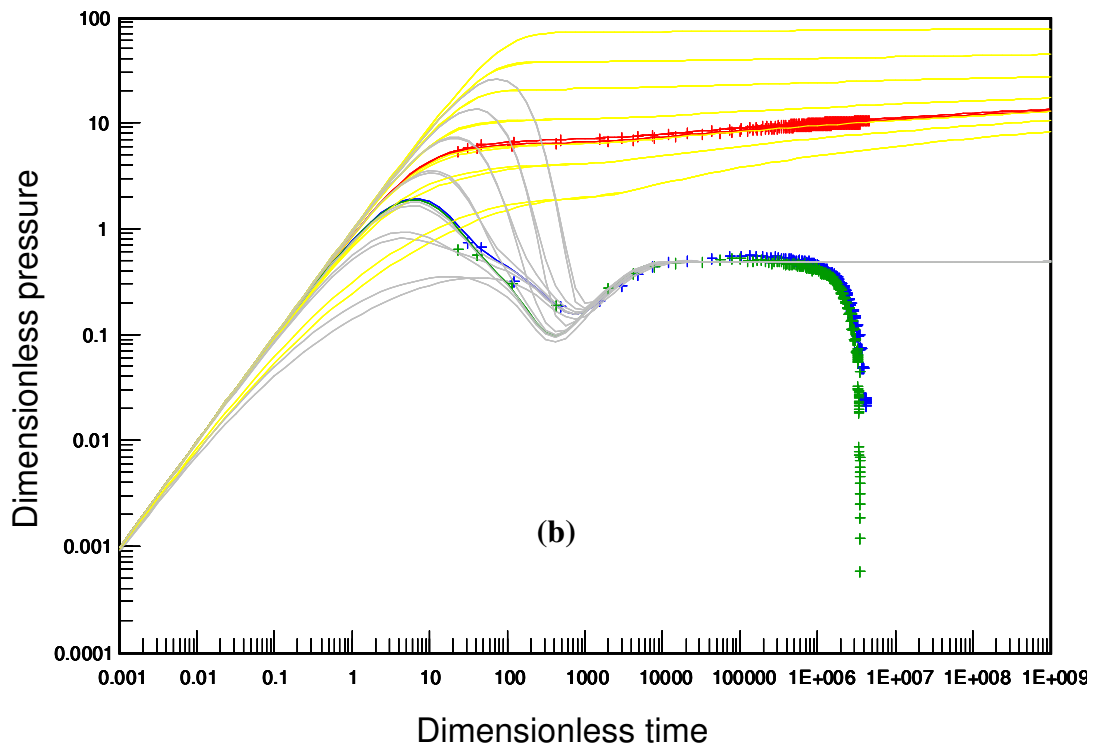
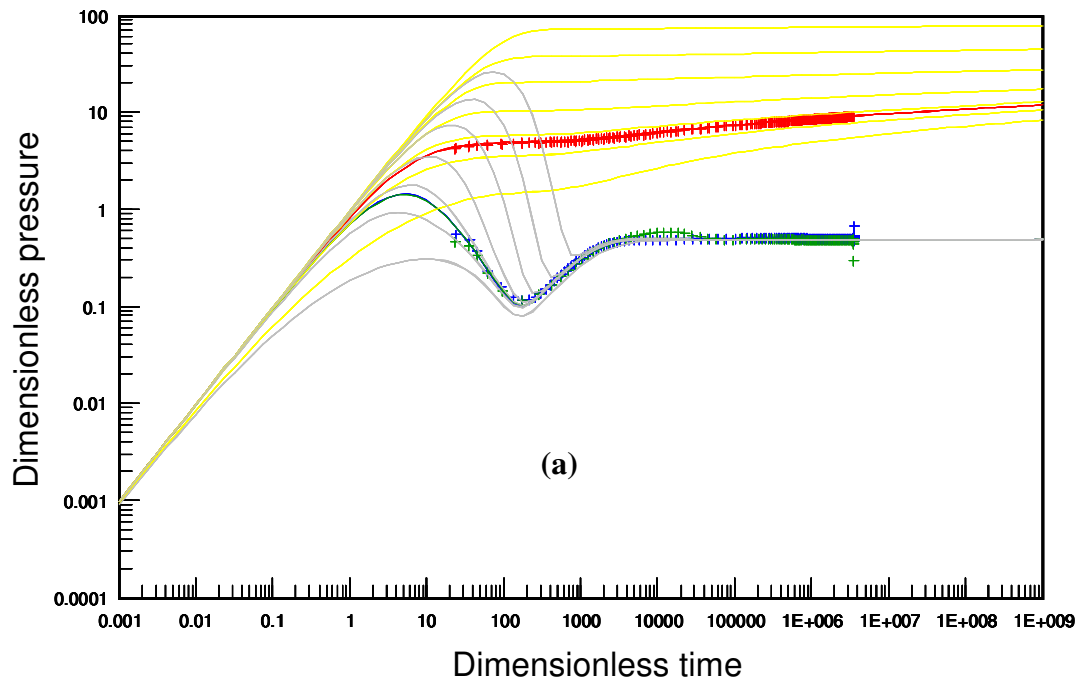


Figure 6.17- Comparison pressure response in radial and cartesian models. (a) K_f/K_m ratio = 10^3 , fracture spacing 3 ft. (b) K_f/K_m ratio = 10^4 , fracture spacing 5 ft.

Table 6.3- Matrix permeability values in x and y directions. Anisotropic matrix permeability case.

K_{mx}	K_{my}	K_{me}	K_{mx}/K_{my}
0.100	0.100	0.100	1
0.200	0.050	0.100	4
0.300	0.033	0.100	9
0.400	0.025	0.100	16
0.500	0.020	0.100	25
0.600	0.017	0.100	36
0.700	0.014	0.100	49
0.800	0.013	0.100	64
0.900	0.011	0.100	81
1.000	0.010	0.100	100

A centrally located producer well flowed at a constant rate of 1,000 STB/day for 30 days and was shut-in for 30 days. Bottom-hole pressure data was extracted and build up pressure information was used to conduct well test analysis. The pressure buildup period of the 10 simulation cases was analyzed using WELLTEST.

Well test analysis results are presented in Table 6.4. Estimated permeability decreases for very large anisotropy ratios, but generally, there is good agreement with fracture permeability input data in simulation. The value of ω is constant for all simulation cases, as expected, since this parameter does not depend on permeability.

The most important changes can be noticed in λ . As anisotropy ratio increases, λ decreases (Figure 6.18). Since all parameters in λ equation remain constant, except matrix permeability, it is apparent that λ is not a function of effective but it is a function of maximum matrix permeability.

Table 6.4- Well test analysis results for anisotropic matrix permeability cases.

Anisotropy ratio	K	λ	ω	Skin
1	95	7.50E-06	0.05	-0.3
4	95	1.10E-05	0.05	-0.3
9	95	1.50E-05	0.05	-0.3
16	95	2.14E-05	0.05	-0.3
25	95	2.42E-05	0.05	-0.3
36	95.3	2.80E-05	0.05	-0.3
49	93	3.20E-05	0.05	-0.5
64	93	3.50E-05	0.05	-0.5
81	85	4.52E-05	0.05	-1
100	88	4.80E-05	0.05	-0.9

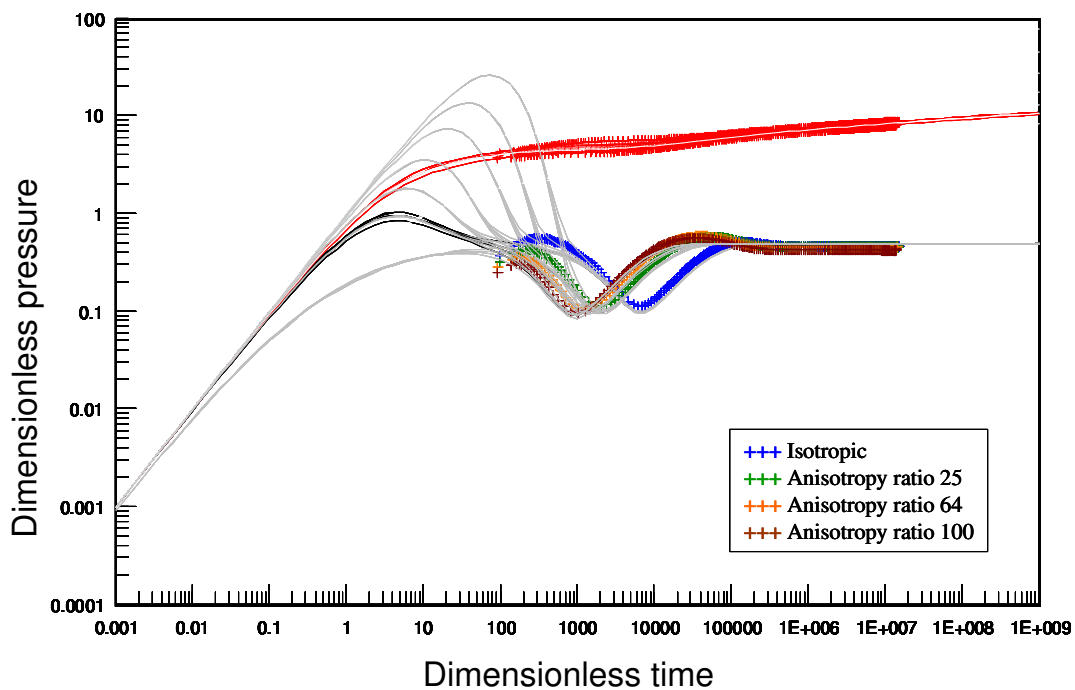


Figure 6.18- Type curve analysis showing the effect of anisotropic matrix permeability on well test response.

Shape factor and fracture spacing were estimated based on fracture permeability and λ from well test, using both matrix permeability values, k_{me} and k_{mx} . Results are presented in Table 6.5. When k_{me} was used, estimated fracture spacing starts at 10.3 ft, very close to simulation input data, 10 ft. As the anisotropy ratio increased the estimated fracture spacing decreased as much as 4.0 ft. Using k_{mx} a better match with simulation input data was achieved, but still different to the simulation input data (13 ft compared to 10 ft). The obtained value is more consistent but overestimates the simulation input data. Thus, the existence of matrix permeability anisotropy causes uncertainty in the well test analysis results.

In most NFR Matrix permeability anisotropy may be negligible. However, in a particular case where the existence of matrix permeability anisotropy is demonstrated, the previous conclusion would be relevant to obtain meaningful estimations of fracture spacing from well test analysis.

Table 6.5- Shape factor and fracture spacing estimation using effective and maximum matrix permeability .

Anisotropy ratio	Simulation Input Lma	λ	K_{me}		K_{mx}	
			Shape factor	Lma	Shape factor	Lma
1	10	7.50E-06	0.114	10.3	0.114	10.3
4	10	1.10E-05	0.167	8.5	0.084	12.0
9	10	1.50E-05	0.229	7.2	0.076	12.6
16	10	2.14E-05	0.325	6.1	0.081	12.1
25	10	2.42E-05	0.368	5.7	0.074	12.8
36	10	2.80E-05	0.427	5.3	0.071	13.0
49	10	3.20E-05	0.476	5.0	0.068	13.3
64	10	3.50E-05	0.521	4.8	0.065	13.6
81	10	4.52E-05	0.618	4.4	0.068	13.3
100	10	4.80E-05	0.676	4.2	0.068	13.3

6.5 Anisotropic Fracture Permeability Model

A cartesian, homogeneous, black oil model was built with the same characteristics presented in Table 6.1. Fracture spacing and matrix permeability were set constant, 10 ft and 0.1 mD respectively. Effective fracture permeability was set at 100 mD. A total of 10 simulation cases, including one isotropic case, were run. Fracture permeability combinations used in each case are shown in Table 6.6.

A centrally located producer well flowed at a constant rate of 1,000 STB/day for 30 days and was shut-in for 30 days. Build up pressure data was used to conduct well test analysis for all 10 cases.

Table 6.6- Fracture permeability values in x and y directions. Anisotropic fracture permeability case.

K_{fx}	K_{fy}	K_{fe}	K_{fx}/K_{fy}
100	100.00	100	1
200	50.00	100	4
300	33.33	100	9
400	25.00	100	16
500	20.00	100	25
600	16.67	100	36
700	14.29	100	49
800	12.50	100	64
900	11.11	100	81
1000	10.00	100	100

Cases with anisotropy ratios lower than 25 showed all dual-porosity flow regimes and the interpretation results are presented in Table 6.7. The estimated shape factor and fracture spacing are close to simulation input data, whereas permeability values obtained from well test are close to the assigned effective fracture permeability.

Cases with anisotropy ratios higher than 36 are increasingly distorted at late times. Figure 6.19 illustrates the incremental distortion in pressure response. High fracture permeability anisotropy ratios cause such a significant distortion in pressure response that it becomes difficult or nearly impossible to conduct well test analysis. In those cases, system radial regime was not properly defined because the distortion in pressure. Henceforth, those tests could not be interpreted with conventional well test techniques, as the result will be inaccurate.

6.6 Heterogeneous Field Model

Most oil and gas reservoirs exhibit different degrees of heterogeneity. In NFR, fracture properties are highly heterogeneous. The effect of heterogeneity on pressure response was investigated in relation to two variables, fracture permeability and fracture spacing.

Table 6.7- Well test analysis results. Anisotropic fracture permeability cases.

Anisotropy ratio	K	λ	ω	S
1	100	6.61E-06	0.045	-0.2
4	95	6.96E-06	0.045	-0.45
9	96.9	6.84E-06	0.045	-0.5
16	95	7.02E-06	0.045	-0.9
25	97	6.99E-06	0.045	-0.9

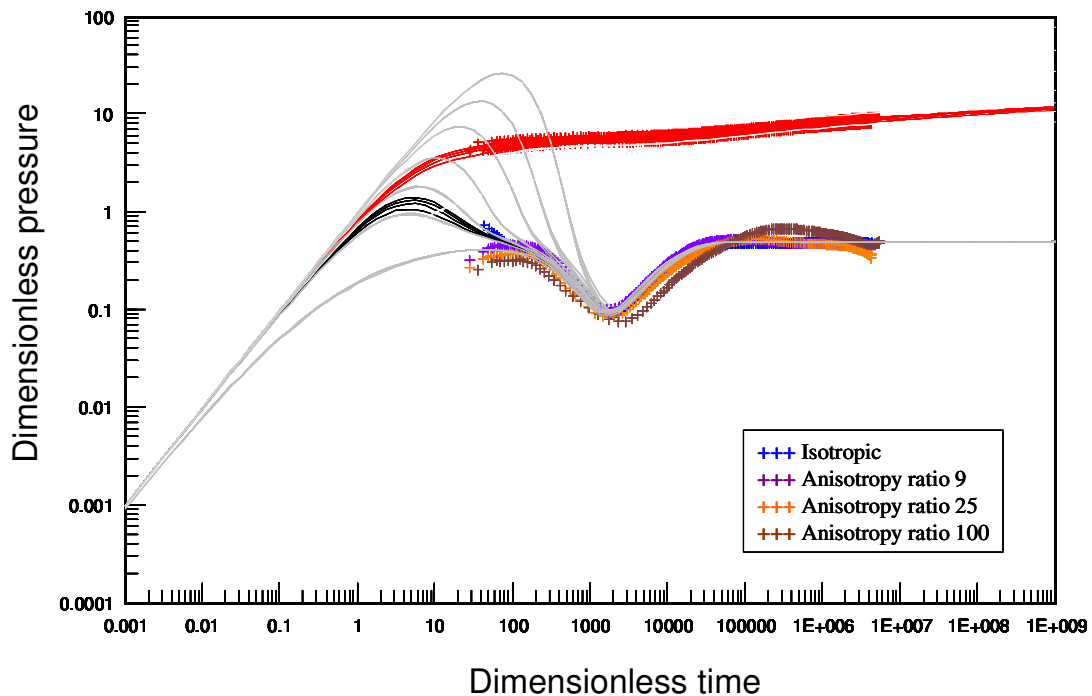


Figure 6.19- Type curve analysis showing the effect of anisotropic fracture permeability on well test response.

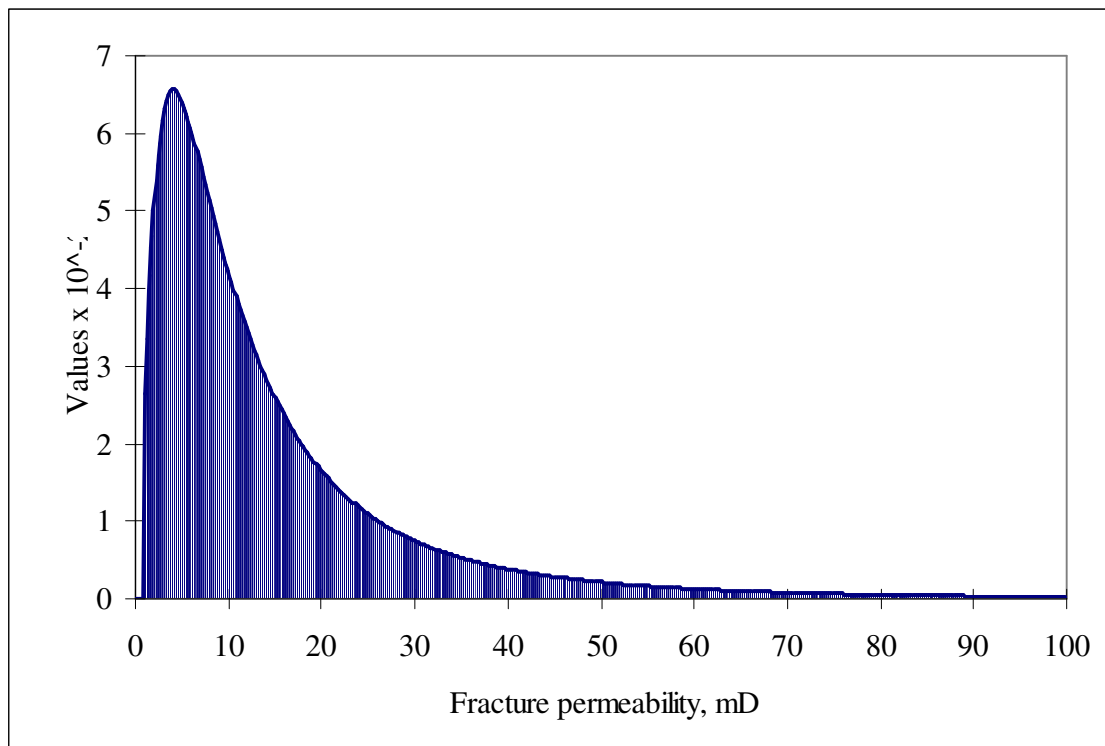
Matrix permeability was set constant at 0.1 mD. Fracture permeability was randomly generated from a log normal distribution as shown in Figure 6.20. Values are in the range of 1 to 100 mD, with a mode of 10 mD.

Matrix relative permeabilities were generated from correlations and fracture permeabilities were set as straight lines. Capillary pressures were ignored for both matrix and fracture.

Other reservoir characteristics used in the heterogeneous field model are shown in Table 6.8

Table 6.8- Main reservoir characteristics; heterogeneous field model.

Reservoir Parameter	Values
Grid cell dimensions	200 ft x 200 ft
Reservoir thickness	30 ft
Initial pressure	3626 psi
Reservoir temperature	120 °F
Matrix porosity	20%
Matrix compressibility	$6.8 \times 10^{-7} \text{ psi}^{-1}$
Fracture porosity	1.0%
Fracture compressibility	$6.8 \times 10^{-7} \text{ psi}^{-1}$
Connate water saturation	20%

**Figure 6.20- Log normal distribution used to generate fracture permeability values.**

Fracture spacing was assumed equal in x , y and z directions. The values were randomly generated according to a triangular distribution with a minimum of 2 ft, a most likely of 5 ft and a maximum of 50 ft, as shown in Figure 6.21.

A total of 25 producer wells were located in the model. Locations are shown in Figure 6.22. Blocks where well were located were locally refined using the hybrid approach. Each well was produced at a constant rate of 500 STB/day for 30 days and was shut-in for 30 days. While one well was tested the remaining 24 were shut-in to avoid interference effects in pressure response. Flowing bottom-hole pressure was monitored to avoid values below bubble point and two-phases flow. For Well 15, where flowing bottom-hole pressure fell below saturation pressure the oil rate was modified to 200 STB/day and simulation was rerun.

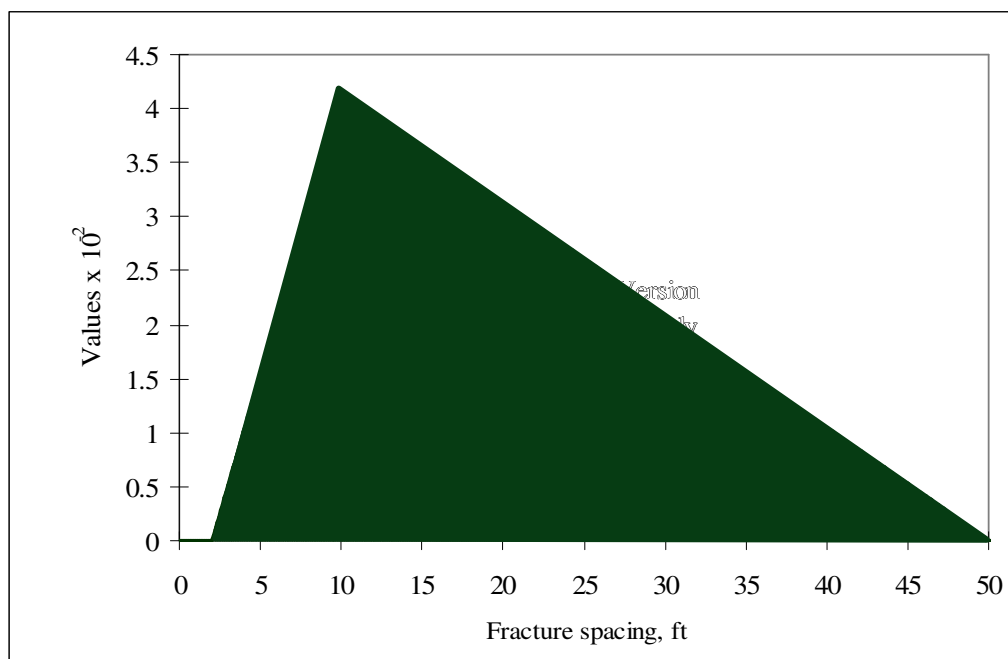


Figure 6.21- Triangular distribution used to generate fracture spacing values.

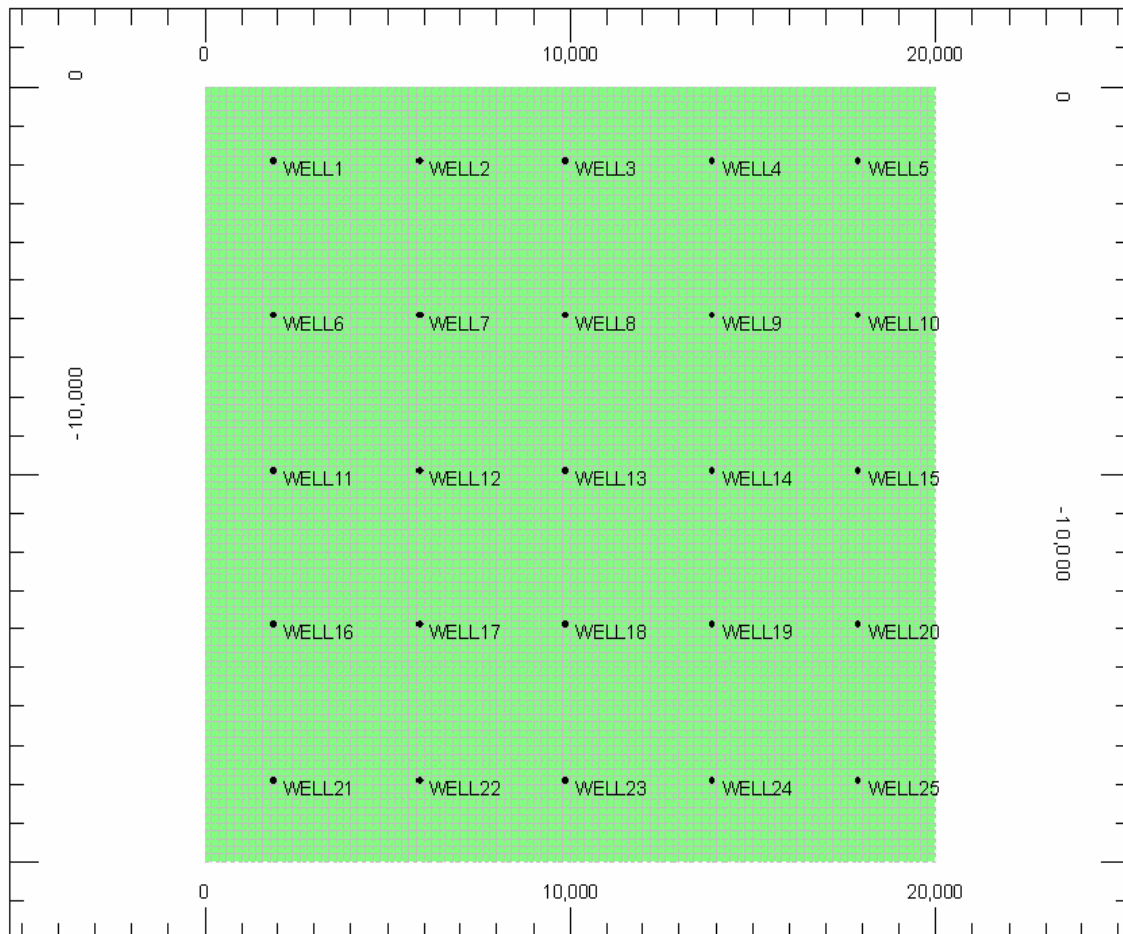


Figure 6.22- Well locations in heterogeneous field model.

Bottom-hole pressure data from shut-in period was extracted and interpreted. The following parameters were reported: permeability, λ , ω and the radius of investigation (r_i) to the first pressure distortion after transition flow regime. Minimum r_i is 100 ft, which is the distance from the well, centrally located in the block, to the neighboring blocks.

There were some difficulties in interpreting several of the tests because of the distortion that mainly affected system radial flow and thus very poor matches were obtained. In those cases, parameters obtained from well tests are very inaccurate. Summary of well test results is presented in Table 6.9.

Table 6.9- Well test results for heterogeneous field model.

Well	K, mD	λ	ω	r_i , ft
1	34	4.48E-06	0.05	1300
2	35	3.36E-06	0.035	2000
3	39	3.70E-06	0.04	2000
4	17.2	7.00E-06	0.04	300
5	32	1.90E-06	0.04	700
6	7.4	9.50E-06	0.03	200
7	11.2	1.73E-05	0.05	200
8	15	4.44E-05	0.05	100
9	32.7	1.59E-05	0.046	2000
10	24	4.50E-05	0.046	700
11	12.75	3.70E-06	0.04	100
12	37	6.91E-06	0.05	500
13	31	1.82E-06	0.04	1200
14	18.2	6.38E-06	0.048	200
15	4.1	1.30E-04	0.05	100
16	31	2.65E-06	0.045	700
17	16.3	2.61E-05	0.045	100
18	20	7.54E-05	0.045	200
19	45	8.45E-06	0.055	500
20	33.4	8.50E-06	0.055	2000
21	10.5	5.13E-06	0.035	300
22	29	3.41E-06	0.045	1500
23	40	5.91E-06	0.06	500
24	16.4	1.14E-05	0.05	200
25	81	4.74E-06	0.05	700

Three different behaviors were identified from observed pressure responses:

1) Pressure response resemble homogeneous model, as is shown in Figure 6.23. Fracture radial, transition and system radial flow regimens can easily be identified. Well test interpretation results are reliable. r_i is higher than 1,000 ft. A total of 7 wells exhibited this behavior. In these cases, fracture permeability simulation input data showed low heterogeneity around the wellbore.

2) Pressure response distortion is observed after system radial flow regime, Figure 6.24. Well test results are less accurate than in the type 1, but still are fair enough to estimate reservoir parameters. A total of 14 wells showed this behavior. Fracture permeability simulation input data showed moderate heterogeneity in the zone surrounding the wellbore.

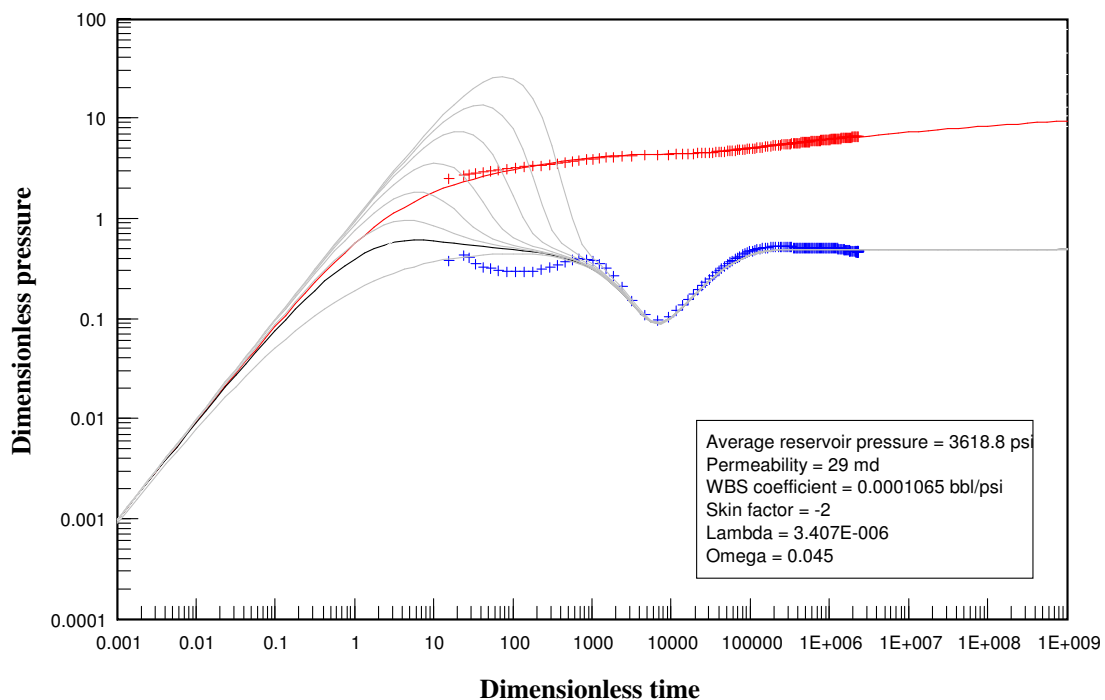


Figure 6.23- Example of pressure response in a low fracture permeability heterogeneity zone. Well 22.

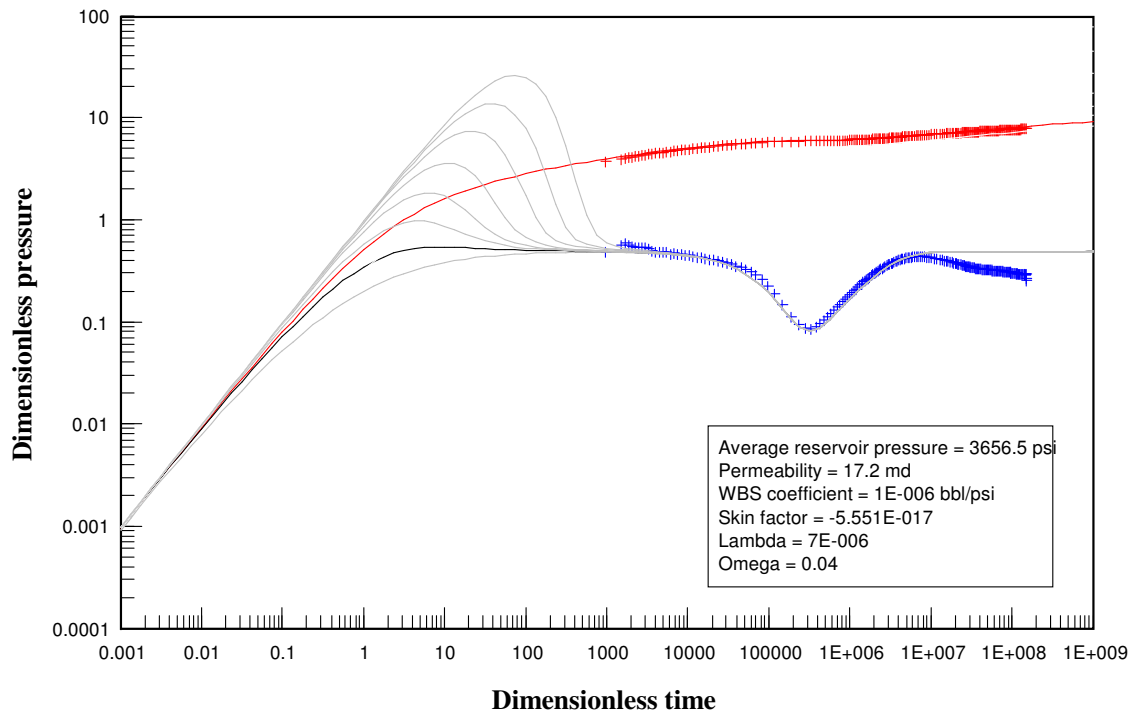


Figure 6.24- Example of pressure response in a moderate fracture permeability heterogeneity zone. Well 4.

- 3) Highly distorted pressure response. System radial flow is difficult to identify. As can be observed in Figure 6.25 (a), the two straight lines in semilog analysis are not parallel. The two radial flows, if present, are at a different pressure derivative value, as shown in Figure 6.25(b). Consequently, well test analysis becomes unreliable. The 4 wells that lied in this category are: Well 6, Well 11, Well 15 and Well 25. Fracture permeability simulation input data showed high heterogeneity around wellbore.

Heterogeneous field model results

Wells that showed type 3 pressure response behavior as described earlier were not considered for further analyses.

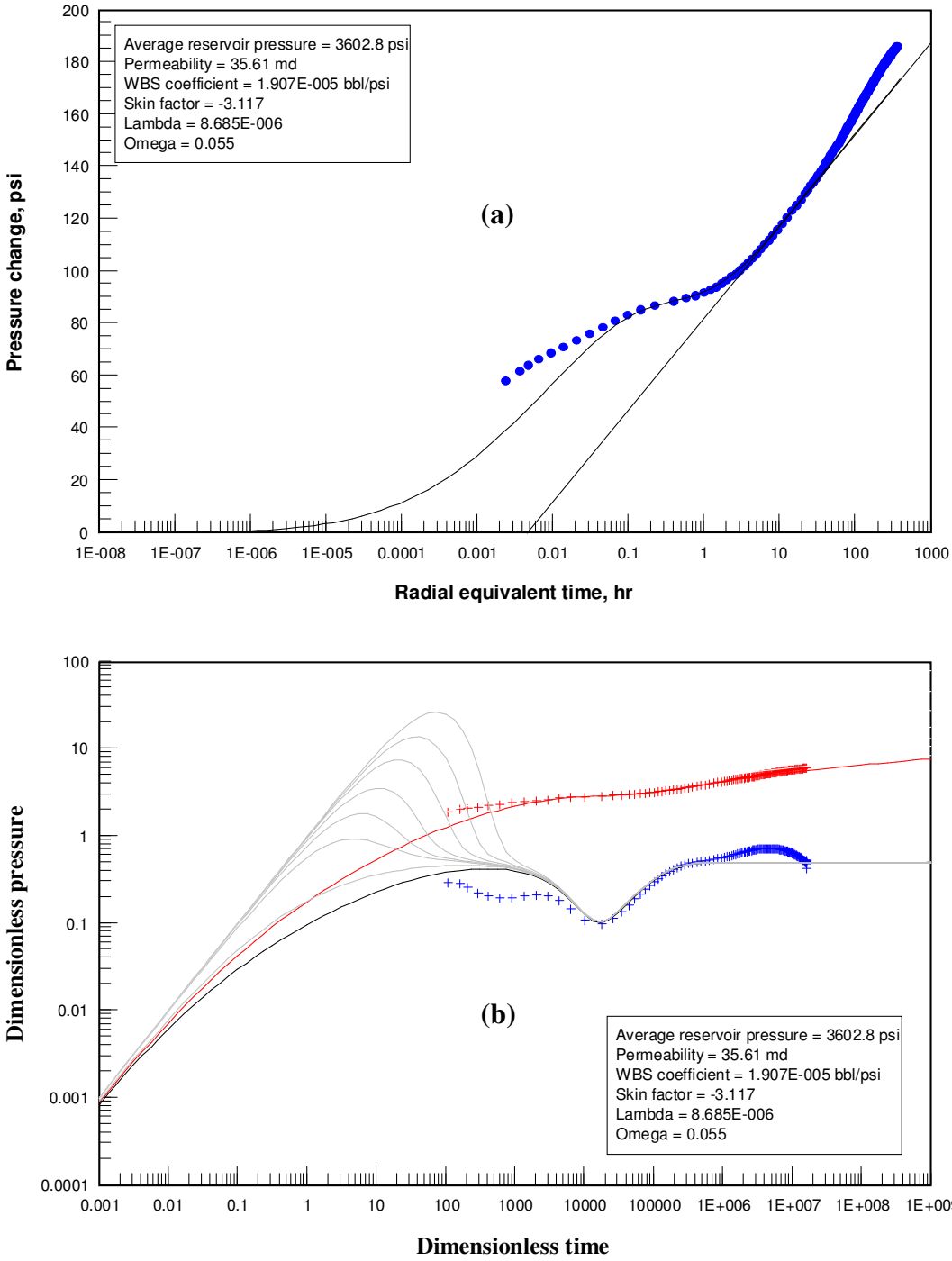
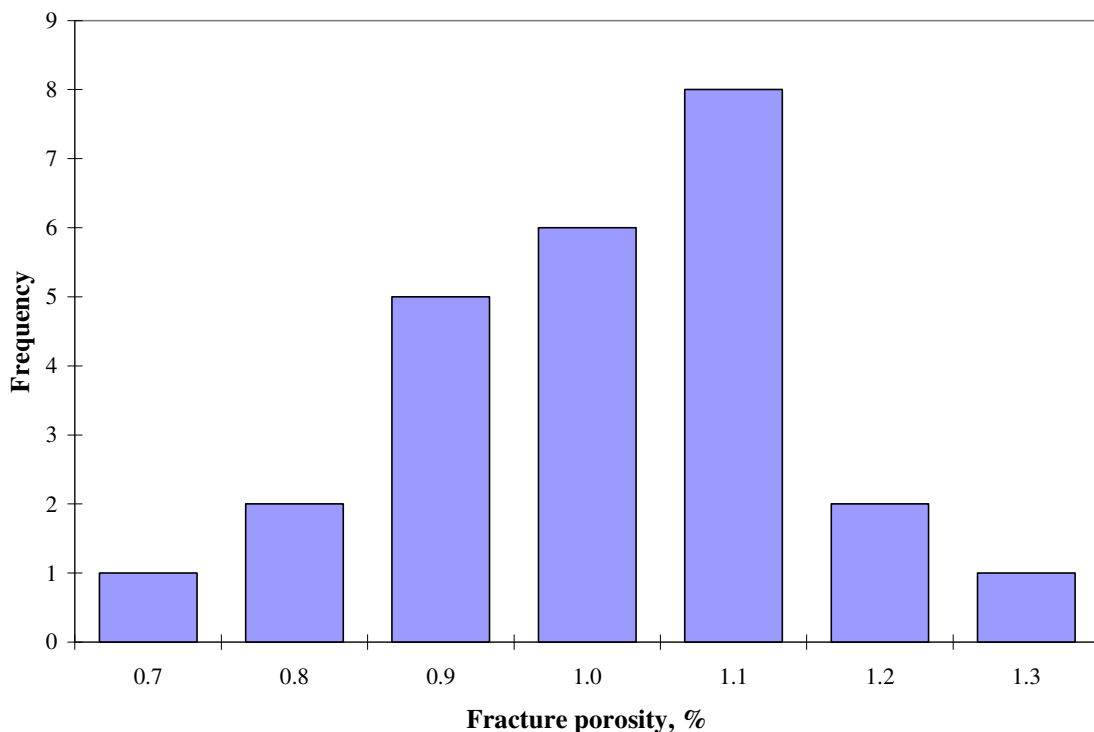


Figure 6.25- Example of pressure response in a high fracture permeability heterogeneity zone. (a) Semilog plot and (b) Type curve. Well 25.

Well test results show that ω values ranged from 0.3 to 0.6. Fracture porosity was estimated based on these values and the results are presented in Figure 6.26. Most of the values are close to the input data that is 1.0%. Since porosity was not considered heterogeneous, results are consistent with the previous results for homogeneous models. ω is a good estimator of fracture porosity.

Shape factor and fracture spacing were estimated using permeability and λ from well test. Permeability and fracture spacing estimated from well test were then compared to the values on the grid blocks where wells were located. Figure 6.27 shows the correlation between the simulation input data vs. well test results for fracture permeability.



6.26- Fracture porosity estimated from well test storativity ratio for heterogeneous field model.

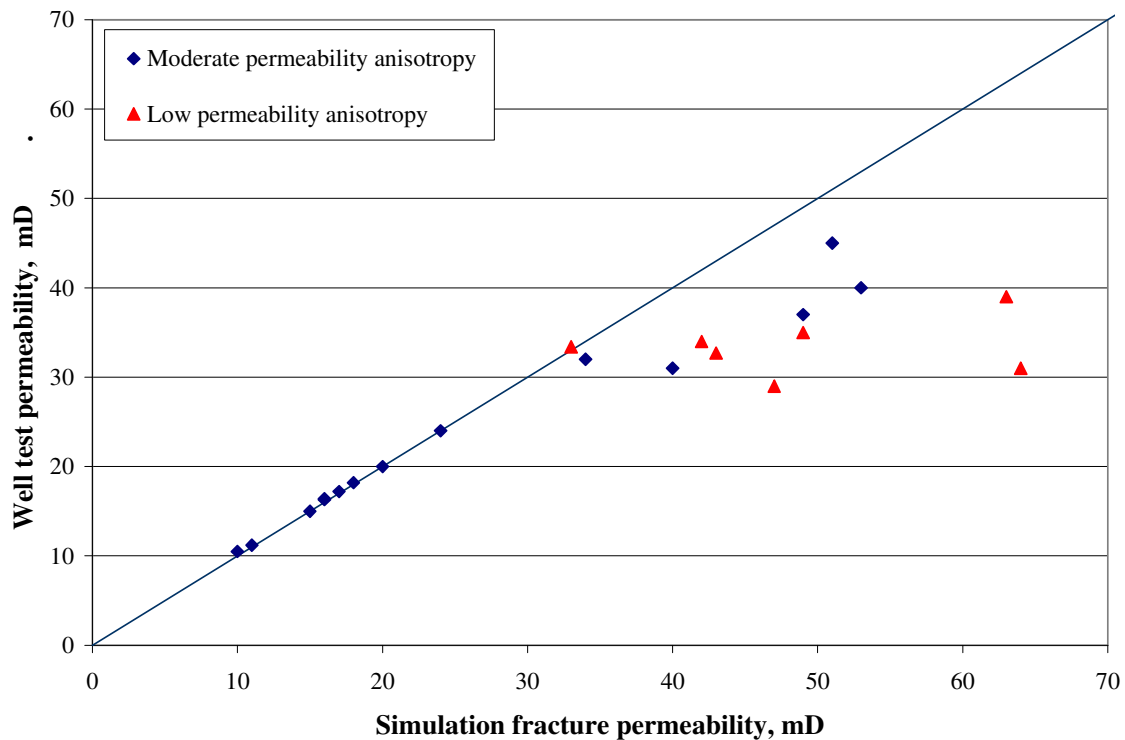


Figure 6.27- Well block fracture permeability vs. well test estimated permeability.

All moderate permeability anisotropy cases where r_i was less than 200 ft showed a consistency between input and the output values. , Only one low permeability anisotropy case showed consistency. Data points showing inconsistency correspond to cases with r_i higher than 200 ft.

Figure 6.28 presents the correlation between simulation input values vs. well test estimated fracture spacing. Surprisingly, most data points showed a good consistency regardless permeability anisotropy or r_i .

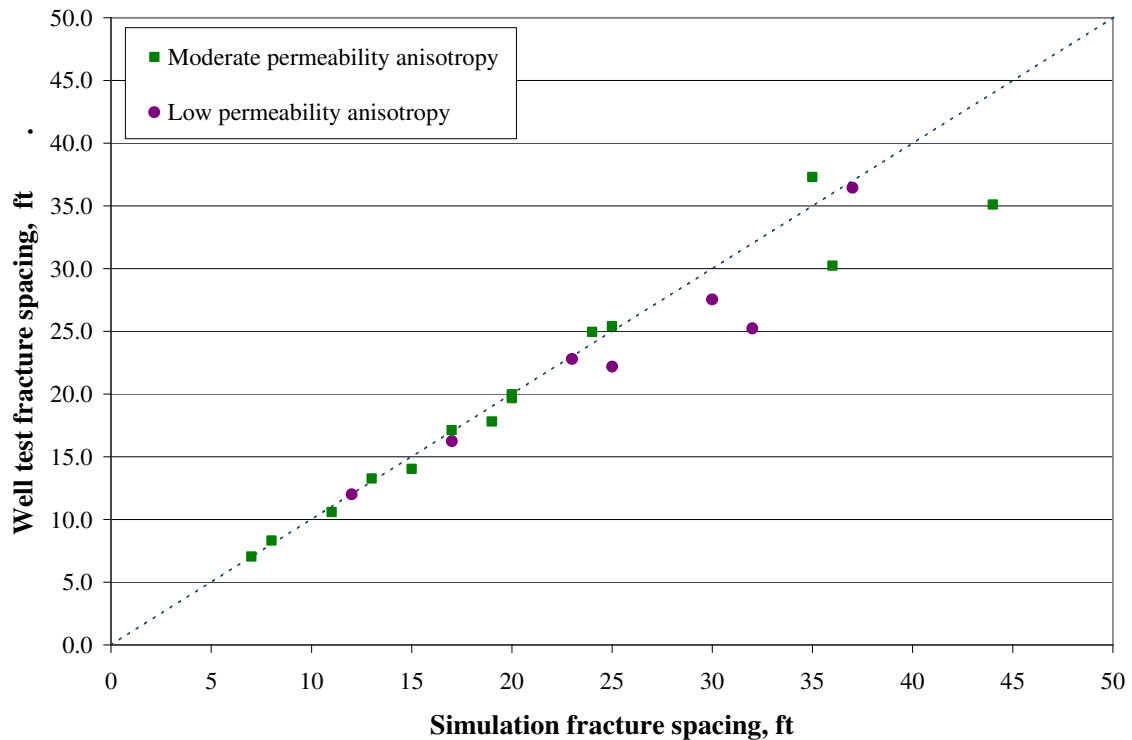


Figure 6.28- Well block vs. well test estimated fracture spacing correlation

To determine the existence of any relationship between values estimated from well test analysis and the actual input values in a wide zone, average fracture permeability and fracture spacing surrounding the well block were calculated.

Average simulation fracture permeability around the well was calculated at different distances up to 1300 ft, which in grid block size is equivalent to 5 contiguous blocks from the well, in all directions. Arithmetic (KA), geometric (KG) and harmonic (KH) averages of fracture permeability were calculated. Averages were named after the number of values used in calculation. For example, $KG9$ is the geometric average of fracture permeability value in the block where the well is located and the surrounding 8 blocks. Figure 6.29 illustrates this concept.

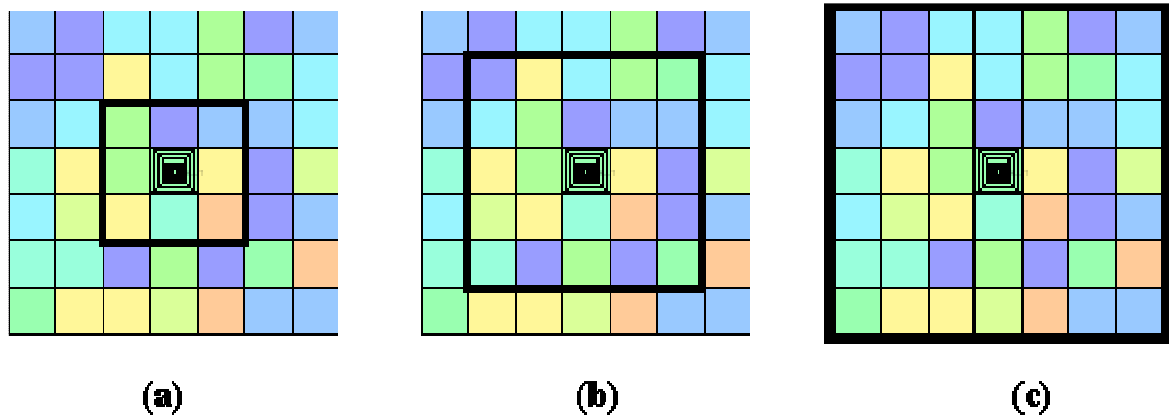


Figure 6.29- Example of fracture permeability averages. (a) K9, (b) K25, and (c) K49.

Fracture spacing averages were estimated following the same methodology as described from fracture permeability. Arithmetic, geometric and harmonic averages were named *LA*, *LG* and *LH* respectively.

Table 6.10 presents the average value that closely matches well test estimations, both for fracture permeability and fracture spacing. Several observations can be made from this table: 1) Permeability estimated from well test matched with geometric averages for all cases with r_i higher than 100; 2) Fracture spacing estimated from well test matched with well block value for most of the cases, as was stated before; 3) In cases where fracture spacing did not match to well block value, the closest values came from arithmetic averages; and 4) In most cases, permeability averaged area did not correspond to fracture spacing averaged area.

Table 6.10- Average input values that closely matched well test results.

Well	r_i , ft	CLOSEST VALUE TO WELL TEST ESTIMATION	
		Kf	Lma
1	1300	KG9	LA25
2	2000	KG25	LA25
3	2000	KG49	LA49
4	300	Kblock	Lmblock
5	700	KG49	Lmblock
7	200	Kblock	Lmblock
8	100	Kblock	Lmblock
9	2000	KG25	Lmblock
10	700	KG25	Lmblock
12	500	KG25	LA25
13	1200	KG125	Lmblock
14	200	Kblock	Lmblock
16	700	KG25	Lmblock
17	100	Kblock	Lmblock
18	200	Kblock	Lmblock
19	500	KG9	LA9
20	2000	KG49	Lmblock
21	300	Kblock	Lmblock
22	1500	KG125	Lmblock
23	500	KG9	LA9
24	200	K1	Lmblock

Figure 6.30 presents the correlation between permeability from well test and the closest average reported in Table 6.9. All data points show a good to excellent match. Figure 6.31 presents the correlation between fracture spacing estimated from well test and the closest average reported in Table 6.9. The improvement in correlation is not as evident as in permeability case, since most of well test results matched with well block input value.

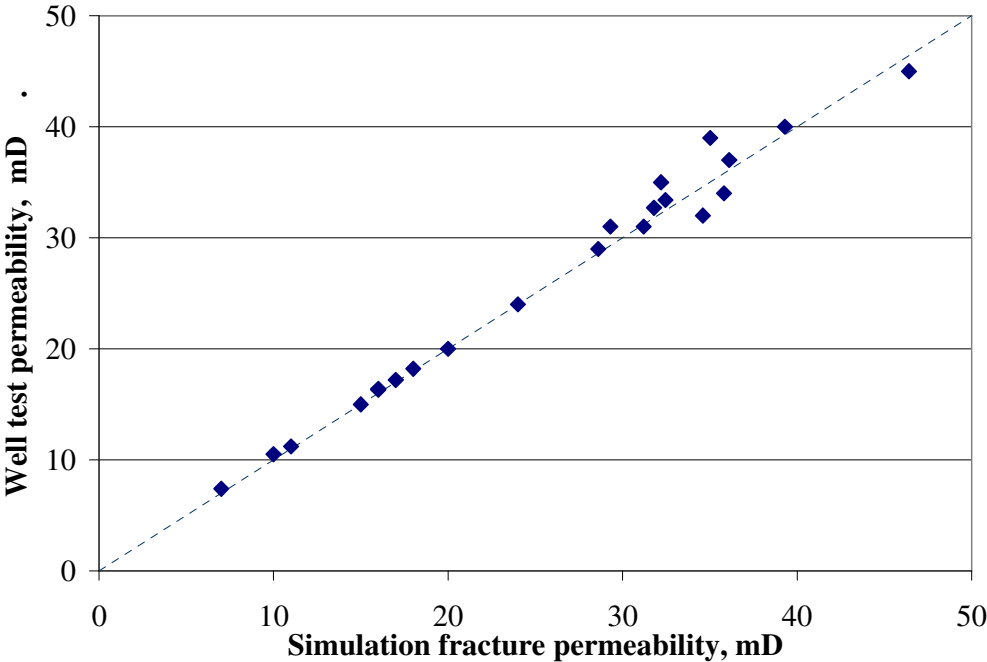


Figure 6.30- Simulation average vs. well test estimated fracture permeability.

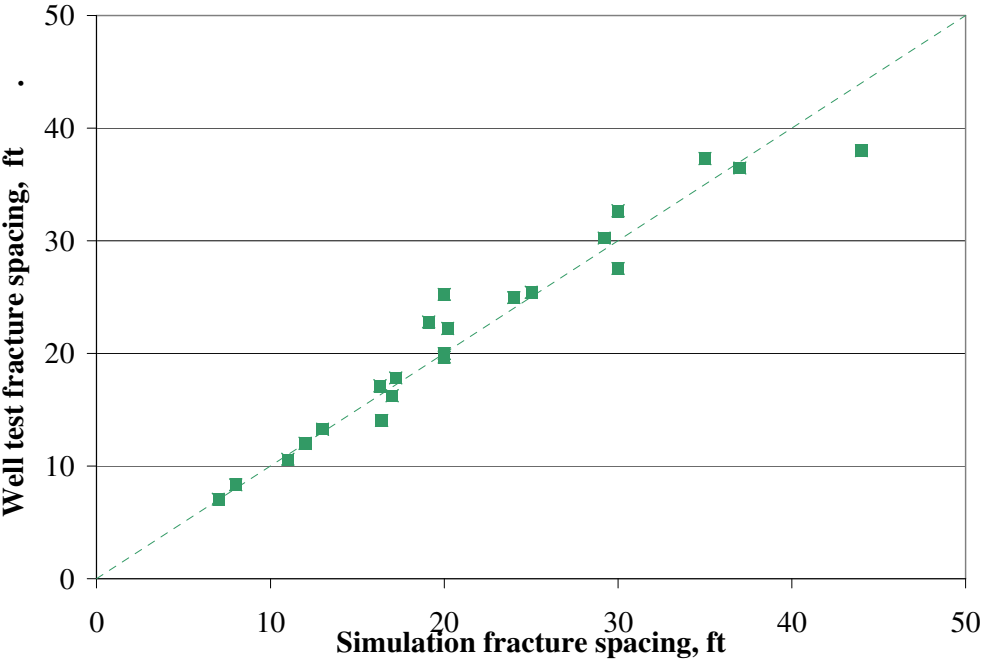


Figure 6.31- Simulation average vs. well test estimated fracture spacing.

6.7 Anisotropic Field Model

Anisotropy is one of the most prominent characteristics of a fracture system. A simulation model with heterogeneous and anisotropic properties was built. Porosity, permeability, fracture spacing, and fracture permeability anisotropy were set in the ranges reported in the literature for typical NFR.

To represent an anisotropic reservoir, the previously used heterogeneous model was modified as follows:

- Matrix permeability was randomly generated using a uniform distribution ranging from 0.01 to 1.0 mD.
- Fracture porosity was changed from 1.0% to 0.1%.
- Only two fracture sets were considered, in x and y directions.
- Fracture permeability in x direction was randomly generated using a log normal distribution. Values are in the range of 5 to 150 mD, with a mode of 20 mD.
- Fracture spacing in x direction was randomly generated using a log normal distribution ranging from 1.5 to 30 ft, with a mode of 5 ft.
- Fracture permeability in y direction was obtained from a fracture anisotropy ratio (K_{fx}/K_{fy}) of 6:1.
- Fracture spacing in y direction was randomly generated using a uniform distribution ranging from 25 to 40 ft.

All other rock and fluid properties remained the same.

A total of 25 producer wells were placed in the same locations as in the heterogeneous model. Cells where well were located were locally refined using the hybrid approach. Each well was produced at a constant rate of 100 STB/day for 30 days and then shut-in for 30 days. While one well was tested the remaining 24 were shut-in to avoid interference effects in pressure response. Flowing bottom-hole pressure was monitored to avoid values below bubble point and two-phases flow.

Bottom-hole pressure data from shut-in period was extracted and interpreted. The following parameters were reported: permeability, λ , ω and radius of investigation (r_i).

Three types of pressure responses were obtained:

1) Pressure response that exhibits the complete three flow regimes. Both type curve and semilog analyses can be performed as usual. A total of 10 cases showed this behavior.

2) Fracture radial flow is not present, but transition and system radial flow are well developed. Semilog analysis can not be done, since the first semilog straight line is not present. Only type curve analysis was performed. This behavior was observed in 11 cases.

3) Fracture radial flow is not present and transition flow is incomplete or absent. Well test analysis can not be conducted under these circumstances. A total of 4 wells showed this behavior, and then were excluded for further analyses.

Anisotropic field model results

Table 6.11 presents well test analysis results for the 21 cases. It must be noted that 18 cases exhibited r_i less than or equal to 500 ft, from which in 12 cases r_i is 100 ft. From these results, it could be expected that most of the cases show a good consistency between well test results and simulation input values in the well block.

The results show that ω values ranged from 0.004 to 0.007. Fracture porosity was estimated using Equation 5.4 and the results are presented in Figure 6.32. Although most of the values matched with the simulation input data (0.1%), some values exhibit a difference of 40% in respect to the input data.

Table 6.11- Well test results. Anisotropic field model.

Well	K, mD	λ	ω	r_i , ft
1	20.5	6.75E-05	0.005	1000
2	13.8	8.00E-05	0.005	100
3	9	6.29E-05	0.005	100
4	11	1.06E-04	0.005	100
5	21.5	5.87E-05	0.006	300
6	12.5	5.69E-06	0.005	500
7	15.8	1.22E-05	0.005	500
8	6.3	9.54E-05	0.005	100
9	14	3.43E-05	0.007	500
10	24	4.84E-05	0.007	100
11	28.5	9.06E-05	0.007	1000
12	12.8	1.40E-04	0.007	100
13	10.6	1.02E-04	0.007	100
14	10	2.91E-05	0.007	200
15	15.8	6.34E-06	0.006	500
18	4.5	1.17E-04	0.005	100
20	25.4	2.29E-05	0.007	1300
21	7.2	1.14E-04	0.004	100
22	22	1.30E-05	0.006	500
23	9.8	5.99E-05	0.006	100
24	9.8	1.19E-04	0.004	100

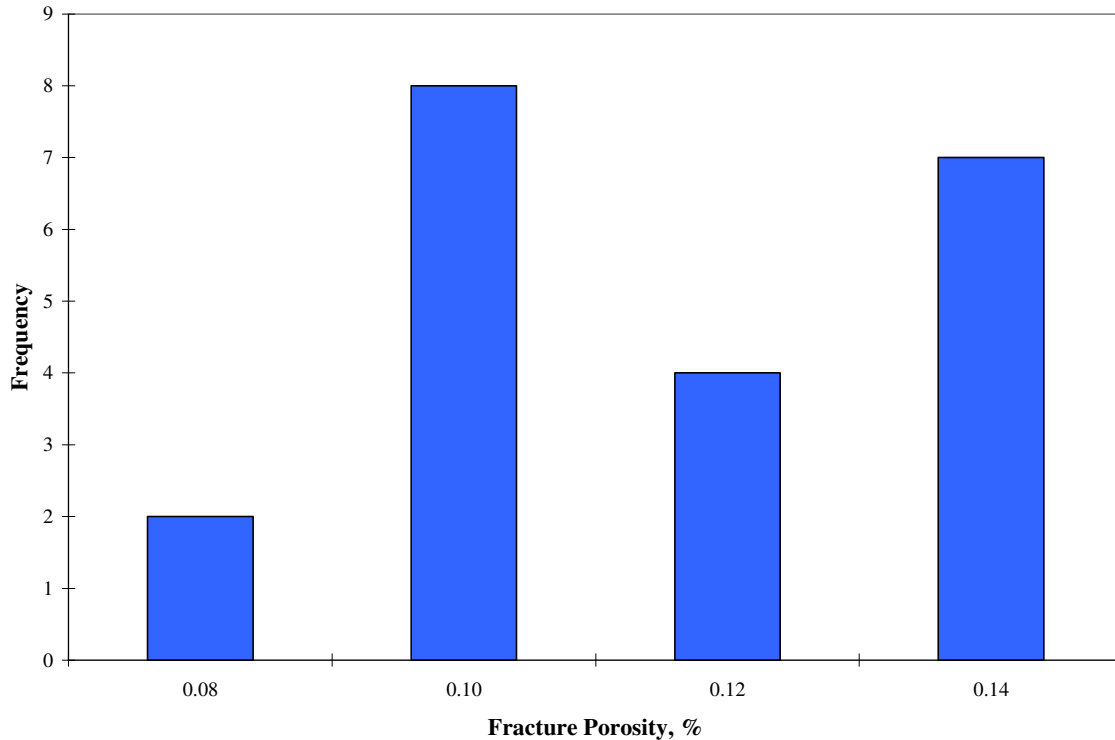


Figure 6.32- Fracture porosity estimated from well test storativity ratio.

Once again, ω is a good indicator of the magnitude of porosity but the results must be taken with careful consideration, depending on the importance of fracture porosity in overall reservoir performance.

Based on simulation input data of K_{fx} and K_{fy} , K_{fe} well block was estimated using Equation 6.2. K_{fe} and shape factor from simulation data were compared to well test estimations.

Figure 6.33 shows well test permeability vs. simulation K_{fe} . In general, the figure shows a good consistency between the input and output values, regardless the pressure response behavior. Points with highest discrepancies correspond to those cases where r_i is larger than 100 ft.

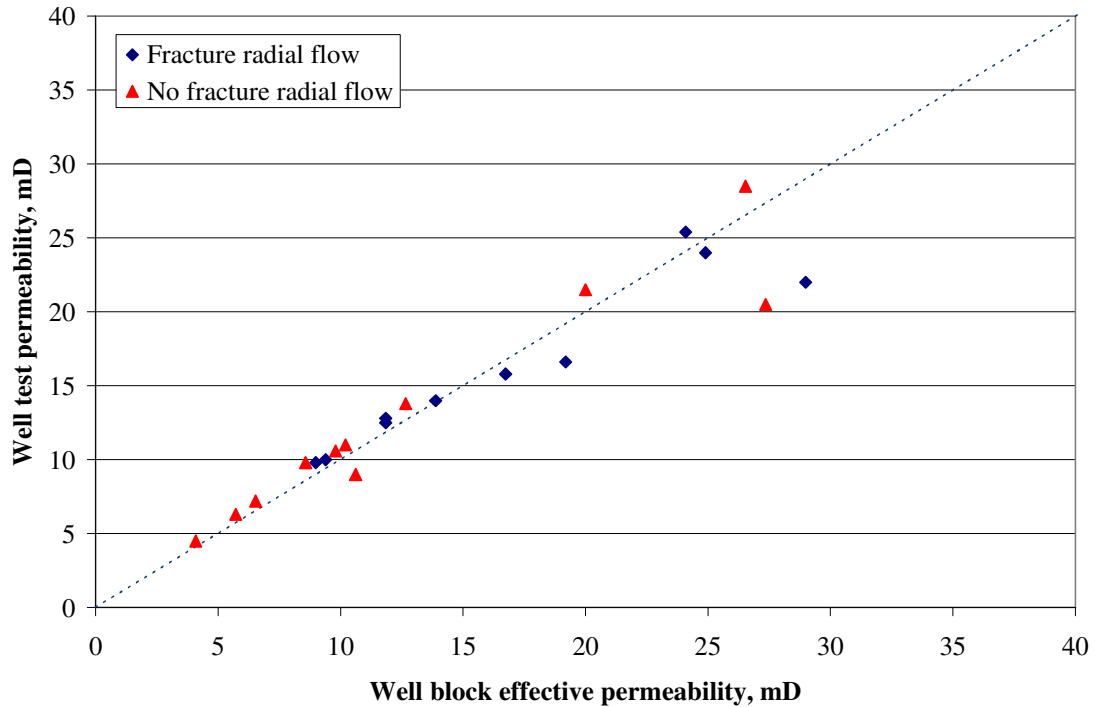


Figure 6.33- Well block vs. well test estimated effective fracture permeability correlation.

Shape factor used in simulation was estimated using Equation 5.1. Well test shape factor was estimated using λ , K_{fe} from well test and matrix permeability used in simulation. Figure 6.34 presents the input (simulation) vs. output (welltest) values of shape factor.

Two trends were identified from Figure 6.34. Cases where pressure response exhibited fracture radial flow showed reasonable consistent results, except for those cases where r_i was larger than 500 ft. On the other hand, cases which did not exhibit fracture radial flow had poor correlations, regardless of r_i .

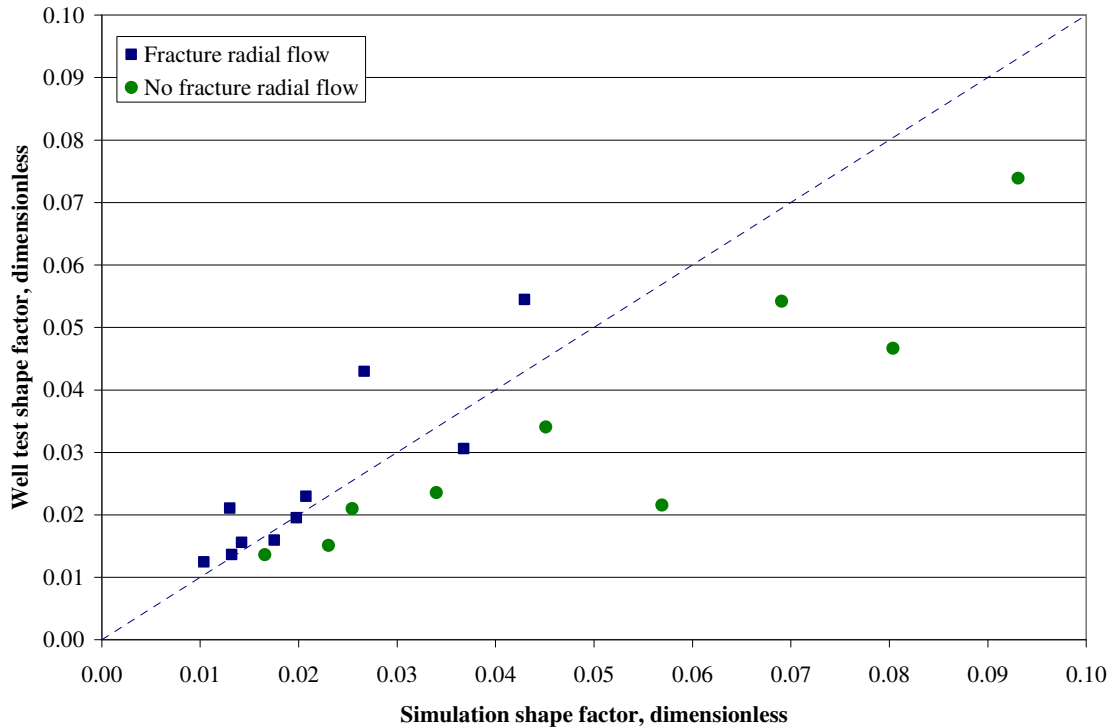


Figure 6.34- Well block vs. well test estimated shape factor correlation.

The values of average effective permeability and shape factor used in simulation were estimated using the same methodology as in the heterogeneous field model. To improve the correlation, well test results were compared to average simulation input values but the results were very inconclusive. In some cases with high r_i , the estimated values matched with well block values while in other cases did not match with either the well block nor the average values.

The requirement of a matrix permeability value to estimate shape factor and fracture spacing have been pointed out before. For anisotropic cases, shape factor was estimated using the well block matrix porosity. Under actual conditions, the best case would be to have a range of values, not a single point value. Recalling that matrix permeability

values were in range of 0.01 to 1.0 mD, this could impact the variation in shape factor values up to 3 orders of magnitude.

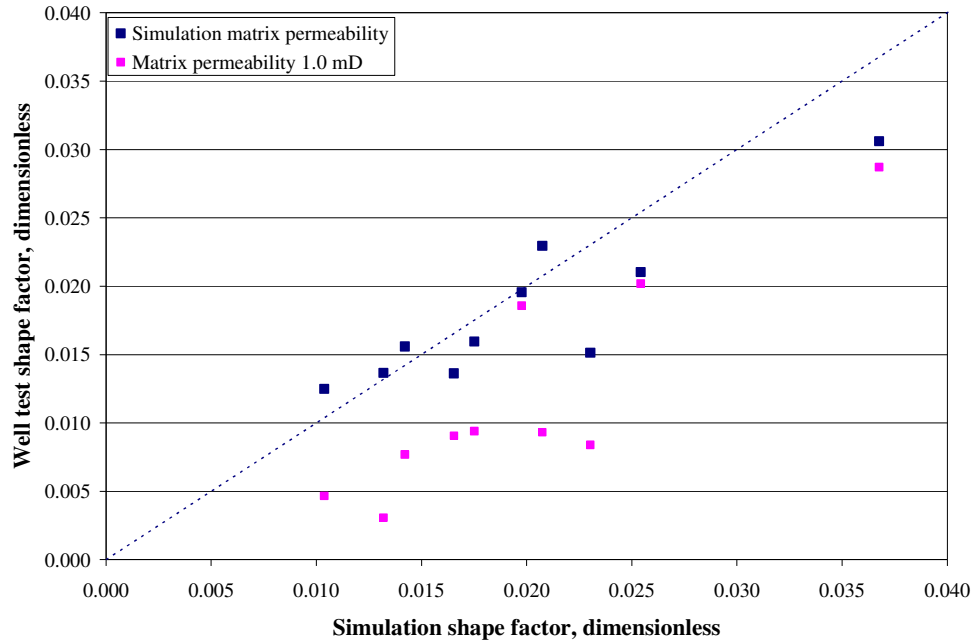


Figure 6.35- Effect of matrix permeability value on shape factor estimation.

To illustrate this effect, Figure 6.35 shows shape factors estimated using a constant matrix permeability value of 1.0 mD for those cases that previously showed a good correlation between simulation input data and well test results.

Estimation of fracture spacing from well test results is a tricky process when L_x and L_y have different values. To solve this problem, shape factor can be used in two ways. First, if fracture spacing in one direction is known, then the unknown fracture spacing can be estimated using shape factor. Second, if the ratio of fracture spacing is known, shape factor equation can be simplified to one unknown and solved as follows.

For the anisotropic case, L_y/L_x follows a log normal distribution with a mode of 3.0 ft. Then, using $L_y = 3 L_x$, shape factor equation was expressed as a function of L_x as follows:

$$\sigma = 4 \left[\frac{1}{L_x^2} + \frac{1}{9L_x^2} \right] \dots\dots\dots (6.3)$$

Then L_x and L_y were calculated using shape factor from well test analysis and matrix permeability from simulation input. Figures 6.36 and 6.37 show the comparison between simulation input values and output values from well test analysis. L_x showed a good match (Figure 6.36), while L_y correlation was very poor (Figure 6.37). However, it must be noted that all L_y values estimated were in the same order of magnitude of the input values.

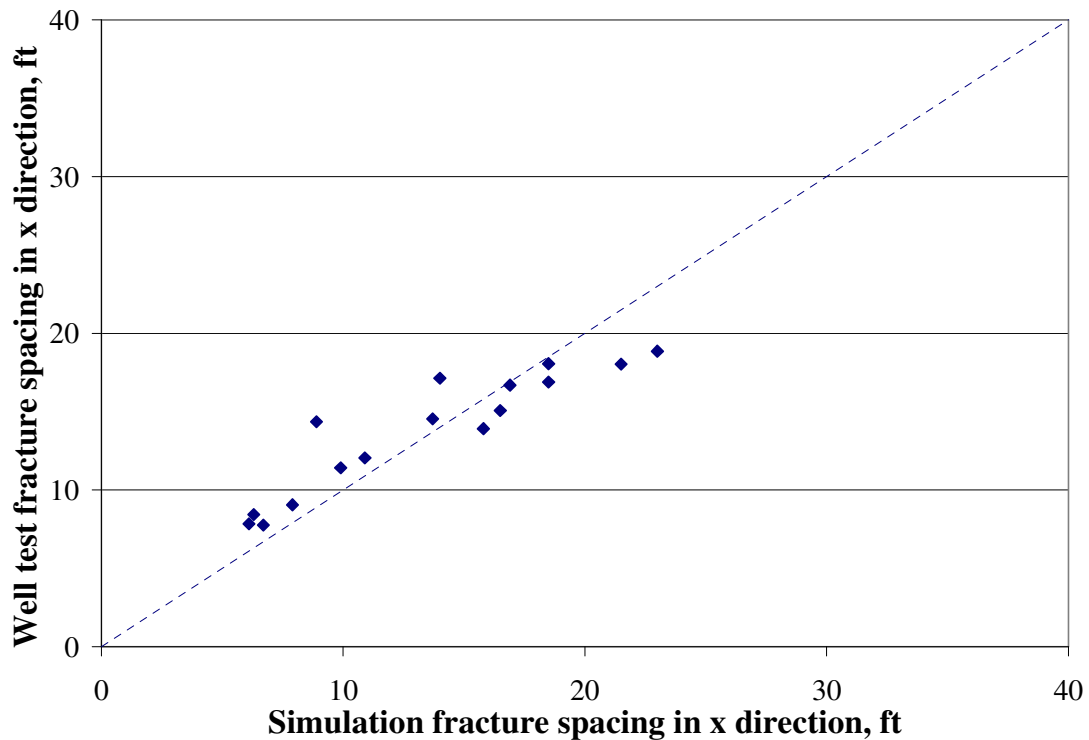


Figure 6.36- Well block vs. well test estimated fracture spacing in x direction.

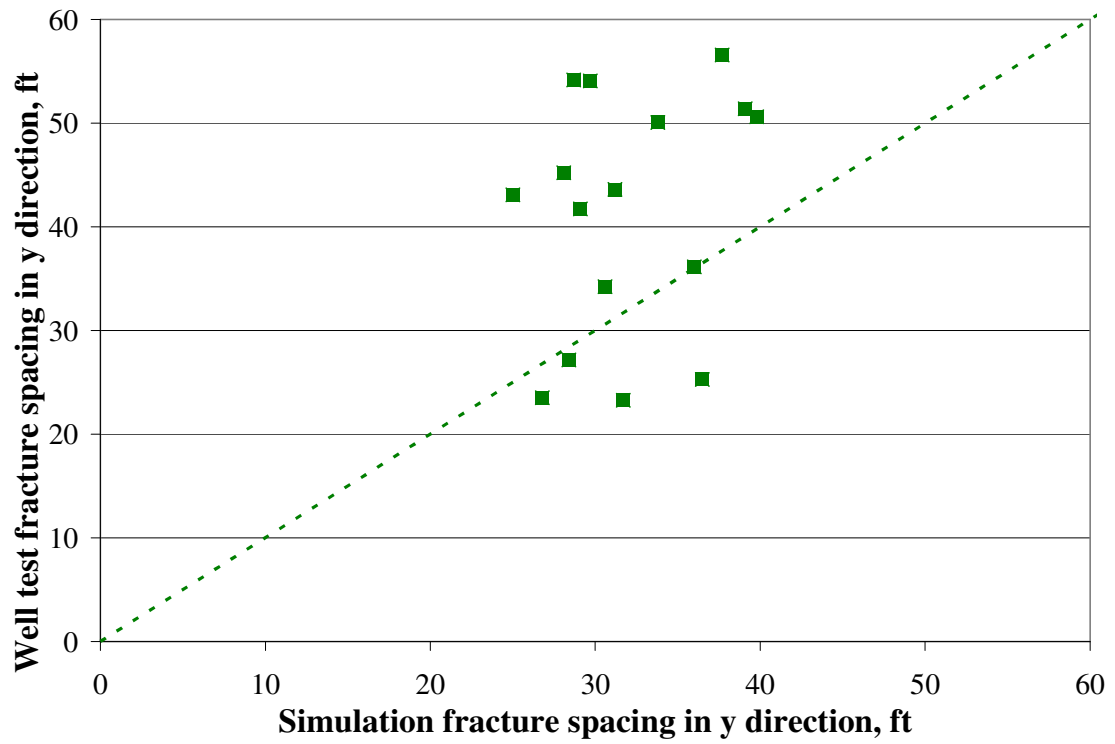


Figure 6.37- Well block vs. well test estimated fracture spacing in y direction.

CHAPTER VII

CONCLUSIONS

Based upon work performed for this thesis the following conclusions were drawn.

1. Storativity ratio obtained from well test analysis can provide a good estimate of the fracture porosity magnitude.
2. Interporosity flow coefficient obtained from well test analysis can also be used to estimate the shape factor magnitude provided that the matrix permeability value is known.
3. Well test pressure response should exhibit a complete flow regimes (fracture radial flow, transition flow, and system radial flow) in order to obtain reliable estimates of storativity ratio and interporosity flow coefficient.
4. The existence of matrix permeability anisotropy causes uncertainty in the well test analysis result.
5. In reservoirs with fracture spacing smaller than 1.0 ft, the estimation of fracture porosity and shape factor from well test results is not reliable because the pressure responses do not exhibit any fracture radial flows.
6. In reservoirs with high fracture permeability, the transition and system radial flows could be distorted or masked because of boundary effects. As a result, the estimation of fracture porosity and shape factor from well test analysis is unreliable.

7. In reservoirs with low or moderate heterogeneity and permeability anisotropy, interporosity flow coefficient from well test analysis provides a good approximation to shape factor.
8. The use of fracture porosity and spacing estimated from well test analysis must be limited to the region within the radius of investigation defined by the distance at which point pressure response distorts from a typical trend of system radial flow.

The above conclusions are valid for cases with the following assumptions: 1) fracture and matrix compressibilities are equal; 2) no wellbore storage and skin; 3) pseudo-steady state; and 4) single phase flow.

Recommendations

The following tasks are recommended based on the result of this study:

1. To investigate the applicability of well test results for building simulation models using other geometries such as non-orthogonal corner point, voronoi, and others.
2. To consider unequal compressibilities between fracture and matrix in order to validate the use of storativity ratio to obtain a more accurate fracture porosity estimation.
3. To validate the results of this study using actual field data.

NOMENCLATURE

A = Arithmetic average
 c = total system compressibility, 1/psi
 D = Fracture spacing, ft, m
 e = Fracture width, in, cm
 G = Geometric average
 H = Harmonic average
 k = permeability, md
 L = Fracture spacing, ft
 r_i = Radius of investigation, ft
 r_w = wellbore radius, ft
 ϕ = porosity
 μ = viscosity, cp
 ρ = fluid density, lb_m/ft³
 σ = Shape factor, ft⁻²
 ω = Storativity ratio
 λ = Interporosity flow coefficient
 Δx = Block dimension in x direction

Subscripts

e = effective
 m = matrix
 f = fracture

REFERENCES

1. Warren J.E. and Root P.J.: "The Behavior of NFR," *SPEJ* (September 1963) 245.
2. Nelson, R.A.: *Geologic Analysis of Naturally Fractured Reservoirs*, Gulf Professional Publishing, Woburn, MA, 2001.
3. Pollard, P.: "Evaluation of Acid Treatments form Pressure Buildup Analysis," *Trans. AIME* (1959) **216**, 38.
4. Pirson, R.S. and Pirson, S.J.: "An Extension of the Pollard Analysis Method of Well Pressure Build-Up and Drawdown Tests," paper SPE 101 presented at the 1961 SPE Annual Fall Meeting, Dallas, Texas, 8-11 October.
5. Mavor, M.J. and Cinco-Ley, H.: "Transient Pressure Behavior of NFR," paper SPE 7977 presented at the 1979 SPE California Regional Meeting, Ventura, California, 18-20 April.
6. Kazemi, H.: "Pressure Transient Analysis of NFR with Uniform Fracture Distribution," *SPEJ* (December 1969) 451.
7. De Swaan O. A.: "Analytic Solutions for Determining NFR Properties by Well Testing," *SPEJ* (June 1976) 117.
8. Najurieta, H.L.: "A Theory for the Pressure Transient Analysis in NFR," paper SPE 6017 presented at the 1976 SPE Annual Technical Conference, New Orleans, 3-6 October.
9. Moench, A.F.: "Double-Porosity Models for a Fissured Groundwater Reservoir With Fracture Skin," *Water Resources Research* (July 1984) 831.
10. Cinco-Ley, H., Samaniego V.F., and Dominguez, A.N.: "Unsteady-State Flow Behavior for a Well Near a Natural Fracture," paper SPE 6019 presented at the 1976 SPE Annual Technical Conference and Exhibition, New Orleans, 3-6 October.
11. Bourdet, D., Ayoub J., Whittle T., Pirard Y., and Kniazeff V.: "Interpreting Well Tests in Fractured Reservoirs," *World Oil* (October 1983) 77.

12. Bourdet D., Whittle T., Douglas A. and Pirard Y.: "New Type Curves Aid Analysis of Fissured Zone Well Tests," *World Oil* (April 1984) 111.
13. Abdassah, D. and Ershaghi, I.: "Triple-porosity Systems for Representing Naturally Fractured Reservoirs," *SPE Formation Evaluation* (April 1986), 113.
14. Dreier, J., Ozkan, E., and Kazemi, H.: "New analytical pressure-transient models to detect and characterize reservoirs with multiple fracture systems," paper SPE 92039. . presented at the 2004 International Petroleum Conference, Puebla, Mexico, 8-9 November 2004.
15. Gilman, J. and Kazemi, H.: "Improvements in Simulation of NFR," *SPEJ* (August 1983) 675.
16. Pruess, K. and Narasimhan, T.N.: "A Practical Method for Modeling Fluid and Heat Flow in Fractured Porous Media," *SPEJ* (February 1985) 14.
17. Saidi, A.M.: "Simulation of NFR," paper SPE 12270 presented at the 1983 Symposium on Reservoir Simulation, San Francisco, 16-18 November.
18. Dean, R.H. and Lo, L.L.: "Development of a Natural Fracture Simulator and Examples of Its Use," paper SPE 14110 presented at the 1996 International Meeting on Petroleum Engineering, Beijing, 17-20 March.
19. Carlson, E.S. and Latham, G.V.: "Naturally Fractured or Single-Porosity? The Importance of Reservoir Flow Model for Performance Assessment of Stimulated Tight Gas Wells," paper SPE 25477 presented at the 1993 Production Operations Symposium, Oklahoma City, Oklahoma, 21-23 March.
20. Wei, L., Hadwin, J., Chaput, E., Rawnsley, K. and Peter S.: "Discriminating Fracture Patterns in Fractured Reservoirs by Pressure Transient Tests," paper SPE 49233 presented at the 1998 SPE Annual Technical Conference and Exhibition, New Orleans, 27-30 September.
21. Wei, L.: "Well Test Pressure Derivatives and the Nature of Fracture Networks," paper SPE 59014 presented at the 2000 SPE International Petroleum Conference and Exhibition, Villahermosa, Mexico, 1-3 February.

22. Bourbiaux, B., Basquet R., Cacas M., Daniel J. and Sarda S.: “An Integrated Workflow to Account for Multi-Scale Fractures in Reservoir Simulation Models: Implementation and Benefits,” paper SPE 78489 presented at the 2002 International Petroleum Exhibition and Conference, Abu Dhabi, UAE, 13-16 October.
23. Bahaer, A., Ates H., Ald-Deeb M.H., Salem, S.A., Badaam, H. et al.: “Practical Approach in Modeling Naturally Fractured Reservoir: A Field Case Study,” paper SPE 84078 presented at the 2003 Annual Technical Conference and Exhibition, Denver, 5-8 October.
24. Gilman, J.R.: Practical Aspects of Simulation of Fractured Reservoirs. International Forum on Reservoir Simulation, Bühl, Germany, June 23-27 2003.

APPENDIX A

RADIAL MODEL – GAS SYSTEM. WELL TEST RESULTS

SIMULATION INPUT DATA				WELL TEST RESULTS			COMMENTS
K_m	K_f	r_w	L_{ma}	K	λ	ω	
0.001	1	0.25	1	1	6.86E-04	0.0476	
0.001	1	0.25	2	1	1.72E-04	0.0476	
0.001	1	0.25	3	1	7.57E-05	0.042	
0.001	1	0.25	5	1	2.65E-05	0.042	
0.001	1	0.25	10	1	6.67E-06	0.042	
0.001	1	0.25	20				System radial flow not reached
0.001	1	0.25	30				System radial flow not reached
0.001	1	0.25	50				System radial flow not reached
0.001	1	0.354	1	1	1.38E-03	0.044	
0.001	1	0.354	2	1	3.56E-04	0.044	
0.001	1	0.354	3	1	1.44E-04	0.044	
0.001	1	0.354	5	1	5.34E-05	0.044	
0.001	1	0.354	10	1	1.32E-05	0.041	
0.001	1	0.354	20				System radial flow not reached
0.001	1	0.354	30				System radial flow not reached
0.001	1	0.354	50				System radial flow not reached
0.001	1	0.51	1	1	2.85E-03	0.043	
0.001	1	0.51	2	1	7.22E-04	0.043	
0.001	1	0.51	3	1	3.02E-04	0.043	
0.001	1	0.51	5	1	1.15E-04	0.042	
0.001	1	0.51	10	1	2.70E-05	0.042	
0.001	1	0.51	20				System radial flow not reached
0.001	1	0.51	30				System radial flow not reached
0.001	1	0.51	50				System radial flow not reached
0.001	10	0.25	1	10	8.00E-05	0.055	
0.001	10	0.25	2	10	1.85E-05	0.055	
0.001	10	0.25	3	10	8.00E-06	0.055	
0.001	10	0.25	5	10	3.03E-06	0.055	
0.001	10	0.25	10	10	7.20E-07	0.055	
0.001	10	0.25	20	10	1.35E-07	0.04	
0.001	10	0.25	30				System radial flow not reached
0.001	10	0.25	50				System radial flow not reached
0.001	10	0.354	1	10	1.70E-04	0.06	
0.001	10	0.354	2	10	4.00E-05	0.06	
0.001	10	0.354	3	10	1.70E-05	0.057	
0.001	10	0.354	5	10	6.00E-06	0.056	
0.001	10	0.354	10	10	1.39E-06	0.052	
0.001	10	0.354	20	10	2.80E-07	0.04	
0.001	10	0.354	30				System radial flow not reached
0.001	10	0.354	50				System radial flow not reached
0.001	10	0.51	1	10	3.08E-04	0.055	

SIMULATION INPUT DATA				WELL TEST RESULTS			COMMENTS
K_m	K_f	r_w	L_{ma}	K	λ	ω	
0.001	10	0.51	2	10	7.56E-05	0.055	
0.001	10	0.51	3	10	3.33E-05	0.055	
0.001	10	0.51	5	10	1.19E-05	0.055	
0.001	10	0.51	10	10	3.09E-06	0.055	
0.001	10	0.51	20	10	6.00E-07	0.04	
0.001	10	0.51	30				System radial flow not reached
0.001	10	0.51	50				System radial flow not reached
0.001	100	0.25	1	100	7.93E-06	0.07	
0.001	100	0.25	2	100	1.93E-06	0.07	
0.001	100	0.25	3	100	8.35E-07	0.07	
0.001	100	0.25	5	100	2.97E-07	0.07	
0.001	100	0.25	10	100	6.84E-08	0.07	
0.001	100	0.25	20				System radial flow not reached
0.001	100	0.25	30				System radial flow not reached
0.001	100	0.25	50				System radial flow not reached
0.001	100	0.354	1	100	1.49E-05	0.07	
0.001	100	0.354	2	100	3.30E-06	0.07	
0.001	100	0.354	3	100	1.71E-06	0.07	
0.001	100	0.354	5	100	5.87E-07	0.07	
0.001	100	0.354	10	100	1.35E-07	0.07	
0.001	100	0.354	20				System radial flow not reached
0.001	100	0.354	30				System radial flow not reached
0.001	100	0.354	50				System radial flow not reached
0.001	100	0.51	1	100	2.71E-05	0.07	
0.001	100	0.51	2	100	7.04E-06	0.07	
0.001	100	0.51	3	100	3.47E-06	0.07	
0.001	100	0.51	5	100	1.15E-06	0.07	
0.001	100	0.51	10	100	2.78E-07	0.07	
0.001	100	0.51	20				System radial flow not reached
0.001	100	0.51	30				System radial flow not reached
0.001	100	0.51	50				System radial flow not reached
0.01	1	0.25	1	1	7.00E-03	0.0476	
0.01	1	0.25	2	1	1.81E-03	0.045	
0.01	1	0.25	3	1	7.49E-04	0.045	
0.01	1	0.25	5	1	2.73E-04	0.045	
0.01	1	0.25	10	1	6.75E-05	0.045	
0.01	1	0.25	20	1	1.75E-05	0.045	
0.01	1	0.25	30	1	8.13E-06	0.045	
0.01	1	0.25	50	1	3.00E-06	0.035	
0.01	1	0.354	1	1	1.30E-02	0.045	
0.01	1	0.354	2	1	3.64E-03	0.045	
0.01	1	0.354	3	1	1.55E-03	0.045	
0.01	1	0.354	5	1	5.90E-04	0.045	
0.01	1	0.354	10	1	1.45E-04	0.045	
0.01	1	0.354	20	1	3.50E-05	0.045	

SIMULATION INPUT DATA				WELL TEST RESULTS			COMMENTS
K_m	K_f	r_w	L_{ma}	K	λ	ω	
0.01	1	0.354	30	1	1.59E-05	0.045	System radial flow not reached
0.01	1	0.354	50	1	6.00E-06	0.035	
0.01	1	0.51	1	1	2.69E-02	0.045	
0.01	1	0.51	2	1	7.37E-03	0.045	
0.01	1	0.51	3	1	3.34E-03	0.045	
0.01	1	0.51	5	1	1.13E-03	0.045	
0.01	1	0.51	10	1	3.08E-04	0.045	
0.01	1	0.51	20	1	7.68E-05	0.045	
0.01	1	0.51	30	1	3.00E-05	0.04	
0.01	1	0.51	50	1			
0.01	10	0.25	1	10	8.19E-04	0.048	
0.01	10	0.25	2	10	1.86E-04	0.048	
0.01	10	0.25	3	10	8.17E-05	0.048	
0.01	10	0.25	5	10	2.79E-05	0.048	
0.01	10	0.25	10	10	6.58E-06	0.048	
0.01	10	0.25	20	10	1.75E-06	0.048	
0.01	10	0.25	30	10	7.47E-07	0.048	
0.01	10	0.25	50	10	2.55E-07	0.048	
0.01	10	0.354	1	10	1.45E-03	0.048	
0.01	10	0.354	2	10	3.61E-04	0.048	
0.01	10	0.354	3	10	1.64E-04	0.048	
0.01	10	0.354	5	10	5.42E-05	0.048	
0.01	10	0.354	10	10	1.27E-05	0.048	
0.01	10	0.354	20	10	3.37E-06	0.048	
0.01	10	0.354	30	10	1.48E-06	0.048	
0.01	10	0.354	50	10	4.94E-07	0.048	
0.01	10	0.51	1	10	2.99E-03	0.048	
0.01	10	0.51	2	10	7.70E-04	0.048	
0.01	10	0.51	3	10	3.61E-04	0.048	
0.01	10	0.51	5	10	1.19E-04	0.048	
0.01	10	0.51	10	10	2.98E-05	0.048	
0.01	10	0.51	20	10	6.54E-06	0.048	
0.01	10	0.51	30	10	2.88E-06	0.048	
0.01	10	0.51	50	10	1.06E-06	0.048	
0.01	100	0.25	1	100	6.63E-05	0.08	
0.01	100	0.25	2	100	1.75E-05	0.08	
0.01	100	0.25	3	100	8.71E-06	0.08	
0.01	100	0.25	5	100	2.98E-06	0.08	
0.01	100	0.25	10	100	7.91E-07	0.08	
0.01	100	0.25	20	100	1.92E-07	0.08	
0.01	100	0.25	30	100	8.74E-08	0.08	
0.01	100	0.25	50	100			
0.01	100	0.354	1	100	1.37E-04	0.08	
0.01	100	0.354	2	100	3.11E-05	0.08	
0.01	100	0.354	3	100	1.71E-05	0.08	

SIMULATION INPUT DATA				WELL TEST RESULTS			COMMENTS	
K_m	K_f	r_w	L_{ma}	K	λ	ω		
0.01	100	0.354	5	100	5.65E-06	0.08	System radial flow not reached	
0.01	100	0.354	10	100	1.32E-06	0.08		
0.01	100	0.354	20	100	3.77E-07	0.08		
0.01	100	0.354	30	100	1.46E-07	0.08		
0.01	100	0.354	50					
0.01	100	0.51	1	100	3.03E-04	0.08		
0.01	100	0.51	2	100	6.70E-05	0.08		
0.01	100	0.51	3	100	3.92E-05	0.08		
0.01	100	0.51	5	100	1.50E-05	0.08		
0.01	100	0.51	10	100	3.02E-06	0.08		
0.01	100	0.51	20	100	8.27E-07	0.08		
0.01	100	0.51	30	100	3.21E-07	0.08		
0.01	100	0.51	50					
0.1	1	0.25	1	1	6.57E-02	0.065		Fracture radial flow not present
0.1	1	0.25	2	1	1.72E-02	0.042		Fracture radial flow not present
0.1	1	0.25	3	1	6.78E-03	0.042		
0.1	1	0.25	5	1	2.80E-03	0.042		
0.1	1	0.25	10	1	6.60E-04	0.042		
0.1	1	0.25	20	1	1.75E-04	0.042		
0.1	1	0.25	30	1	7.00E-05	0.042		
0.1	1	0.25	50	1	2.71E-05	0.042		
0.1	1	0.354	1	1				
0.1	1	0.354	2	1	3.41E-02	0.047		
0.1	1	0.354	3	1	1.47E-02	0.045		
0.1	1	0.354	5	1	5.72E-03	0.045		
0.1	1	0.354	10	1	1.34E-03	0.044		
0.1	1	0.354	20	1	3.56E-04	0.044		
0.1	1	0.354	30	1	1.53E-04	0.044		
0.1	1	0.354	50	1	6.07E-05	0.044		
0.1	1	0.51	1	1	2.48E-01	0.06	Fracture radial flow not present	
0.1	1	0.51	2	1	6.50E-02	0.44	Fracture radial flow not present	
0.1	1	0.51	3	1	2.85E-02	0.044		
0.1	1	0.51	5	1	1.08E-02	0.044		
0.1	1	0.51	10	1	2.53E-03	0.044		
0.1	1	0.51	20	1	7.09E-04	0.044		
0.1	1	0.51	30	1	3.24E-04	0.044		
0.1	1	0.51	50	1	1.11E-04	0.044		
0.1	10	0.25	1	10	6.54E-03	0.06		
0.1	10	0.25	2	10	1.87E-03	0.045		
0.1	10	0.25	3	10	8.31E-04	0.05		
0.1	10	0.25	5	10	2.77E-04	0.05		
0.1	10	0.25	10	10	7.43E-05	0.055		
0.1	10	0.25	20	10	1.81E-05	0.055		
0.1	10	0.25	30	10	8.01E-06	0.055		
0.1	10	0.25	50	10	2.94E-06	0.055		

SIMULATION INPUT DATA				WELL TEST RESULTS			COMMENTS
K_m	K_f	r_w	L_{ma}	K	λ	ω	
0.1	10	0.354	1	10	1.28E-02	0.08	Fracture radial flow not present
0.1	10	0.354	2	10	3.32E-03	0.055	
0.1	10	0.354	3	10	1.67E-03	0.055	
0.1	10	0.354	5	10	5.74E-04	0.055	
0.1	10	0.354	10	10	1.49E-04	0.055	
0.1	10	0.354	20	10	3.84E-05	0.055	
0.1	10	0.354	30	10	1.70E-05	0.055	
0.1	10	0.354	50	10	5.85E-06	0.055	
0.1	10	0.51	1				Fracture radial flow not present
0.1	10	0.51	2	10	7.62E-03	0.06	
0.1	10	0.51	3	10	3.80E-03	0.06	
0.1	10	0.51	5	10	1.23E-03	0.06	
0.1	10	0.51	10	10	3.19E-04	0.06	
0.1	10	0.51	20	10	7.78E-05	0.06	
0.1	10	0.51	30	10	3.44E-05	0.06	
0.1	10	0.51	50	10	1.23E-05	0.06	
0.1	100	0.25	1				Fracture radial flow not present
0.1	100	0.25	2	100	1.63E-04	0.08	
0.1	100	0.25	3	100	6.98E-05	0.08	
0.1	100	0.25	5	100	2.90E-05	0.08	
0.1	100	0.25	10	100	5.86E-06	0.08	
0.1	100	0.25	20	100	1.91E-06	0.08	
0.1	100	0.25	30	100	6.90E-07	0.08	
0.1	100	0.25	50	100	2.69E-07	0.06	
0.1	100	0.354					Fracture radial flow not present
0.1	100	0.354	2	100	3.01E-04	0.06	
0.1	100	0.354	3	100	1.56E-04	0.06	
0.1	100	0.354	5	100	5.14E-05	0.06	
0.1	100	0.354	10	100	1.45E-05	0.06	
0.1	100	0.354	20	100	3.73E-06	0.06	
0.1	100	0.354	30	100	1.54E-06	0.06	
0.1	100	0.354	50	100	5.47E-07	0.06	
0.1	100	0.51					Fracture radial flow not present
0.1	100	0.51	2	100	5.77E-04	0.05	
0.1	100	0.51	3	100	2.86E-04	0.05	
0.1	100	0.51	5	100	1.07E-04	0.05	
0.1	100	0.51	10	100	2.51E-05	0.05	
0.1	100	0.51	20	100	6.88E-06	0.05	
0.1	100	0.51	30	100	2.84E-06	0.05	
0.1	100	0.51	50	100	1.07E-06	0.05	

APPENDIX B

RADIAL MODEL – OIL SYSTEM. WELL TEST RESULTS

SIMULATION INPUT DATA				WELL TEST RESULTS			COMMENTS	
K_m	K_f	r_w	L_{ma}	K	λ	ω		
0.1	100	0.25	1	74.5	5.55E-04	0.05	Fracture radial flow not present	
0.1	100	0.25	2	103	1.51E-04	0.05		
0.1	100	0.25	3	103	6.43E-05	0.05		
0.1	100	0.25	5	103	2.29E-05	0.05		
0.1	100	0.25	10	103	5.66E-06	0.05		
0.1	100	0.25	20	103	1.50E-06	0.05		
0.1	100	0.25	30	103	6.79E-07	0.05		
0.1	100	0.25	50	103	2.22E-07	0.05		
0.1	100	0.354	1					Fracture radial flow not present
0.1	100	0.354	2	103	2.89E-04	0.055		
0.1	100	0.354	3	103	1.27E-04	0.055		
0.1	100	0.354	5	103	4.74E-05	0.055		
0.1	100	0.354	10	103	1.17E-05	0.055		
0.1	100	0.354	20	103	3.08E-06	0.055		
0.1	100	0.354	30	103	1.27E-06	0.055		
0.1	100	0.354	50	103	4.52E-07	0.055		
0.1	100	0.51	1				Fracture radial flow not present	
0.1	100	0.51	2	103	6.03E-04	0.059		
0.1	100	0.51	3	103	2.68E-04	0.055		
0.1	100	0.51	5	103	1.05E-04	0.055		
0.1	100	0.51	10	103	2.70E-05	0.055		
0.1	100	0.51	20	103	6.49E-06	0.055		
0.1	100	0.51	30	103	3.02E-06	0.055		
0.1	100	0.51	50	103	1.01E-06	0.055		
0.1	1000	0.25	1					Fracture radial flow not present
0.1	1000	0.25	2	1000	1.38E-05	0.055		
0.1	1000	0.25	3	1000	6.35E-06	0.055		
0.1	1000	0.25	5	1000	2.45E-06	0.055		
0.1	1000	0.25	10	1000	6.06E-07	0.055		
0.1	1000	0.25	20	1040	1.68E-07	0.055		
0.1	1000	0.25	30	1040	6.87E-08	0.055		
0.1	1000	0.25	50				System radial flow not present	
0.1	1000	0.354	1	800	5.34E-05	0.05	Fracture radial flow not present	
0.1	1000	0.354	2	1000	2.21E-05	0.055		
0.1	1000	0.354	3	1000	1.07E-05	0.055		
0.1	1000	0.354	5	1000	5.28E-06	0.055		
0.1	1000	0.354	10	1000	1.19E-06	0.055		
0.1	1000	0.354	20	1000	3.24E-07	0.055		
0.1	1000	0.354	30	1000	1.38E-07	0.055		
0.1	1000	0.354	50					System radial flow not present
0.1	1000	0.51	1	800	1.29E-04	0.08		Fracture radial flow not present

SIMULATION INPUT DATA				WELL TEST RESULTS			COMMENTS
K_m	K_f	r_w	L_{ma}	K	λ	ω	
0.1	1000	0.51	2	1000	5.27E-05	0.046	
0.1	1000	0.51	3	1000	2.22E-05	0.05	
0.1	1000	0.51	5	1000	1.02E-05	0.05	
0.1	1000	0.51	10	1000	2.67E-06	0.04	
0.1	1000	0.51	20	1000	6.14E-07	0.042	
0.1	1000	0.51	30	1000	2.67E-07	0.045	
0.1	1000	0.51	50				System radial flow not present
0.1	5000	0.25	1				Fracture radial flow not present
0.1	5000	0.25	2	5000	2.56E-06	0.08	
0.1	5000	0.25	3	5200	1.06E-06	0.09	
0.1	5000	0.25	5	4850	4.10E-07	0.05	
0.1	5000	0.25	10	5200	1.07E-07	0.055	
0.1	5000	0.25	20	5000	2.74E-08	0.052	
0.1	5000	0.25	30	5200	1.11E-08	0.07	
0.1	5000	0.25	50	3800	1.87E-09	0.055	System radial flow not present
0.1	5000	0.354	1				Fracture radial flow not present
0.1	5000	0.354	2	5060	6.09E-06	0.05	
0.1	5000	0.354	3	5160	2.15E-06	0.08	
0.1	5000	0.354	5	5000	1.04E-06	0.08	
0.1	5000	0.354	10	5220	2.62E-07	0.08	
0.1	5000	0.354	20	5200	5.55E-08	0.06	
0.1	5000	0.354	30				System radial flow not present
0.1	5000	0.354	50				System radial flow not present
0.1	5000	0.51	1				Fracture radial flow not present
0.1	5000	0.51	2				Fracture radial flow not present
0.1	5000	0.51	3	5100	4.62E-06	0.08	
0.1	5000	0.51	5	5200	2.20E-06	0.08	
0.1	5000	0.51	10	5140	6.60E-07	0.08	
0.1	5000	0.51	20	5200	1.23E-07	0.08	
0.1	5000	0.51	30				System radial flow not present
0.1	5000	0.51	50				System radial flow not present
0.5	100	0.25	1				Fracture radial flow not present
0.5	100	0.25	2				Fracture radial flow not present
0.5	100	0.25	3				Fracture radial flow not present
0.5	100	0.25	5	103	1.23E-04	0.05	
0.5	100	0.25	10	103	2.89E-05	0.05	
0.5	100	0.25	20	100.3	7.90E-06	0.05	
0.5	100	0.25	30	100.6	3.24E-06	0.05	
0.5	100	0.25	50	103	1.12E-06	0.05	
0.5	100	0.354					Fracture radial flow not present
0.5	100	0.354					Fracture radial flow not present
0.5	100	0.354					Fracture radial flow not present
0.5	100	0.354	5	100.8	2.11E-04	0.048	
0.5	100	0.354	10	100	5.66E-05	0.048	
0.5	100	0.354	20	100	1.49E-05	0.048	

SIMULATION INPUT DATA				WELL TEST RESULTS			COMMENTS
K_m	K_f	r_w	L_{ma}	K	λ	ω	
0.5	100	0.354	30	102	6.49E-06	0.048	
0.5	100	0.354	50	101.3	2.28E-06	0.048	
0.5	100	0.51	1				Fracture radial flow not present
0.5	100	0.51	2				Fracture radial flow not present
0.5	100	0.51	3				Fracture radial flow not present
0.5	100	0.51	5	100.9	4.43E-04	0.051	
0.5	100	0.51	10	100	1.29E-04	0.051	
0.5	100	0.51	20	100	3.14E-05	0.051	
0.5	100	0.51	30	100.7	1.36E-05	0.051	
0.5	100	0.51	50	101.3	5.38E-06	0.051	
0.5	1000	0.25	1				Fracture radial flow not present
0.5	1000	0.25	2				Fracture radial flow not present
0.5	1000	0.25	3				Fracture radial flow not present
0.5	1000	0.25	5	1050	1.10E-05	0.08	
0.5	1000	0.25	10	1050	3.37E-06	0.08	
0.5	1000	0.25	20	1050	8.08E-07	0.08	
0.5	1000	0.25	30	1006	3.66E-07	0.06	
0.5	1000	0.25	50	1040	1.26E-07	0.06	
0.5	1000	0.354	1				Fracture radial flow not present
0.5	1000	0.354	2				Fracture radial flow not present
0.5	1000	0.354	3				Fracture radial flow not present
0.5	1000	0.354	5	985.2	1.51E-05	0.05	
0.5	1000	0.354	10	1040	6.90E-06	0.08	
0.5	1000	0.354	20	996	1.47E-06	0.06	
0.5	1000	0.354	30	1030	7.44E-07	0.08	
0.5	1000	0.354	50	1040	2.52E-07	0.08	
0.5	1000	0.51	1				Fracture radial flow not present
0.5	1000	0.51	2				Fracture radial flow not present
0.5	1000	0.51	3				Fracture radial flow not present
0.5	1000	0.51	5	1040	4.49E-05	0.09	
0.5	1000	0.51	10	990	1.38E-05	0.05	
0.5	1000	0.51	20	1000	3.47E-06	0.05	
0.5	1000	0.51	30	1040	1.43E-06	0.09	
0.5	1000	0.51	50	1040	4.99E-07	0.06	
0.5	5000	0.25	1				Fracture radial flow not present
0.5	5000	0.25	2				Fracture radial flow not present
0.5	5000	0.25	3				Fracture radial flow not present
0.5	5000	0.25	5				Fracture radial flow not present
0.5	5000	0.25	10	5100	3.78E-07	0.05	
0.5	5000	0.25	20	5100	1.40E-07	0.053	
0.5	5000	0.25	30	5180	6.45E-08	0.055	
0.5	5000	0.25	50	5180	6.45E-08	0.055	System radial flow not present
0.5	5000	0.354	1				Fracture radial flow not present
0.5	5000	0.354	2				Fracture radial flow not present
0.5	5000	0.354	3				Fracture radial flow not present

SIMULATION INPUT DATA				WELL TEST RESULTS			COMMENTS
K_m	K_f	r_w	L_{ma}	K	λ	ω	
0.5	5000	0.354	5				Fracture radial flow not present
0.5	5000	0.354	10	5200	1.16E-06	0.08	
0.5	5000	0.354	20	5200	3.59E-07	0.08	
0.5	5000	0.354	30	5220	1.38E-07	0.07	
0.5	5000	0.354	50	5230	3.96E-08	0.09	
0.5	5000	0.51	1				Fracture radial flow not present
0.5	5000	0.51	2				Fracture radial flow not present
0.5	5000	0.51	3				Fracture radial flow not present
0.5	5000	0.51	5				Fracture radial flow not present
0.5	5000	0.51	10	5220	2.33E-06	0.09	
0.5	5000	0.51	20	5150	7.30E-07	0.06	
0.5	5000	0.51	30	5220	2.69E-07	0.09	
0.5	5000	0.51	50	5220	8.94E-08	0.09	
1	100	0.25	1				Fracture radial flow not present
1	100	0.25	2				Fracture radial flow not present
1	100	0.25	3				Fracture radial flow not present
1	100	0.25	5	99.5	2.27E-04	0.05	
1	100	0.25	10	103	5.87E-05	0.05	
1	100	0.25	20	103	1.53E-05	0.05	
1	100	0.25	30	102.3	7.27E-06	0.05	
1	100	0.25	50	103	2.50E-06	0.055	
1	100	0.354	1				Fracture radial flow not present
1	100	0.354	2				Fracture radial flow not present
1	100	0.354	3				Fracture radial flow not present
1	100	0.354	5				Fracture radial flow not present
1	100	0.354	10	100	1.13E-04	0.055	
1	100	0.354	20	100.3	3.21E-05	0.055	
1	100	0.354	30	100.2	1.42E-05	0.05	
1	100	0.354	50	102.1	5.24E-06	0.055	
1	100	0.51	1				Fracture radial flow not present
1	100	0.51	2				Fracture radial flow not present
1	100	0.51	3				Fracture radial flow not present
1	100	0.51	5	103		0.055	Fracture radial flow not present
1	100	0.51	10	103	2.54E-04	0.055	
1	100	0.51	20	103	6.56E-05	0.055	
1	100	0.51	30	103	2.64E-05	0.055	
1	100	0.51	50	103	1.01E-05	0.055	
1	1000	0.25	1				Fracture radial flow not present
1	1000	0.25	2				Fracture radial flow not present
1	1000	0.25	3				Fracture radial flow not present
1	1000	0.25	5				Fracture radial flow not present
1	1000	0.25	10	995	5.76E-06	0.054	
1	1000	0.25	20	1040	1.70E-06	0.051	
1	1000	0.25	30	1040	7.63E-07	0.051	
1	1000	0.25	50	1040	2.49E-07	0.051	

SIMULATION INPUT DATA				WELL TEST RESULTS			COMMENTS
K_m	K_f	r_w	L_{ma}	K	λ	ω	
1	1000	0.354	1				Fracture radial flow not present
1	1000	0.354	2				Fracture radial flow not present
1	1000	0.354	3				Fracture radial flow not present
1	1000	0.354	5				Fracture radial flow not present
1	1000	0.354	10	1018	1.16E-05	0.08	
1	1000	0.354	20	1000	3.07E-06	0.05	
1	1000	0.354	30	970	1.49E-06	0.055	
1	1000	0.354	50	1040	4.85E-07	0.06	
1	1000	0.51	1				Fracture radial flow not present
1	1000	0.51	2				Fracture radial flow not present
1	1000	0.51	3				Fracture radial flow not present
1	1000	0.51	5				Fracture radial flow not present
1	1000	0.51	10	970	2.54E-05	0.05	
1	1000	0.51	20	994	6.43E-06	0.05	
1	1000	0.51	30	1006	2.84E-06	0.05	
1	1000	0.51	50	1028	9.55E-07	0.05	
1	5000	0.25	1				Fracture radial flow not present
1	5000	0.25	2				Fracture radial flow not present
1	5000	0.25	3				Fracture radial flow not present
1	5000	0.25	5				Fracture radial flow not present
1	5000	0.25	10	4985	1.06E-06	0.05	
1	5000	0.25	20	5200	3.51E-07	0.08	
1	5000	0.25	30	5200	1.06E-07	0.08	
1	5000	0.25	50	5200	4.30E-08	0.08	
1	5000	0.354	1				Fracture radial flow not present
1	5000	0.354	2				Fracture radial flow not present
1	5000	0.354	3				Fracture radial flow not present
1	5000	0.354	5				Fracture radial flow not present
1	5000	0.354	10	5030	1.90E-06	0.07	
1	5000	0.354	20	4950	5.91E-07	0.05	
1	5000	0.354	30	5210	2.82E-07	0.08	
1	5000	0.354	50	5250	8.96E-08	0.08	
1	5000	0.51	1				Fracture radial flow not present
1	5000	0.51	2				Fracture radial flow not present
1	5000	0.51	3				Fracture radial flow not present
1	5000	0.51	5				Fracture radial flow not present
1	5000	0.51	10	5200	3.88E-06	0.08	
1	5000	0.51	20	5050	1.27E-06	0.05	
1	5000	0.51	30	5200	5.66E-07	0.08	
1	5000	0.51	50	5200	1.73E-07	0.08	
5	100	0.25	1				Fracture radial flow not present
5	100	0.25	2				Fracture radial flow not present
5	100	0.25	3				Fracture radial flow not present
5	100	0.25	5				Fracture radial flow not present
5	100	0.25	10				Fracture radial flow not present

SIMULATION INPUT DATA				WELL TEST RESULTS			COMMENTS
K_m	K_f	r_w	L_{ma}	K	λ	ω	
5	100	0.25	20	100.1	7.41E-05	0.055	
5	100	0.25	30	99.5	3.32E-05	0.055	
5	100	0.25	50	110.9	1.18E-05	0.055	
5	100	0.354	1				Fracture radial flow not present
5	100	0.354	2				Fracture radial flow not present
5	100	0.354	3				Fracture radial flow not present
5	100	0.354	5				Fracture radial flow not present
5	100	0.354	10	103.1	5.62E-04	0.055	
5	100	0.354	20	103.6	1.51E-04	0.055	
5	100	0.354	30	103	6.62E-05	0.055	
5	100	0.354	50	99	2.63E-05	0.055	
5	100	0.51	1				Fracture radial flow not present
5	100	0.51	2				Fracture radial flow not present
5	100	0.51	3				Fracture radial flow not present
5	100	0.51	5				Fracture radial flow not present
5	100	0.51	10	101.1	1.20E-03	0.055	
5	100	0.51	20	103.1	3.15E-04	0.055	
5	100	0.51	30	102	1.45E-04	0.055	
5	100	0.51	50	100	5.15E-05	0.055	
5	1000	0.25	1				Fracture radial flow not present
5	1000	0.25	2				Fracture radial flow not present
5	1000	0.25	3				Fracture radial flow not present
5	1000	0.25	5				Fracture radial flow not present
5	1000	0.25	10	1040	2.79E-05	0.055	
5	1000	0.25	20	985	7.19E-06	0.055	
5	1000	0.25	30	975	3.31E-06	0.055	
5	1000	0.25	50	1000	1.21E-06	0.055	
5	1000	0.354	1				Fracture radial flow not present
5	1000	0.354	2				Fracture radial flow not present
5	1000	0.354	3				Fracture radial flow not present
5	1000	0.354	5				Fracture radial flow not present
5	1000	0.354	10	1020	4.67E-05	0.05	
5	1000	0.354	20	1000	1.50E-05	0.05	
5	1000	0.354	30	1000	6.97E-06	0.05	
5	1000	0.354	50	995	2.27E-06	0.05	
5	1000	0.51	1				Fracture radial flow not present
5	1000	0.51	2				Fracture radial flow not present
5	1000	0.51	3				Fracture radial flow not present
5	1000	0.51	5				Fracture radial flow not present
5	1000	0.51	10	966	1.01E-04	0.05	
5	1000	0.51	20	960	2.74E-05	0.05	
5	1000	0.51	30	1000	1.51E-05	0.05	
5	1000	0.51	50	1000	5.42E-06	0.05	
5	5000	0.25	1				Fracture radial flow not present
5	5000	0.25	2				Fracture radial flow not present

SIMULATION INPUT DATA				WELL TEST RESULTS			COMMENTS
K_m	K_f	r_w	L_{ma}	K	λ	ω	
5	5000	0.25	3				Fracture radial flow not present
5	5000	0.25	5				Fracture radial flow not present
5	5000	0.25	10				Fracture radial flow not present
5	5000	0.25	20	4950	1.47E-06	0.05	
5	5000	0.25	30	5140	8.17E-07	0.05	
5	5000	0.25	50	5100	2.34E-07	0.05	
5	5000	0.354	1				Fracture radial flow not present
5	5000	0.354	2				Fracture radial flow not present
5	5000	0.354	3				Fracture radial flow not present
5	5000	0.354	5				Fracture radial flow not present
5	5000	0.354	10				Fracture radial flow not present
5	5000	0.354	20	5000	2.84E-06	0.05	
5	5000	0.354	30	5070	1.78E-06	0.05	
5	5000	0.354	50	5050	6.04E-07	0.05	
5	5000	0.51	1				Fracture radial flow not present
5	5000	0.51	2				Fracture radial flow not present
5	5000	0.51	3				Fracture radial flow not present
5	5000	0.51	5				Fracture radial flow not present
5	5000	0.51	10				Fracture radial flow not present
5	5000	0.51	20	5200	4.52E-06	0.05	
5	5000	0.51	30	5150	2.34E-06	0.05	
5	5000	0.51	50	5150	1.02E-06	0.05	

VITA

Name: Laura Elena Perez Garcia

Permanent Address: Calle 37 No. 8-43 Piso 12
Bogota, Colombia

Email: laura.perez@ecopetrol.com.co

Education: B. S., Petroleum Engineering,
Universidad Surcolombiana
Neiva, Colombia
(December 1993)

M.S., Petroleum Engineering
Texas A&M University
College Station, TX 77843-3116, U.S.A.
(December 2005)